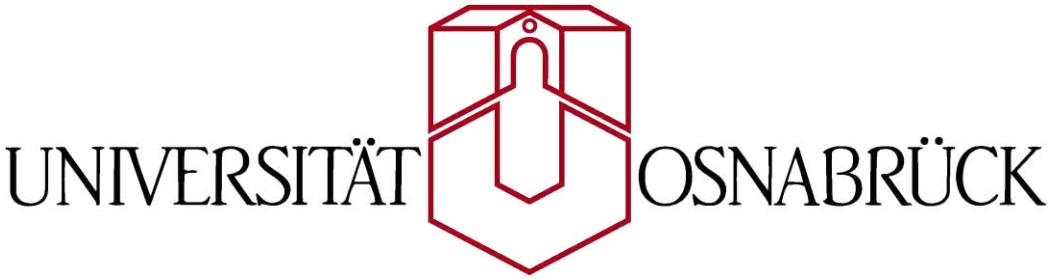

Complex sphingolipid profiling and identification of an inositol phosphorylceramide synthase in *Dictyostelium discoideum*

Dissertation

submitted to the Department of Biology/Chemistry of the
University of Osnabrück, Germany

to obtain the degree '*Doctor Rerum Naturalium*' (Dr. rer. nat.)

Presented by

Stevanus Aditya Listian

Born in Jakarta, Indonesia

Osnabrück, August 2023

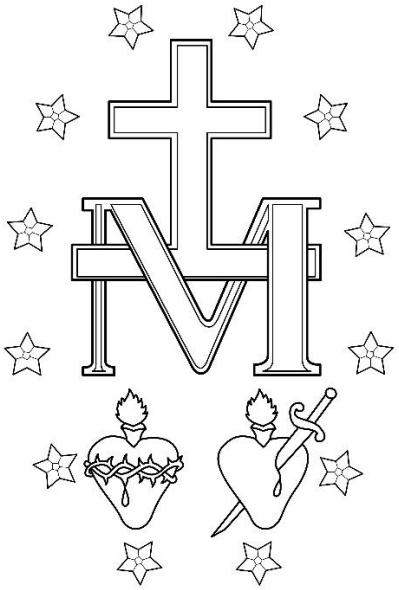

Buat Ama, Mami, Papi, Niko dan Christo;

Juga untuk Ibu Tresnawati Purwadaria dan Ibu Noviana Ingrid

Referees:

Prof. Dr. Caroline Barisch
Center for Structural Systems Biology, Hamburg

Prof. Dr. Joost Holthuis
Molecular Cell Biology, University of Osnabrück

TABLE OF CONTENTS

PUBLICATIONS

Listian SA, Kol M, Ufelmann E, Eising S, Froehlich F, Walter S, Holthuis JCM, Barisch C (2023). Complex Sphingolipid Profiling and Identification of an Inositol Phosphorylceramide Synthase in *Dictyostelium discoideum.* BioRxiv. doi:10.1101/ 2023.07.07.548115.

Anand A, Mazur A-C, Rosell-Arevalo P, Franzkoch R, Breitsprecher L, **Listian SA**, Hüttel SV, Müller D, Schäfer DG, Vormittag S, Hilbi H, Maniak M, Gutierrez MG, Barisch C (2023). ER-dependent membrane repair of mycobacteria-induced vacuole damage. accepted for publication in mBio. doi:10.1101/2023.04.17.537276.

Foulon M, **Listian SA**, Soldati T, Barisch C (2022). Chapter 6. Conserved mechanisms drive host lipid access, import and utilisation in *Mycobacterium tuberculosis* and *M. marinum*. In Developments in Microbiology, Biology of Mycobacterial Lipids, Academic Press. Edited by Fatima Z, Canaan S. Review.

Kjeldgaard B*, **Listian SA***, Ramaswamhi V, Richter A, Kiesewalter HT, Kovács AT (2019). Fungal hyphae colonization by *Bacillus subtilis* relies on biofilm matrix components. Biofilm. doi:10.1016/j.bioflm.2019.100007.

ABSTRACT

Dictyostelium discoideum is a free-living social amoeba at the crossroads between uni- and multicellular life. It is often used as a model organism to investigate cellular processes related to the recognition, engulfment and infection course of intracellular pathogens. Sphingolipids are found in high abundance in the plasma membrane. They are cholesterol-binding lipids that control membrane properties, mediate signaling and act as adhesion molecules in recognition mechanisms essential to infection and immunity. In plants, animals and fungi, the sphingolipid pathway is largely established. However, in *D. discoideum*, neither the identity of the sphingolipids nor the biosynthesis pathway are well characterised. Using lipidomics, I observed that *D. discoideum* generates inositol-phosphorylceramide (IPC) with predominantly phytoceramide backbones. The candidates for IPC synthase were narrowed down using a bio-IT-based cloning strategy, and the activity of each candidate was analysed using a cell-free expression (CFE) system within defined lipid environments, which takes into account the selectivity of headgroup transfer from phosphatidylinositol (PI) to Ceramide (Cer). This led to the identification of *Dd*IPCS1, a protein sharing multiple sequence motifs with yeast IPC and human sphingomyelin (SM) synthases. *Dd*IPCS1 is localised at the Golgi apparatus and the contractile vacuole (CV) of *D. discoideum*. These ground-breaking findings pave the way for further research into the role of sphingolipids in phagocytosis and infection, bridging a large evolutionary gap.

ZUSAMMENFASSUNG

Dictyostelium discoideum ist eine freilebende soziale Amöbe, die sich an der Schnittstelle zwischen dem ein- und mehrzelligem Leben befindet. Sie wird häufig als Modellorganismus verwendet, um zelluläre Prozesse im Zusammenhang mit der Erkennung, der Aufnahme und dem Infektionsverlauf von intrazellulären Krankheitserregern zu untersuchen. Sphingolipide befinden sich in großer Menge in der Plasmamembran. Sie sind cholesterinbindende Lipide, die Membraneigenschaften steuern, Signale vermitteln und als Adhäsionsmoleküle in Erkennungsmechanismen wirken, welche für Infektion und Immunität wesentlich sind. In Pflanzen, Tieren und Pilzen ist der Sphingolipid-Stoffwechselweg bereits weitgehend etabliert. In *D. discoideum* sind jedoch weder die Identität der Sphingolipide noch der Biosyntheseweg bisher charakterisiert. Mit Hilfe von Lipidomics konnte ich feststellen, dass *D. discoideum* überwiegend Inositol-Phosphorylceramid (IPC) mit einem Phytoceramid-Grundgerüst erzeugt. Die möglichen Kandidaten für die IPC-Synthase wurden mit Hilfe einer bio-IT-basierten Klonierungsstrategie ausgewählt. Die Aktivität der Kandidaten wurde mit einem zellfreien Expressionsystems (CFE) in definierten Lipidumgebungen untersucht, welches die Selektivität des Kopfgruppentransfers von Phosphatidylinositol (PI) zu Ceramid (Cer) berücksichtigt. Dies führte zur Identifizierung von *Dd*IPCS1, einem Protein, das mehrere Sequenzmotive mit der IPC-Synthase der Hefe und der Sphingomyelin-Synthasen (SM) des Menschen teilt. *Dd*IPCS1 ist im Golgi Apparat und der kontraktilen Vakuole (CV) von *D. discoideum* lokalisiert. Diese bahnbrechenden Ergebnisse ebnen den Weg für die weitere Erforschung der Rolle von Sphingolipiden bei der Phagozytose sowie bei der Infektion und schließen eine große evolutionäre Lücke.

INTRODUCTION

The structural diversity of lipids and how their composition influences cell function

Lipids are remarkably diverse. This diversity affects lipid properties and plays a role in regulating cellular processes. Harayama and Riezman defined the diversity of lipids into two categories: Structural and compositional (ratio of different lipids). Lipids differ chemically in their basic structure, head group, charge, number, length and saturation state of acyl chains (Fig. 1). Conversely, in terms of their compositional diversity, different organisms, tissues, cells, organelles, membrane leaflets or membrane sub-domains have different lipid compositions. Both lipid structure and composition influence cellular processes, mainly through protein-lipid interactions (Harayama and Riezman, 2018).

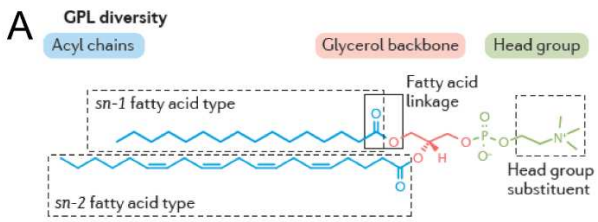

GPL	Head group substituent
Phosphatidic acid	–
PtdCho	Choline
PtdEtn	Ethanolamine
PtdSer	Serine
PtdIns	Inositol
PtdGro	Glycerol
Cardiolipin	PtdGro
LBPA	LPA
PtdGlc	Glucose

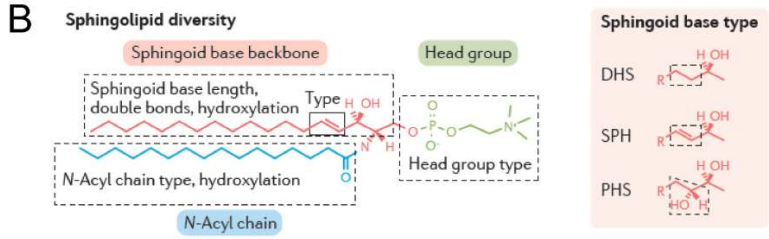

Sphingolipid	Head group
Cer	Hydroxyl
Sphingomyelin	Phosphocholine
CerPE	Phosphoethanolamine
GlcCer	Glucose
GalCer	Galactose
Complex GSLs	Oligosaccharides
C1P	Phosphate

Fig. 1. The diversity of mammalian membrane lipids. **A:** The molecular diversity of phospholipids/glycerophospholipids or GPLs. Glycerophospholipids are acylated at the *sn-1* and/or *sn-2* position. Different phospho headgroup moeities constitute different glycerophospholipid classes. The fatty acid linkage at the *sn-1* position can be either an ester or an ether bond. **B:** The molecular diversity of sphingolipids. Sphingolipids vary in their respective sphingoid long chain bases (LCB), headgroups and N-acyl chain. Different chain lengths of LCB may exist. Unsaturation and hydroxylation at the LCB define the base type, while the headgroup defines the sphingolipid name. Every Cer that receives a headgroup is called a complex sphingolipid. Unlike glycerophospolipids, the headgroup of sphingolipids may or may not be phosphorylated. The N-acyl chain also differ in terms of chain length and hydroxylation. Figure addapted from Harayama and Riezman (2018).

How lipid structure influences protein-mediated cell function is exemplified by the recognition of phosphoinositides (PIPs) with lipid binding proteins, which regulates a variety of processes. PIPs are phosphorylated PIs, which act as a signpost for lipid-binding proteins and regulate phagosomal maturation in *D. discoideum* (Vines and King, 2019). Recently, in *Dictyostelium discoideum*, it was discovered that *Dd*SnxA binds specifically to $PI(3,5)P_2$. The binding of *Dd*SnxA

to the endosomal membrane is abolished when *Dd*PIKfyve, the enzyme responsible for the synthesis of $PI(3,5)P_2$, is ablated (Vines et al., 2023). Aside from the lipid chemical structure, cells also sense and respond to membrane lipid composition. One example is that orosomucoid (Orm) proteins inhibiting the production of sphingolipids (Körner and Fröhlich, 2022). Orms inhibit the rate-limiting serine palmitoyl transferase (SPT). In yeast, *Sc*Slm1 and *Sc*Slm2 sense the membrane stress caused by reduced sphingolipids. The signal was transmitted to Target of Rapamycin Complex 2 (TORC2), which releases the inhibition of Spt through a phosphorylation cascade (Berchtold et al., 2012).

Investigating lipid structure and composition are relevant as mutations in specific lipid metabolising enzymes might cause genetic diseases. For instance, p.Ile62Ser and p.Met64Arg mutations in sphingomyelin synthase 2 (*Hs*SMS2) cause osteoporosis and skeletal dysplasia (Pekkinen et al., 2019). *Hs*SMS2 with these mutations is mislocalised from the Golgi to the endoplasmic reticulum (ER). This mislocalisation leads to bulk production of SM in the ER and perturbs the lipid gradient of the secretory pathway. It was hypothesised that this pertubation impairs normal phosphate and Ca^{2+} secretion from the osteoblast, thereby hindering bone mineralization (Sokoya et al., 2022).

The structural diversity of sphingolipids and the conservation of the sphingolipid pathway between eukaryotes

The structural diversity of sphingolipids is immense. Sphingolipids vary in (i) the length of the LCB, (ii) the length of the N-acyl chain, (iii) the saturation of both the LCB and the N-acyl chain, (iv) hydroxylations of both the LCB and the N-acyl chain and (v) headgroup modification (Fig. 1) (Harayama and Riezman, 2018). Each sphingolipid modification is introduced by distinct enzymes within the sphingolipid pathway (Fig. 2, 3). Hanun and Obeid reviewed each step of the sphingolipid pathway extensively (Hannun and Obeid, 2018). Here, I will focus on the structural diversity of sphingolipids and their conservation between eukaryotes.

The sphingolipid pathway is largely preserved between eukaryotes. However, there are some differences, especially in terms of the sphingolipid headgroup (Fig. 2). For instance, fungi and plants produce IPC, while mammals produce SM (Fig. 2). Figure 3 depicts the sphingolipid pathway of *S. cerevisiae*: First, serine and palmitoyl-Coenzyme A (palmitoyl-CoA) are condensed, generating 3-ketodihydrosphingosine (3-KDS). Second, 3-KDS is reduced to dihydrosphingosines (sphinganine). From sphinganine, the LCB primarily undergoes C4-hydroxylation, yielding trihydroxy phytosphingosine. Both sphinganine and phytosphingosine are N-acylated giving rise to Cer. In *S. cerevisiae*, the fatty acid moiety is predominantly hydroxylated

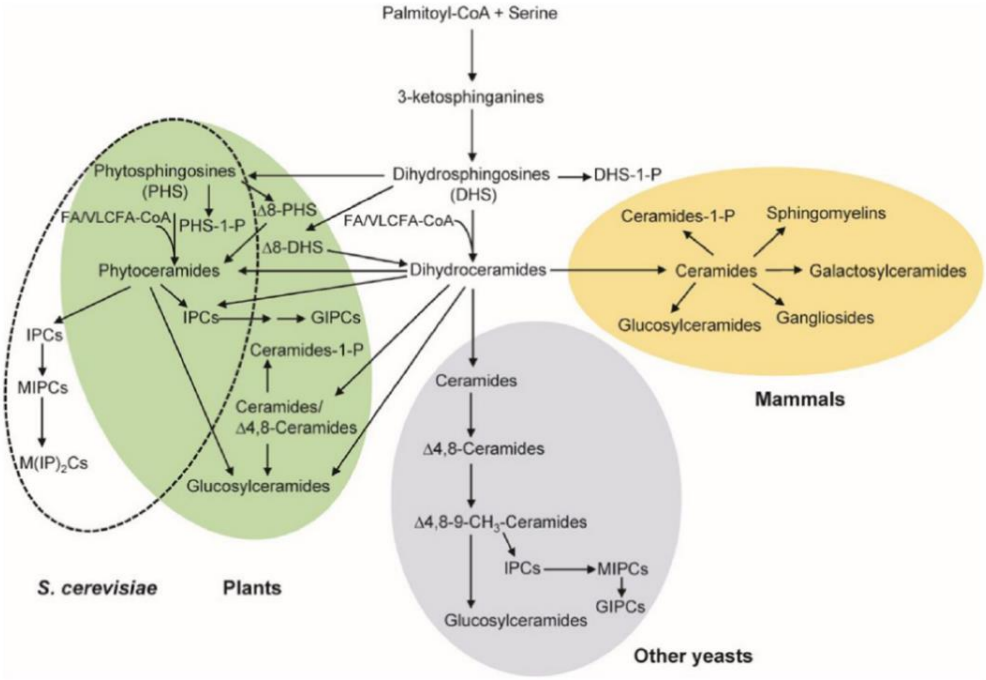

Fig. 2. The sphingolipid pathway is largely conserved between eukaryotes. However, variations might be present in complex sphingolipids. DHS: dihydroceramide. VLCFA: Very Long Chain Fatty Acid. Figure from Marquês et al., (2018).

at position 2 (α-OH), but varying degrees of hydroxylation may occur (Ejsing et al., 2009). Then, a phosphoinositol headgroup is added to Cer by *Sc*Aur1, generating IPC (Fig. 3B). IPC may incorporate mannosyl and then another phosphoinositol group in its inositol headgroup, generating mannosylinositol-phosphorylceramide (MIPC) and mannosyldiinositol-phosphorylceramide ($M(IP)_2C$), respectively (Fig. 3,4) (Lisman et al., 2004; Megyeri et al., 2016). Strikingly, there are differences in sphingolipid structure between fungi. For instance, unlike *S. cerevisiae* where no LCB desaturation occurs, the LCB of *Pichia pastoris* might be desaturated at Δ4 and Δ8 (Fig. 4A) (Ternes et al., 2006). Additionally, in *Kluyveromyces lactis*, Cer may undergo glycosylation, resulting in glycosylceramide (GlcCer) (Fig. 4B) (Saito et al., 2006); also, in *C. neoformans*, a series of sugar moieties are added to MIPC, generating a diverse set of glycosylinositol phosphorylceramides (GIPC) (Fig. 4B). In plants, the sphingolipid pathway is very similar to that of *S. cerevisiae*. In both *S. cerevisiae* and plants, IPC is present and Cers are predominantly α-OH phytoceramides (Ceramides C) (Fig. 3A). However, there are several differences: In *Arabidopsis thaliana*, (i) LCBs might undergo Δ4 and Δ8 desaturations (Fig. 4A), (ii) GlcCer is generated (Fig. 4B) and (iii) IPCs are modified to GIPCs (Fig. 4B). The first sugar residue in the synthesis of GIPC in *A. thaliana* is glucoronic acid. After glucoronic acid, either N-acetyl glucosamine or mannose are added. Further GIPC modifications are poorly characterised (Mamode Cassim et al., 2020).

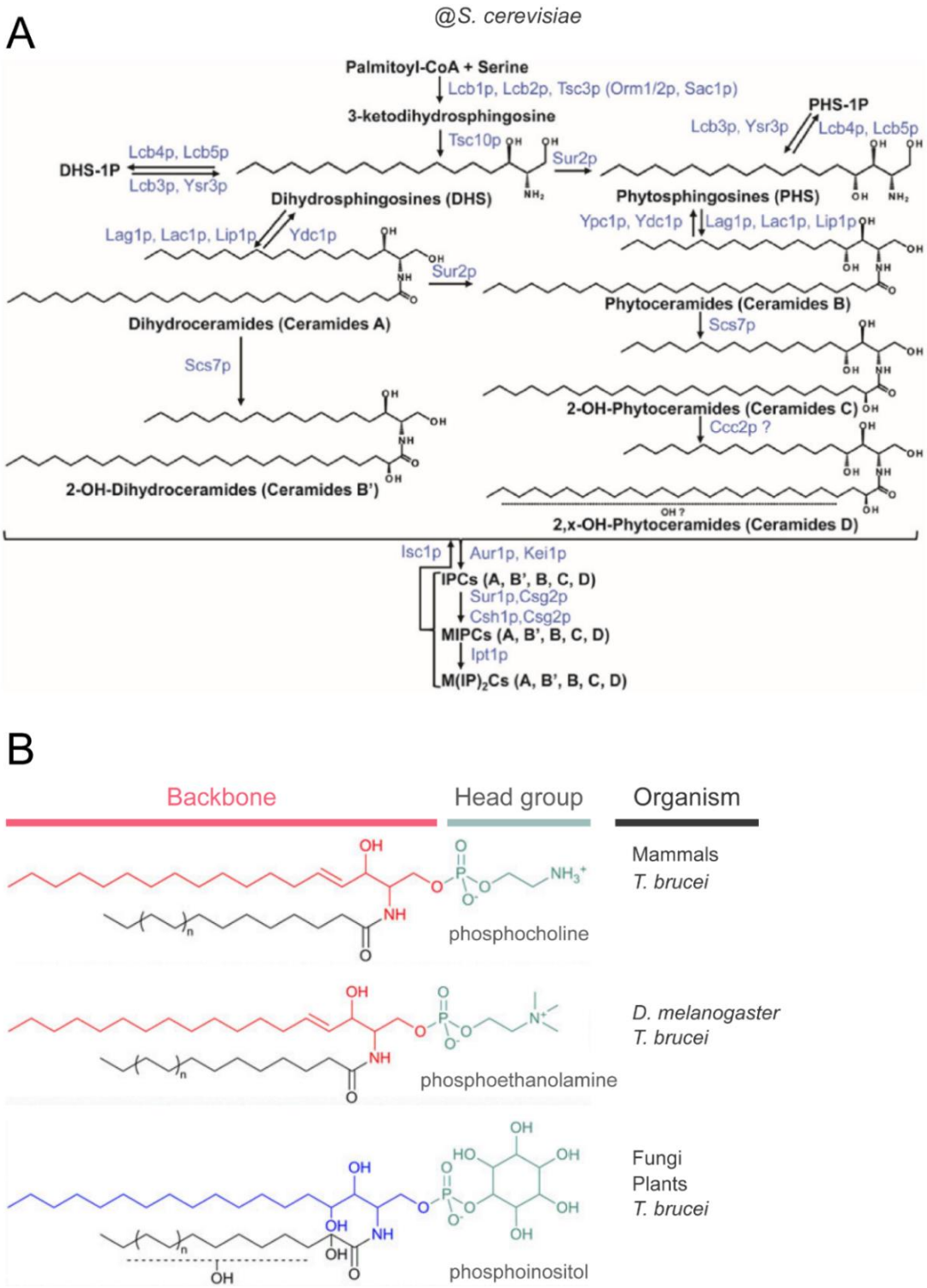

Fig. 3. Hydroxyl and phospho headgroup variations in sphingolipids. **A:** Structural modification of sphingolipids in *S. cerevisiae* with special attention to the hydroxylation of the Cer backbone. Before conversion into complex sphingolipids, hydroxyl groups may be introduced to the LCB and the N-acyl chain. Figure adapted from Marquês et al., (2018). **B:** Headgroup modifications of complex phosphosphingolipid between organism. Figure adapted from Mina and Denny (2018).

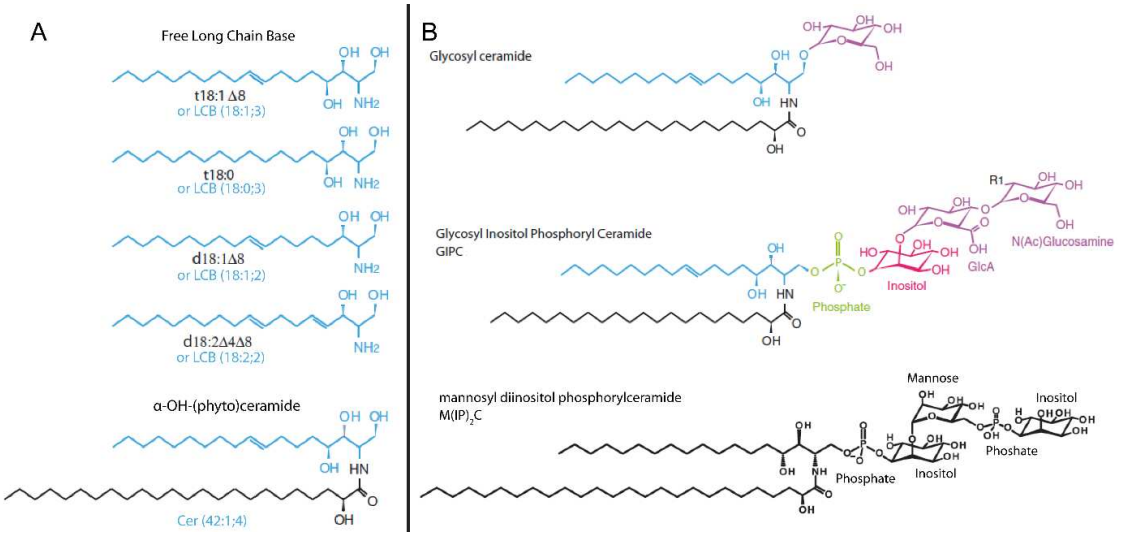

Fig. 4. Double bond and extended headgroup variations of sphingolipids**. A**: Structure and nomenclature of sphingolipids. **B**: Structures of GlcCer, GIPC and $M(IP)_2C$. Figure adapted from Mamode Cassim et al., (2020).

In mammals, phytosphingolipids are not prevalent. The LCBs are typically desaturated at Δ4 (Fig. 3A) (Sokoya *et al.*, 2022). Unlike yeast and plants, mammals do not produce IPC but SM, which has phosphocoline as headgroup instead of phosphoinositol (Fig. 3B) (Huitema et al., 2004). Mammalian cells also produce a trace amount of ethanolamine-phosphorylceramide (EPC) (Fig. 3B), which is synthesised by the transfer of the phosphoethanolamine headgroup from phosphatidylethanolamine (PE) to Cer (Kol et al., 2017). The structural diversity of sphingolipids in mammals, *S. cerevisiae* and *A. thaliana* is summarised in Table 1.

Table 1. The summarised structural diversity of sphingolipids between mammals, *A. thaliana* and *S. cerevisiae*.

Variation	Mammals	*A. thaliana*	*S. cerevisiae*
LCB chain length	mainly C18, sometimes C16 or C20 (Hornemann et al., 2009; Sonnino and Chigorno, 2000).	mainly C18 (Chen et al., 2008; Ternes et al., 2011).	mainly C18, sometimes C20 (Ejsing *et al.*, 2009).
LCB desaturation	usually a double bond at Δ4 (Ternes et al., 2002).	usually a double bonds at Δ4, sometimes at Δ8 (Chen et al., 2012).	non-existent (Ejsing *et al.*, 2009).
LCB hydroxylation	mainly dihydroxylated at C1 and C3, except in some tissues (Robson et al., 1994; Sokoya *et al.*, 2022).	mainly trihydroxylated at C1, C3 and C4 (Chen *et al.*, 2012; Chen *et al.*, 2008).	mainly trihydroxylated at C1, C3 and C4 (Ejsing *et al.*, 2009).
N-acyl chain length	C16-C24, but mainly C16 and C24 (Sokoya *et al.*, 2022; Zhang et al., 2015).	C16-C28, but mainly C24 and C26 (Chen *et al.*, 2008; Ternes *et al.*, 2011).	mainly C26, sometimes C24 and C22 (Ejsing *et al.*, 2009).
N-acyl hydroxylation	α-OH is less prominent than in plants and yeasts; the composition of the N-acyl with α-OH chain varies between tissues (Hama, 2010).	mainly α-OH (Chen *et al.*, 2008).	mainly α-OH (Ejsing *et al.*, 2009), the N-acyl chain sometimes contain hydroxyl groups at unspecified locations (Beeler et al., 1997).
Headgroup modifications	See Figure 1B.	glucose → GlcCer; phosphoinositol → IPC; phosphoinositol and series of sugar residues → GIPC (Mamode Cassim *et al.*, 2020)	phosphoinositol → IPC; mannosyl phosphoinositol → MIPC; mannosyl diphosphoinositol → $M(IP)_2C$ (Megyeri *et al.*, 2016)

In *Drosophilla melanogaster*, EPC is the predominant complex phosposphingolipid (Goh and Guan, 2021). Some protozoa, like *Trypanosoma brucei,* even synthesise both EPC, IPC and SM (Fig. 3B) (Sevova et al., 2010). Taken together, the nature of phosphoheadgroup defines the feature of complex phosposphingolipids.

The discovery of complex sphingolipid synthases (CSS) in various species

Here, CSS refers to a phosphotransferase responsible for the synthesis of complex (phospho)sphingolipids (SM, CPE and IPC) (Fig. 5). The first identified CSS was *Sc*Aur1, the IPC synthase from *S. cerevisiae*. Nagiec et al., (1997) isolated an *S. cerevisiae* strain defective in the incorporation of [^{3}H]inositol into sphingolipids. Transforming the mutant with a plasmid expressing *Sc*Aur1 restored the production of IPC (Heidler and Radding, 1995; Nagiec et al., 1997). Mutations in the *aur1* gene have been identified as the leading cause of resistance to the antifungal drug Aureobasidin A (AbA) in *S. cerevisiae* (Hashida-Okado et al., 1996). This led to the observation that AbA treatment decreases IPC synthesis in *S. cerevisiae* membranes (Levine et al., 2000; Nagiec *et al.*, 1997). Further sequence analysis revealed that the fungal Aur1 and Lipid Phosphate Phosphatase (LPP) families share motif conservations, particularly in the C3 domain (Heidler and Radding, 2000). The shared motif, H-[YFWH]-X2-D-[VLI]-X2-[GA]-X3-[GSTA], was used to track down candidates for metazoan SM synthase. This groundbreaking discovery has led to the identification of SMS1 and SMS2 (Huitema *et al.*, 2004). Consequently, a similar strategy has been used to discover other CSSs from kinetoplastids (Denny et al., 2006; Sevova *et al.*, 2010; Sutterwala et al., 2008). Interestingly, like human SMS2, some of these CSS also have bifunctional activity, such as *Tb*SLS4 from *T. brucei* (Fig. 5) (Sutterwala *et al.*, 2008; Ternes et al., 2009).

In *A. thaliana*, IPC synthase was discovered as a result of a genetic screen for mutations that enhance programmed cell death. Loss of *At*ERH1 or *At*IPCS1 leads to elevated Cer levels, reduced plant stature and resistance to powdery mildew infection (Wang et al., 2008). *A. thaliana* contains three orthologues of IPC synthases (*At*IPCS1-3), and all three display AbA resistance (Fig. 5) (Mina et al., 2010). Strikingly, *D. melanogaster* contains no SMS1 or SMS2 homologues, while EPC generated by SMSr is retained at the ER. In addition, *D. melanogaster* also possesses a non-canonical EPC synthase (*Dm*CPES). *Dm*CPES transfers the phospoethanolamine headgroup from CDP-ethanolamine rather than PE. Like most CSS, *Dm*CPES is also localised at the Golgi (Vacaru *et al.*, 2013).

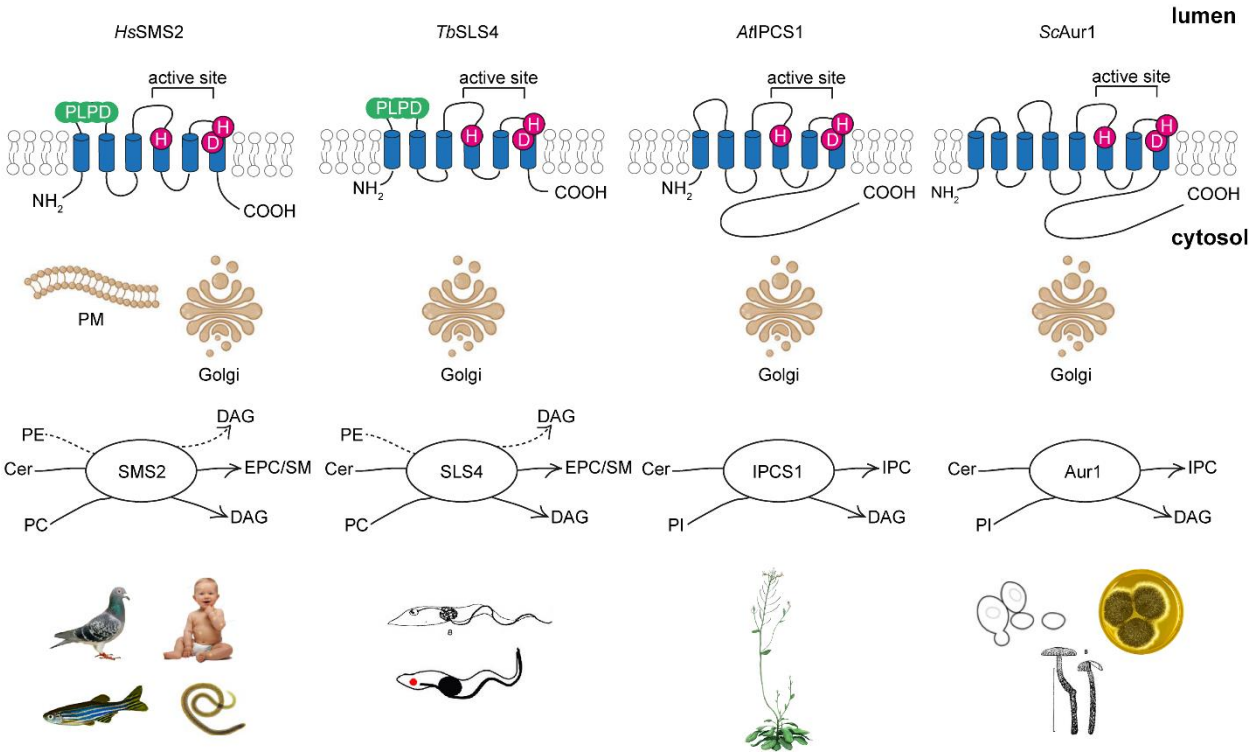

Fig. 5. CSSs of different species. All known CSSs are polytopic transmembrane proteins, and the active site containing the catalytic triad (His-His-Asp) is always facing the lumen. Most CSS reside at the Golgi, but *Hs*SMS2 is located at both the Golgi and the plasma membrane, and *Hs*SMSr at the ER. The reaction entails the transfer of headgroups from PE, phosphatidylcholine (PC), and PI to Cer, resulting in the formation of CPE, SM and IPC as well as diacylglycerol (DAG). Some CSSs, like *Hs*SMS2 and *Tb*SLS4, are bifunctional (Sutterwala *et al.*, 2008; Ternes *et al.*, 2009), producing two or more classes of complex phosphosphingolipids. CSSs are commonly composed of six TMDs, with the exception of fungal Aur1 with eight TMDs. Conserved motifs, such as the PLPD motif, may be shared between CSS from different organisms (e.g. mammalian and protozoa)(Denny *et al.*, 2006). Figure adapted from Jan Parolek's PhD Thesis (2019).

The development of CFE systems accelerated CSS research. Within these systems, the mRNA of the relevant proteins is expressed in a wheat germ extract (WGE). For the investigation of polytopic membrane proteins, liposomes composed of glycerolipids are added to the reaction mix to recruit the protein and prevent misfolding. The newly synthesized proteins are then used for enzymatic assays by adding fluorescently labelled ceramide as an acceptor molecule (Goren et al., 2009). This led to the rapid characterization of four CSSs from *T.brucei* (*Tb*SLS1-4) (Sevova *et al.*, 2010). Using this assay, it was discovered that the amino acid upstream adjacent to the second His of the catalytic triad is important for the specificity of the CSS reaction (e.g. the E271D mutation abolished EPC production by *Hs*SMS2) (Kol *et al.*, 2017; Sevova *et al.*, 2010).

D. discoideum as a model organism for cell biology

D. discoideum is a free living soil amoeba that hunts and phagocytizes bacteria to use them as a nutrition source. This organism is able to alternate between uni- and multicellular life as, during starvation, cells form aggreagate and sporulate. Since the amoeba is one of the earliest branches

from the final common ancestor of all eukaryotes, it has enormous evolutionary significance (Eichinger et al., 2005). Moreover, a proteome-based eukaryotic phylogenetic analysis showed that *D. discoideum* branches soon after the plant-animal split but before the differentiation of fungi (Fig. 6). Despite its earlier divergence, the proteome of *D. discoideum* is more closely related to human orthologues than that of *S. cerevisiae* (Fig. 6) (Eichinger *et al.*, 2005).

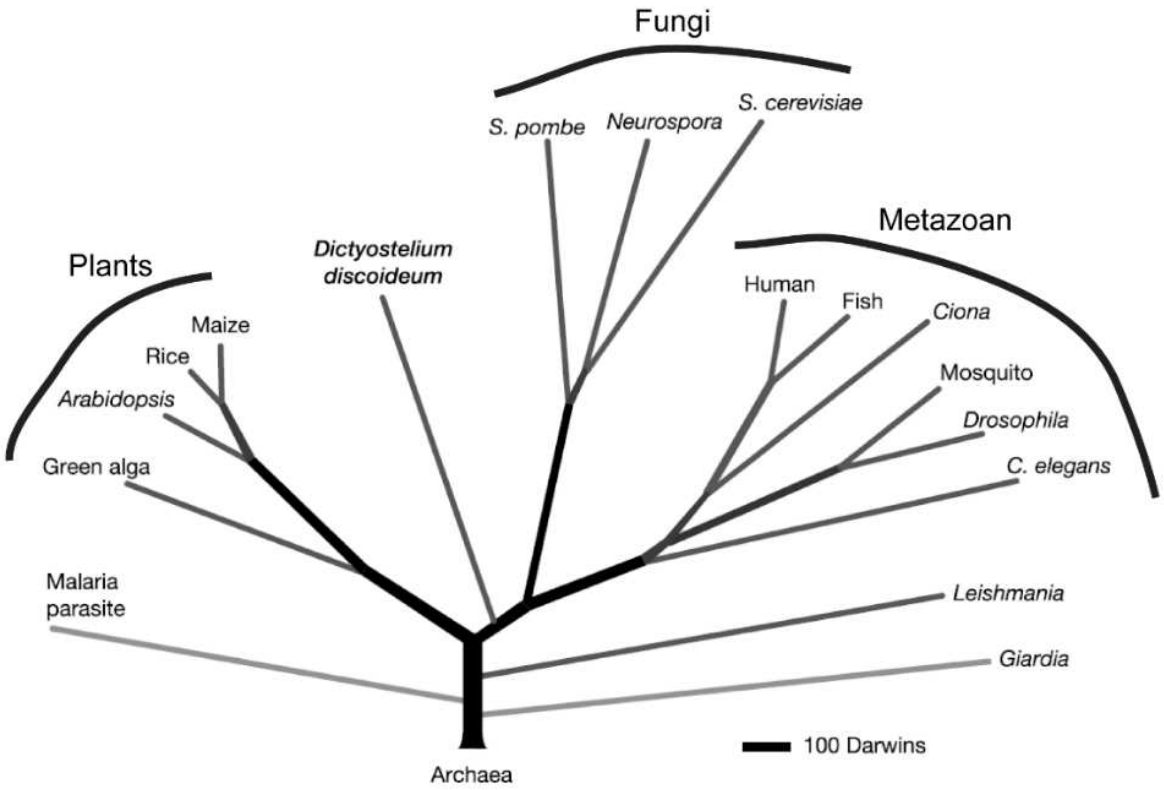

Fig. 6. The phylogenetic tree of *D. discoideum*. Evolutionarily, *D. discoideum* is between fungi and plants. 1 Darwin is defined as 1/2,000 of the divergence between *S. cerevisiae* and humans. The alignment is based on proteomics sequences. Figure was modified from Eichinger et al., (2005).

As a model organism, *D. discoideum* holds some technical advantages. The genetics of *D. discoideum* are highly amenable to manipulation. Well-established protocols exist for extrachromosomal expression, reporter fusion-tagging, mutagenesis through Restriction Enzyme Mediated Integration (REMI), as well as the generation of knock-ins and knock-outs using both homologous recombination and Crispr-Cas9 techniques (Kuspa and Loomis, 1992; Muramoto et al., 2019; Paschke et al., 2018; Veltman et al., 2009; Yamashita et al., 2021). As a consequence, this model organism has been extensively used to investigate phagocytosis, vesicular trafficking, multicellularity, chemotaxis, motility, cell-to-cell signaling and host-pathogen interactions (Barry and Bretscher, 2010; Cardenal-Muñoz et al., 2017; Glöckner et al., 2016; Loomis, 2014; Maniak, 2003; Nichols et al., 2015; Tosetti et al., 2014; Vines and King, 2019). Strikingly, *D. discoideum* has been also used as model system to study the biology of lipids.

D. discoideum **as a powerful tool to study lipid synthesis and dynamics**

D. discoideum produces ether lipids

In mammalian cells, the acyl chains of most glycerolipid species are joined with ester links at the *sn-1* and *sn-2* positions. However, in around 20% of the cases, the ester link at the *sn-1* position is swapped by an ether link (Fig. 7A) (Braverman and Moser, 2012). Such glycerolipids are called ether lipids. Plasmalogens, a subset of ether lipids, is equipped with a *cis* double bond adjacent to the ether bond (Fig. 7A) (Snyder, 1999). Ether lipids appear to be absent in plants and fungi (Braverman and Moser, 2012; Goldfine, 2010). Importantly, ether lipids have been suggested to be physiologically significant since the genetic loss of ether lipid synthetizing genes leads to a severe disease phenotypes in mice (da Silva et al., 2014; da Silva et al., 2012; Dean and Lodhi, 2018). The precursor of ether lipids (ether-lyso-phosphatidic acid, or ether-LPA) is synthesised in the peroxisome. Then, ether-LPAs are transported to the ER, where they are metabolised into ether glycerolipids (neutral or phospholipids).

One role of ether lipids is to act as the lipid backbone for glycosylphosphatidylinositol (GPI) anchored proteins (GPI-AP) (Jiménez-Rojo and Riezman, 2019). GPIs are glycolipids that serve as anchors for many covalently attached membrane proteins. Within eukaryotes, there are some variations within the lipid base of GPI-APs: For instance, in yeast, the GPI-AP has an IPC moiety, whereas in mammalian cells it is mostly ether lipid based (Dean and Lodhi, 2018; Jiménez-Rojo and Riezman, 2019). Remarkably, the majority of free PI within mammalian cells is diacyl, while the predominant form in GPI is alkyl-acyl (Kinoshita and Fujita, 2016). The biosynthetic pathway is detailed in Figure 7B.

D. discoideum has been shown to produce ether lipids. Du *et al*. (2014) reported that *D. discoideum* produces monoalkyl-diacyl-glycerols (MDGs). The production of MDGs is (i) dependent on the TAG synthetizing enzyme *Dd*Dgat1, (ii) increased upon palmitic acid treatment, and (iii) observably less than that of TAGs (Du et al., 2014). Subsequently, the peroxisomal enzyme Fatty-acyl Reductase Acyl Transferase (FARAT), encoded by the *fatA* gene, was found to mediate the synthesis of MDGs. MDGs were nearly abolished when *fatA* was knocked-out (Kappelt et al., 2020). Conversely, *D. discoideum* phosphoinositides are overwhelmingly (~95 mol %) ether-linked (alkyl-acyl). The major PI species, PI (O-34:1), is phosphorylated into PIP, PIP_2 and PIP_3 (Clark et al., 2014). Thus, it appears that a significant portion of the *D. discoideum* lipidome is composed of ether lipids.

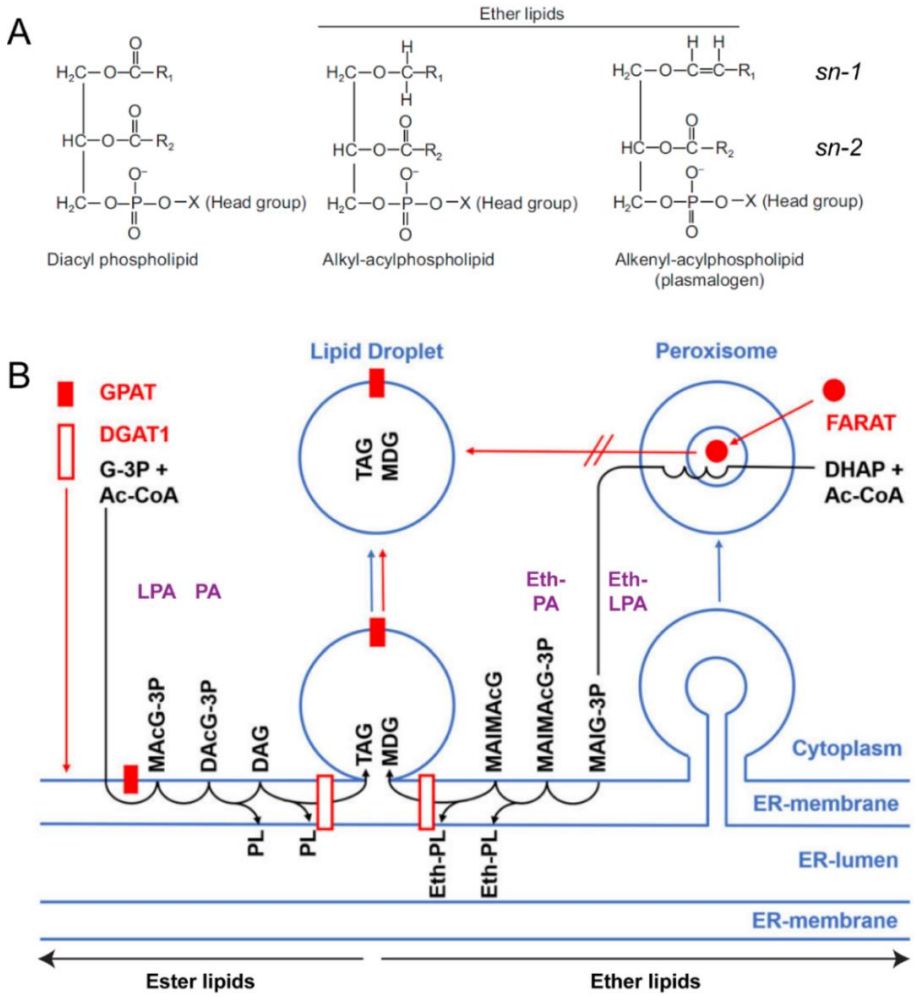

Fig. 7. Ether lipid structure and its biosynthesis in *D. discoideum*. **A:** The structure of ester and ether lipids. Ether lipids with an alkenyl chain (with a cis double bond adjacent to the ether bond) are termed plasmalogens. Figure adapted from Dean and Lodhi (2018). **B:** Model explaining *D. discoideum* ester and ether lipid synthesis. Ester lipid synthesis (left side) starts with the conversion of glycerol-3-phosphate (G-3P) and Acetyl-CoA (Ac-CoA) into monoacylglycerol-3-phosphate (MAcG-3P or LysoPA) by *Dd*GPAT. Subsequently, the second acyl chain is added, forming DAcG-3P or phosphatidic acid (PA). PA is subsequently converted into glycerophospholipids (PL) or DAG. Finally, DAG is converted into TAG before being channelled into LDs. DAG might also undergo conversion into phospholipids via the Kennedy Pathway. The synthesis of ether lipid (right side) is largely similar. FARAT performs the sequential reactions that convert dihydroxyacetone-phosphate (DHAP) and Ac-CoA into monoalkylglycerol-3-phosphate (MAlG-3P) or ether-LPA. After the transfer of ether-LPA into the ER, the reaction follows the same itinerary as for ester lipids. However, due to ether-LPA being used as precursor, ether-PLs and MDG are synthesised as end products. The reaction that catalyses the synthesis of both TAG and MDG is mediated by *Dd*Dgat1. Under normal culture condition, *Dd*GPAT is localised at the ER, but when palmitic acid is added (200 µM, 3 hours), the enzyme translocates to LDs. Figure adapted from Kapelt *et al*., (2020).

D. discoideum produces Lyso-bis-phosphatidic acid (LBPA)

LBPA appears in mammalian cells and other metazoan, but seems to be absent in single celled eukaryotes and fungi (Gruenberg, 2020). Strikingly, unlike other lower eukaryotes, *D. discoideum* also produces LBPA (Nolta et al., 1994). LBPA or bis-monoacylglycero-phosphate (BMP) is a peculiar lipid since its localisation seems to be almost exclusively in endosomes or intraluminal vesicles. In terms of structure, LBPA resembles two LPA molecules connected by a phosphate

molecule (Fig. 8) (Gruenberg, 2020). It can be acylated either at the *sn-2* or *sn-3* position, and due to its unique structure, it is resistant to phospholipase degradation (Fig. 8) (Matsuzawa and Hostetler, 1979). Physiologically, the lipid is of interest because elevated level of LBPAs are found in Niemann-pick C (NPC) and other lysosomal storage diseases (Rouser et al., 1968; Walkley and Vanier, 2009). To date, the biosynthetic pathway of LBPA and its role in phagocytosis remains to be elucidated.

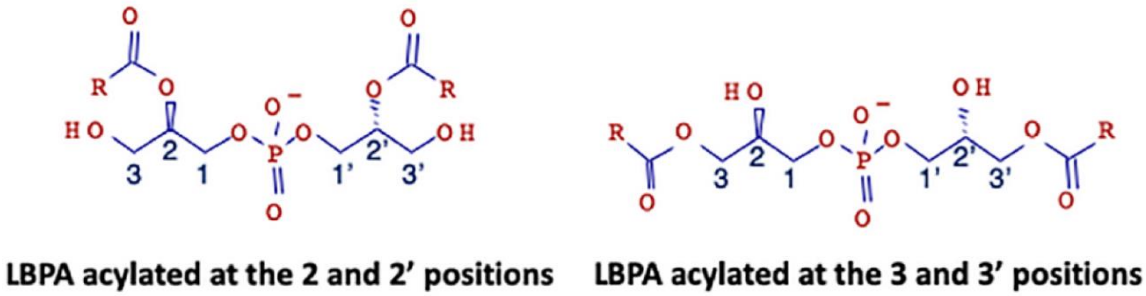

Fig. 8. The structure of LBPA and isoforms. Figure adapted from Gruenberg (2020).

Phagocytosis in *D. discoideum*

Phagocytosis is defined as the uptake of particles > 0.25 µm in diameter into a newly-generated vacuole, or phagosome, aimed at digesting microbes or killing invading pathogens. As the phagosome matures, it undergoes proteomic changes. *D. discoideum* phagocytosis is divided into four phases (Fig. 9) (Maniak, 2003):

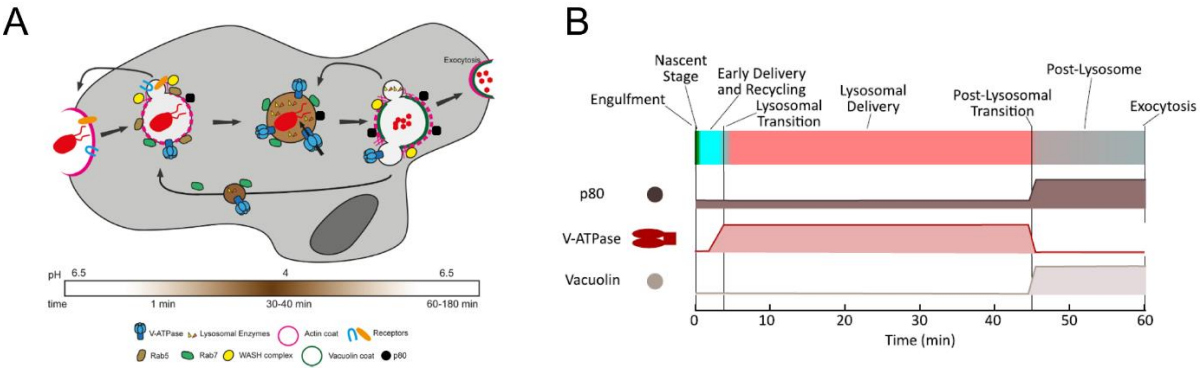

Fig. 9. Phagocytosis in *D. discoideum*. **A:** Maturation of phagosomes in *D. discoideum*. *Dd*V-ATPase is recruited to the phagosome during the acidic-digestion (lysosomal) phase, decreasing the vacuolar pH. *Dd*V-ATPase is recycled at the end of the lysosomal phase. *Dd*p80 is ever present throughout the phagocytic cycle, however, it is enriched during the post-lysosomal phase. Conversely, *Dd*Vacuolins are recruited exclusively during the post-lysosomal phase. Figure adapted from Dunn *et al*., (2018). **B:** Scheme explaining the timing of *Dd*p80, *Dd*V-ATPase and *Dd*Vacuolin recruitment to the phagosome. Figure adapted from Vines and King (2019).

1. Initialization: A "phagocytic cup" is formed and the particle is engulfed.
2. Lyosomal phase: The lumen of the phagosome is acidified by fusion with vesicles carrying a proton pump (*Dd*V-ATPase) (Clarke et al., 2010). Afterwards, proteolytic enzymes and other hydrolases are transported to the phagosome by vesicular fusion.

3. Post-lysosomal phase: The phagosome reneutralizes and *Dd*V-ATPase is removed. The copper transporter *Dd*p80, is enriched during post-lysosomes (Ravanel et al., 2001). *Dd*Vacuolin (mammalian Flotilin homolog) is localised at the phagosome (Bosmani et al., 2020).
4. Exocytosis: Indigestible remnants are released from the cell.

The CV, an osmoregulatory organelle in *D. discoideum*

In *D. discoideum* and other protozoa, the CV is a dedicated organelle for the expulsion of water and toxic ions (Fig. 10) (Gabriel et al., 1999). This organelle is required to regulate osmotic pressure. The lysosome-resident *Dd*V-ATPase also localises to that organelle, pumping H^+ and $HCO3^+$ into the CV lumen (Fig. 10). This creates an osmotic gradient, leading to water flowing into the compartment (Heuser et al., 1993). The organelle swells and eventually discharge its contents through the plasma membrane via a “kiss and run” process. During the discharges, the CV and plasma membrane shortly fuse, forming a small pore where the water is expelled. After water is discharged, the CV bladder deflates, fragments, and reintegrates into the CV network. In brief, the CV discharge cycle in *D. discoideum* is regulated by *Dd*Rab8a and *Dd*Rab11a (Du et al., 2008; Essid et al., 2012). The CV is distinct from the endolysosomal system, even though some resident proteins is shared (Gabriel *et al.*, 1999).

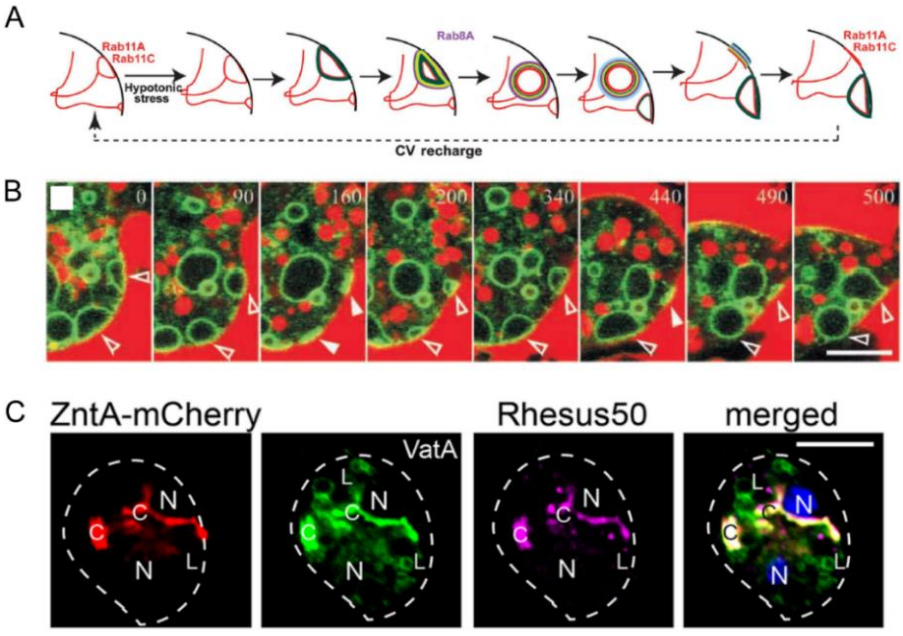

Fig. 10. The CV is an organelle dedicated to water and ion discharge. **A:** Hypotonic stress is proposed to activate the CV discharge cycle in which *Dd*Rab11A, *Dd*Rab11C and *Dd*Rab8a play the regulatory role. Figure modified from Du et al., (2008). **B:** Cells expressing Dajumin-GFP (CV marker) are incubated with the fluid-phase marker TRITC-dextran. Open and filled arrowheads show a filled and discharged CV, respectively. Scale bars: 10 µm. Figure from Gabriel et al., (1999). **C:** *Dd*VatA (a subunit of *Dd*V-ATPase) co-localises with the zinc transporter *Dd*ZntA and the CV marker Rhesus 50. ZntA-mCherry-expressing cells were fixed and stained with an anti-Rhesus50 antibody. Scale bars: 5 µm. Figure from Barisch et al., (2018).

The *D. discoideum* - *Mycobacterium marinum* model system to investigate the pathogenesis of mycobacteria

The cell-autonomous defense system (e.g. the phagocytic and authophagy pathways) is conserved in *D. discoideum* (Gaudet et al., 2016). It is hypothesised that the intracellular killing capacity of metazoan macrophages was inherited from their amoeboid ancestors. Because bacteria and their amoeboid predators share the same habitat, some intracellular pathogens have evolved the ability to withstand intracellular killing and even exploit the host for nutrition. In response, the amoeba have evolved sophisticated strategies to eliminate bacteria, suggesting an ongoing arms race throughout evolution (Boulais et al., 2010; Dunn et al., 2017). Consequently, *D. discoideum* is a suitable macrophage surrogate to investigate host-pathogen interactions (Cardenal-Muñoz *et al.*, 2017; Hilbi et al., 2007; Loomis, 2014). As a result, research using *D. discoideum* as a host has contributed towards a better understanding of the pathogenesis of mycobacteria, *Legionella pneumophilla*, *Vibrio cholera* and *Pseudomonas aeruginosa* (Barisch and Soldati, 2017; Personnic et al., 2019; Pukatzki et al., 2002; Pukatzki et al., 2006).

Tuberculosis, caused by *Mycobacterium tuberculosis*, is a worldwide leading cause of death. Due to *M. tuberculosis* being highly contagious, research using this bacteria is not always feasible. The less pathogenic cousin of *M. tuberculosis*, *M. marinum*, is a valid substitute for *M. tuberculosis* mainly because the molecular pathways related to physiology and virulence, including the type-VII secretion system ESX-1, are conserved in both species (Gröschel et al., 2016; Tønjum et al., 1998). In addition to its conservation with *M. tuberculosis*, the use of *M. marinum* holds some advantages: It grows faster than *M. tuberculosis* (6–8 h vs. 20–24 h) and requires a laboratory with a biosafety level of 2 instead of 3 (Cardenal-Muñoz *et al.*, 2017).

Virulent *M. marinum* strain renders *D. discoideum* endosome permissive for bacterial growth (Solomon et al., 2003). This allows the use of the *D. discoideum* – *M. marinum* system to investigate for example the role of lipids in the pathogenesis of mycobacteria. Using this system, it has been shown that the host Lipid Droplets (LDs) translocate into the Mycobacteria-Containing Vacuole (MCV) lumen during infection (Fig. 11) (Barisch et al., 2015). Subsequently, *M. marinum* imports and metabolises host phospholipids and fatty acids (Fig. 11) (Barisch and Soldati, 2017; Foulon et al., 2022). Moreover, since *M. marinum* induces membrane damage at the MCV, this system has been used to study membrane damage and repair (Cardenal-Muñoz *et al.*, 2017; López-Jiménez et al., 2018; Anand et al., 2023).

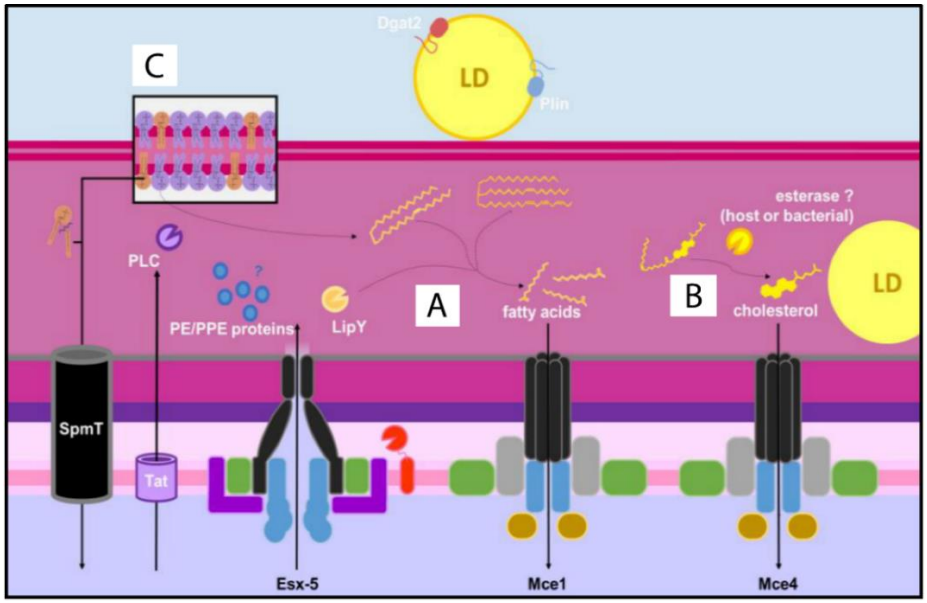

Fig. 11. Access to host-derived lipids by *M. marinum* during the early (intra-vacuolar) stages of infection. Host lipids contained in the MCV or in the cytosol are incorporated into mycobacteria via different pathways: fatty acids derived from Triacyl Glycerols (TAGs) or DAGs (possibly hydrolyzed by *Mm*LipY) or extracted from host membranes are imported through *Mm*Mce1 (A). Subsequently, sterols, possibly also derived from sterol esters, are imported through *Mm*Mce4 (B) and glycerophospholipids (from the MCV or the LD membrane) and sphingolipids might be hydrolyzed by a phospholipase (such as PLC) and the C-terminal domain sphingomyelinase of SpmT, respectively (C). Figure adapted from Foulon et al., (2022).

SCOPE

Lipidomics studies on mammalian and yeast cells have yielded many insights on how membrane lipid composition affects cell function. *D. discoideum* is a tractable model organism that has been extensively used in cell biology research since this amoeba has interesting characteristics such as motility, multicellularity, phagocytic properties, and a great deal of conservation with mammalian cells. In addition, the *D. discoideum* – *M. marinum* model system has been used to investigate the pathogenesis of mycobacteria. For example, it was shown that LDs translocate into the MCV lumen and that *M. marinum* imports host fatty-acids and glycerophospholipids for its own metabolism (Barisch *et al.*, 2015; Barisch and Soldati, 2017). Even ether lipid synthesis has been thoroughly described in *D. discoideum* (Clark *et al.*, 2014; Kappelt *et al.*, 2020), its lipidome and sphingolipidome has been poorly characterised. Consequently, this thesis will pave the way for investigating the role of lipids, especially sphingolipids, in phagocytosis and the pathogenesis of mycobacteria using *D. discoideum* as a model organism. In my paper (Listian et al., 2023), I confirm that *D. discoideum* produces IPC and characterised the enzyme responsible for IPC synthesis. This dissertation is intended to be an extension of the publication. The presentation of experimental results in this thesis is formatted to meet the following key objectives:

1. Reconstruction of the sphingolipid pathway in *D. discoideum.*
2. Characterization of the *D. discoideum* lipidome and sphingolipidome.
3. Development of strategies to hunt for CSS candidates in *D. discoideum* and to investigate their sequence and structure topology as well as their conservation with other CSS.
4. Characterization of *D. discoideum* CSS activity.
5. Determination of *D. discoideum Dd*CSS2/*Dd*IPCS1 localisation.

MATERIAL AND METHODS

Buffer, reagents and standards

Soeresen's Buffer (SB) pH 6.0

2 mM Na2HPO4, 15 mM KH2PO4

Mobile phase A

water/acetonitrile (60:40, volume), 10 mM ammonium formate, 0.1 % formic acid

Mobile phase B

2-propanol/acetonitrile/H2O (88:10:2, volume), 2 mM ammonium formate, 0.02% formic acid

Internal standard mix

Into a MS grade glass vial, 30 μL of 2.5 mM Cer (d18:1_17:0) were pipetted and the volume were set to 3 mL with chloroform/methanol (2:1, volume). When applicable, 120 μL of 2.5 mM Cer (d18:1_6:0), 30 μL of 2.5 mM Cer (d18:1_12:0) and 30 μL of 2.5 mM Cer (d18:1_14:0) were also added to the mix. The standard mix were vortexed vigorously prior use. The internal standards were omitted when calculating Cer composition.

External standard

LightSPLASH™ LIPIDOMIX® Quantitative Mass Spec Primary Standard (330732) serially diluted with with 50:50 mix of mobile phase A and mobile phase B.

Proteinase inhibitor cocktail (PIC)

1 μg/ml aprotinin, 1 μg/ml leupeptin, 1 μg/ml pepstatin, 5 μg/ml antipain, 157 μg/ml benzamidine

2X PNS reaction buffer

100 mM Tris pH 7.4, 20 mM MgCl2, 0.4 % Triton X-100, 2X PIC

PFA/picric acid pH 6.0

4% Paraformaldehyde (PFA), 10 mM PIPES and 15 % picric acid

H40 buffer pH 7.0 (for transformation of *D. discoideum*)

1 mM MgCl2, 40 mM HEPES

Laemmli buffer 2X pH 6.8

0.125 mM Tris base, 0.14 mM SDS, 20 % glycerol, 10 % β-mercapto-ethanol, 2 mg/ml bromphenol blue

5x SDS sample Buffer for SDS-PAGE pH 6.8

10% SDS, 50% Glycerol, 0.025% Bromophenol blue, 0.3 M Tris/HCl and 10% ß-mercaptoethanol

Reducing Urea/SDS sample buffer 2X (pH 6.8) for SDS-PAGE

40 mM Tris-HCl, 1 mM EDTA, 9 M Urea, 5 % SDS, 0.01 % bromophenolblue, 5 % betamercaptoethanol

TGM – Transfer buffer

250 mM Tris base, 2M glycine, 20 % methanol

SDS-PAGE buffer

250 mM Tris base, 2 M glycine, 1 % SDS

SDS-PAGE

Buffer	*Running gel (ml)*	*Stacking gel (ml)*
Tris/HCl pH 8.8	1.89	-
Acryl/Bisacrylamide	9.06	1.26
10 % SDS	0.45	0.17
Tris/HCl pH 6.8	-	1.05
APS	0.23	0.08
TEMED	0.009	0.008
H_2O	11.01	5.83
Total volume	22.6	8.40

***D. discoideum* plasmids, strains and cell culture**

All the *D. discoideum* material used in this study is listed in page 84. Wild type cells (AX2) were grown under static condition in a 10-cm dish at in 10 ml of HL5c medium (Formedium) supplemented with PS (100 U/ml penicillin and 100 mg/ml streptomycin). To create CSS2-overexpressing cells, *css2* (DDB_G0268928) was amplified from *D. discoideum* cDNA (FastGene Scriptase Basic Kit, Nippon Genetics) and cloned into N- and C-terminal mCherry-fusion plasmids pDM1208 and pDM1210, respectively. The primers for cloning into pDM1208 were oMIB154 (5'-AGATCTATGGGAGTACAACAACAATCGG-3') and oMIB155 (5'-ACTAGTCTATTTAT TATTAAATTTTGATAAAATATTTTG-3'), while the primers for pDM1210 cloning were oMIB156 (5'-AGATCTAAAATGGGAGTACAACAACAATCGG-3') and oMIB157 (5' ACTAGTTTTATTATTA AATTTTGATAAAATATTTTG-3'). To generate the ZntD-GFP construct, ZntD was cleaved with SpeI and BglII from pDM1044-ZntD-mCherry (Barisch *et al.*, 2018) and cloned into pDM1045. To generate D4H-GFP construct, D4H fragment was amplified from pMCB_1058 (Sokoya *et al.*, 2022) using oMIB99 (5'-CCA GAT CTG CCA AGG GAA AAA TAA ACT TAG A-3') and oMIB100 (5'-CCA CTA GTG AAT TCT TAA TTG TAA GTA ATA CTA G-3'). The PCR product was cloned into pDM 1043. All plasmids used in this study are listed in page 84. Plasmids were electroporated into *D. discoideum* and selected with the appropriate antibiotic. Hygromycin was used at a concentration of 50 μg/ml, and neomycin (G418) at a concentration of 5 μg/ml.

Lipidomics

Sample preparation

Confluent cells grown on tissue culture dish were washed with 10 mL of ice cold SB. After being spun (5 min, 4°C, 500 xg), the cells were re-washed with 1 mL of ice cold SB. After another round of centrifugation (5 min, 4°C, 4000 rpm), the cells were re-suspended with 150 μL of SB. Separate aliquots of cell suspension were prepared for protein determination. The cells were snap-frozen with liquid nitrogen and stored in -80°C.

Folch's lipid extraction (Eising et al., 2019; Folch *et al.*, 1957)

Into one glass vial (Ref 0193, MS grade, Chromatographie service), an equal amount of cell suspension worth 200 µg of protein is added. The volume is set to 200 µL with 150 mM ammonium formate (Sigma) dissolved in HPLC grade water. Then, 25 µL of internal standard mix and 1 mL of chloroform/methanol (2:1, v:v) were added to the vial. For each extraction round, one vial of extraction blank were prepared. The vial were then shaken in thermomixer (Eppendorf, 60 min, 22°C, 1400 rpm), before being spun (2 min, 4°C, 1000 xg). The organic lower phase were

extracted with gastight syringe (Hamilton, 58643) and moved to a new vial. Care was taken not to harvest the white protein precipitate that might clog the LC-MS instrument. The organic phase, was then evaporated in Vacuum Concentrator (Christ, 45 min, 45 °C). The dried lipid extracts were stored in -20°C for no longer than one week prior to the LC-MS run.

Sullard's lipid extraction (Fröhlich et al., 2015; Sullards et al., 2011)

Into one glass vial, an equal amount of cell suspension worth 60 µg of protein is added. The volume is set to 200 µL with 150 mM ammonium formate (Sigma) dissolved in MS grade water. Then, 25 µL of internal standard mix and 1 mL of methanol/dichloromethane (2:1, v:v) were added to the vial. For each extraction round, one vial of extraction blank were prepared. The vials were then sonicated for 1 min and incubated in thermomixer (overnight, 48°C, 1400 rpm). Subsequently, the mix were added with 150 µL 1M KOH (dissolved in a MS grade water), sonicated for 1 min and shaken at thermomixer (120 min, 37°C, 1400 rpm) to hydrolise glyceophospholipids. The mix were neutralized with 7 µL of glacial acetic acid (MS grade) and were shaken at thermomixer (10 min, 22°C, 1400 rpm). Then, the mix were spun down (5 min, 4°C, full speed), have the supernatant transferred to a new vial and dried down in Vacuum Concentrator (3 hrs, 45 °C). The dried lipid extracts were stored in -20°C for no longer than one week prior to the LC-MS run.

LC-MS preparation and run

After extraction, the dried lipids were mixed with 50:50 mix of mobile phase A and mobile phase B (65:35 for the case of Folch extraction samples) before the analysis. The mix were shaken in thermomixer (3 min, 22°C, 700 rpm), spun down to remove the contaminants (5 min, 4°C, 8600 rpm) and have the supernatant moved to a new glass vial with MS inlet. The HPLC run was done using a C30 reverse-phase column (Thermo Acclaim C30, 2.1 250 mm, 3 mm, operated at 40˚ C; Thermo Fisher Scientific) connected to a Shimadzu LC-20AD HPLC system and a QExactivePLUS orbitrap mass spectrometer (Thermo Fisher Scientific) equipped with a heated electrospray ionization (HESI) probe. All analysis were done in positive and negative ion mode. For each ion mode, 10 µL of lipid suspension were injected. The elution was performed with a gradient of 20 min. For samples extracted with Folch extraction: during 0–1 min, elution starts with 30% B and increases to 100%; in a linear gradient over 13 mins. 100% B is maintained for 3 mins. Afterwards solvent B was decreased to 30% and maintained for another 4 min for column re-equilibration. For samples extracted with Sullards extraction: during 0–1 min, elution starts with 40% B and increases to 100%; in a linear gradient over 13 mins. 100% B is maintained for 3 mins.

Afterwards solvent B was decreased to 40% and maintained for another 4 min for column re-equilibration. The flow-rate was set to 0.3 mL/min. MS spectra of lipids were acquired in full-scan/ data-dependent MS2 mode. The maximum injection time for full scans was 100 ms, with a target value of 3,000,000 at a resolution of 70,000 at m/z 200 and a mass range of 200–1200 m/z in both, positive and negative mode The 5 and 10 most intense ions from the survey scan were selected and fragmented with high-energy collision dissociation with normalized collision energy of 25, 30, 35 (samples extracted with Folch) and 25, 30 (samples extracted with Sullards), respectively. Target values for MS/MS were set at 100,000 with a maximum injection time of 50 ms at a resolution of 35,000 at m/z 200. To avoid repetitive sequencing, the dynamic exclusion of sequenced lipids was set at 10 s.

Lipid quantification (Lipid Search)

For the quantification of total lipids, ether/ester lipids and glycerophospholipids, peaks were analysed using the Lipid Search algorithm (Thermo Fisher Scientific). Product ion (MS2) and precursor ion (MS1) peaks were defined from scanning through raw files. From the intensities of external lipid standards (LightSPLASH™ LIPIDOMIX®), the absolute values for each lipid classes in mol % were calculated. SM, PC, Lyso-phosphatidyl Choline (LPC), DAG, TAG and Cer were acquired in the positive ion mode, while PE, PI, Phosphatidyl Glycerol (PG), Phosphatidyl Serine (PS) and Lyso-phosphatidyl Ethanolamine (LPE) were acquired in negative ion mode. Candidate molecular species were identified by a database search for positive (+H+; +NH4+) or negative ion adducts (-H-; +COOH-). Mass tolerance was set to 20 ppm and 5 ppm for the precursor mass from the positive ion mode and the negative ion mode, respectively. For the peak alignment between samples, the retention time (RT) tolerance were set to 0.5 and 0.21 min for the positive and negative ion mode, respectively. Samples were aligned within a time window and results were combined in a single report.

Lipid quantification (FreeStyle)

For the quantification of IPC from samples extracted by Folch extraction, the software FreeStyle™ 1.8 SP2 (Thermo Fisher Scientific) was used. The peak area of precursor ions normalized to the internal standard were calculated. To confirm that the quantified peak represents IPC, the presence of MS/MS fragments characteristic to IPC (m/z 241 representing inositol-1,2-cyclic phosphate anion and m/z 259 representing inositol monophosphate anion) in all IPC species was checked (Han, 2016).

Lipid quantification (Skyline/Lipid Creator)

For the quantification of IPC and Cers from samples extracted by Sullards's extraction, the peaks were analysed with Skyline (MacLean et al., 2010; Peng et al., 2020). The top thirteen most abundant IPC species were selected. To confirm that the quantified peak represents IPC, the presence of MS/MS fragments characteristic to IPC (m/z 241 representing inositol-1,2-cyclic phosphate anion and m/z 259 representing inositol monophosphate anion) in all IPC species was checked (Han, 2016). The peak area of precursor ions from each IPC species was normalized against the total IPC signal from each sample.

NBD-Cer lysate assay

Generation of the Post Nuclear Supernatant (PNS)

D. discoideum cells were grown in 200 ml of HL5c at 150 rpm at RT until an approximate density of $5x10^6$ c/ml. Cells were pelleted, washed twice with ice cold SB and re-suspended in SB containing 1x PIC. Subsequently, cells were lysed using the Balch homogenizer (8.008 mm ball bearing, approximately 13 cycles) and centrifuged (5 min, 4°C, 600 xg) to separate the nuclei from the PNS. The PNS was snap frozen and stored at -80°C. For further use its protein concentration was determined using the Pierce BCA kit (Thermo Fischer Scientific). The preparation of PNS of *S. cerevisiae* expressing SMS1, SMS2, and Empty Vector (EV) was performed as described previously (Kol *et al.*, 2017).

Analysis of CSS activity in lysates

Catalytic activity of CSS enzymes in *D. discoideum* and *S. cerevisiae* extracts was analysed as previously described (Vacaru et al., 2009). Briefly, 50 µl of *D. discoideum* PNS (containing 200 µg of protein) were added in addition to 50 µl ice cold 2X PNS reaction buffer and 25 µM of NBD-Cer (Avanti Polar Lipids) to a tube containing dried PI (62.5 µg/ml 1-palmitoyl-2-oleoyl PI (Sigma) or 250 µg/ml Soybean PI (Sigma)). The mixture was vortexed vigorously, incubated first for 10 min on ice and then incubated at 22°C for 2 hrs under shaking conditions. Reactions were stopped by adding 375 µl of $CHCl_3$:MeOH (1:2, v:v) and then stored at -20°C prior to lipid extraction with modified (Bligh and Dyer, 1959).

Modified Bligh and Dyer's lipid extraction (Bligh and Dyer, 1959) and TLC

The terminated assay mix was vortexed (5 min, 1000 rpm), centrifuged (10 min, 4°C, 15000 rpm) and the supernatant was mixed with 100 µl of $CHCl_3$ and 125 µl of 0.45% NaCl. After another mixing (5 min, 1000 rpm) and centrifugation round (10 min, 4°C, 15000 rpm), the lower phase

was harvested and mixed with 350 µl of MeOH:NaCl 0.45% (1:1, v:v). After a final shaking (5 min, 1000 rpm) and centrifugation cycle (10 min, 4°C, 15000 rpm), the lower phase was transferred to a fresh tube and dried in vacuum concentrator (40 min, 40 °C). Dried lipids were re-suspended with $CHCl_3$:MeOH (2:1, v:v) and the reaction products were analysed by TLC using $CHCl_3$:MeOH:25% NH_4OH (50:25:6, v:v) as running solvent. Fluorescent lipids were visualised with a Typhoon FLA 9500 biomolecular imager (GE Healthcare).

Preparation of liposomes

Liposomes were prepared as previously mentioned (Kol *et al.*, 2017). In brief, glycerophospholipid stocks were prepared in $CHCl_3$:MeOH (9:1, v:v) and stored at -20°C. Glycerophospholipid concentration was determined following (Bartlett and Lewis, 1970). Using a mini extruder (Avanti Polar Lipids), unilamellar liposomes were generated from a defined lipid mixture as stated in the figure legends: egg PC: DOPE: wheat germ PI 2:2:1 mol %, egg PC: DOPE 1:1 mol %; egg PC: wheat germ PI 1:1 mol %; and DOPE: wheat germ PI 1:1 mol %. To create a lipid film, 20 µmol of total lipids were dried with nitrogen gas. Dried lipids were re-suspended in 1 ml lipid rehydration buffer (25 mM HEPES (pH 7.5) and 100 mM NaCl) to create a 20 mM lipid suspension. After six freeze-thaw cycles, liposomes were extruded through 0.4 µM and 0.1 µM polycarbonate membrane filter (Whatman-Nucleopore) to obtain a average diameter of 100 nm. Liposome suspensions were snap-frozen and stored at -80°C.

CSS activity assay of cell-free expressed CSS

The CFE expression of CSS was conducted as previously described (Kol *et al.*, 2017). In brief, proteinase K was used to remove trace amounts from RNAse from pEU-Flexi-CSS1, pEU-Flexi-CSS2 and pEU-Flexi-SMS2 expression constructs (page 84). *Dd*CSS1 and *Dd*CSS2 were synthesized together with a V5-tag using GeneArt DNA Synthesis (Thermo Fisher Scientific) and then cloned into pEU-Flexi. After phenol/$CHCl_3$ extraction, the constructs were dissolved in water at 1.8 µg/µl. The mRNA was transcribed in a 120 µl reaction volume containing 21.6 µg of DNA; 2 mM each of ATP, GTP, CTP, and UTP; 45,6 units of SP6 RNA polymerase; 96 units of RNase inhibitor in 80 mM HEPES-KOH (pH 7.8); 20 mM of Mg-acetate; 2 mM of spermidine hydrochloride and 10 mM of DTT (Goren *et al.*, 2009). After a 4 hr incubation at 37°C and a centrifugation at 3,400 g for 5 min at RT, the supernatant was collected and subsequently used for the cell-free translation reaction. Each 100 µl translation reaction contained: 2 mM of liposomes, 40 µg/ml of creatine kinase, 15 OD_{260} of WEPRO2240 WGE, 0.3 mM each of all 20 amino acids, 5 mM of HEPES-KOH (pH 7.8), 50 mM of potassium acetate, 1.25 mM of Mg-

acetate, 0.2 mM of spermidine, 0.6 mM of ATP, 125 µM of GTP, 8 mM of creatine phosphate and 20 µl of the mRNA-containing supernatant. The translation mixture was then incubated for 4 hrs at 26 °C. The translation products were directly used for the CSS assay. Protein expression was confirmed using immunoblots and anti-V5.

For the CSS activity assay, the reaction volume was set to 100 µl: 50 µl of the CFE product were first incubated with 5 µM of NBD-Cer, 25 mM of HEPES (pH 7.4), 75 mM of NaCl and 1 mM of $MgCl_2$ for 10 min on ice. This was followed by a 60 min incubation at 22°C under shaking condition. The reaction was ended by adding 375 µL of $CHCl_3$:MeOH (1:2, v:v) and stored at -20°C prior to Bligh and Dyer's lipid extraction and TLC analysis.

Live fluorescence microscopy

To observe the subcellular distribution of CSS2-mCherry or mCherry-CSS2 by live imaging, cells were transferred to either 4- or 8-well µ-ibidi slides and imaged in low fluorescent medium (LoFlo, Foremedium, UK) with a Zeiss Cell observer spinning disc (SD) microscope using the 63x oil objective (NA 1.46). Images were processed and analysed with ImageJ.

Immunofluorescence

The anti-vatA, anti-vacA, anti-p80 and anti-Golgi antibodies were acquired from the Geneva antibody facility (Geneva, Switzerland). The anti-PDI antibody was provided from Markus Maniak (University of Kassel, Germany) and the anti-RFP antibody was purchased from Chromotek (5F8). As secondary antibodies, goat anti-rabbit, anti-mouse and anti-rat IgG coupled to Alexa546 (Thermo Fisher Scientific), CF488R (Biotium), CF568 (Biotium) or CF640R (Biotium) were used. Filipin III (Sigma) were dissolved in DMSO with a working concentration of 100 µg/mL.

To prepare cells for immunostaining, *D. discoideum* was either fixed with 4 % PFA/picric acid or with cold MeOH as described previously (Hagedorn et al., 2006). Where indicated cells were incubated overnight with 3 µm latex beads (Sigma Aldrich) before the fixation. Cells were embedded using ProlongGold antifade or ProlongGold antifade with DAPI (Molecular Probes). Images were recorded with an Olympus IX83-P2ZF confocal microscope and the 60 x PLAPON-SC 1.4 NA oil immersion objective. To improve signal-to-noise, indicated images were deconvolved using Huygens Software from Scientific Volume Imaging (Netherlands). The images were processed and analysed with ImageJ.

SDS-PAGE and Western blotting

For Western blotting of mCherry-tagged CSS2, cells were washed, harvested and incubated with 2X Laemmli buffer. For Western blotting of V5 tagged proteins, samples were added to urea buffer containing 5% ß-mercaptoethanol instead. After SDS-PAGE, proteins were transferred for 50 min at 120 V to a nitrocellulose membrane (Amersham™ Protran™, Premium 0,45 µm NC). To check the efficiency Ponceau S staining was performed. For the detection of mCherry-tagged proteins, the membranes were blocked and incubated with an anti-mCherry primary (Rockland) and a goat anti-rabbit secondary antibody coupled to horseradish peroxidase (HRP) (BioRad). For V5-tagged proteins, anti-V5 primary (Invitrogen; 1:4000) and a goat anti-mouse secondary antibody coupled to horseradish peroxidase (HRP) (BioRad, 1:4000) were used. The detection of HRP was accomplished using the Pierce™ ECL Western Blotting Substrate (Thermo Scientific).

Selection and topology prediction of *D. discoideum* CSS

The *D. discoideum* AX4 proteome was obtained from UniProt (ID: UP000002195) and searched using Prosite (https://prosite.expasy.org/) for the presence of the H-X3-D-X3-[GA]-X3-[GSTA] motif. The fasta files of all 52 protein hits were collected and submitted as queries to TMHMM 2.0 to search for the presence of TMDs (Krogh et al., 2001). Proteins with >3 TMDs were selected for further screening. Among the seven remaining candidates, proteins with known biochemical function (with annotation at dictybase.org or identification by BLAST search) were excluded yielding two potential CSS candidates.

AlphaFold and MembraneFold was used to predict the membrane topology of CSS1 and CSS2 (Gutierrez et al., 2022; Hallgren et al., 2022; Jumper et al., 2021). MAFFT version 7 algorithm (https://mafft.cbrc.jp/) was used to construct phylogenetic tree and protein sequences (Katoh et al., 2019). The following parameters was adopted for MAFFT alignment: G-INS-1 strategy, unalignlevel 0.0 and “try to align gappy regions away”. NJ conserved sites and the JTT substitution model was used to generate a phylogenetic tree in phylo.ilo. Numbers on the branches indicate bootstrap support for nodes from 100 bootstrap replicates.

***M. marinum* intracellular growth assay**

D. discoideum was grown to 80% confluency on 10-cm dishes. The medium was replaced with 3.5 mL of HL5C-filtered. Luciferase expressing *M. marinum* was grown in 7H9/OADC and kanamycin for > 24 hours to an approximate OD600 of 1 at 32°C. Approximately $5*10^8$ bacteria were pelleted (3500 RPM, 10 min) to generate a multiplicity of infection (MOI) of 10 and washed once with HL5C-filtered medium. Subsequently, the pellet was resuspended in 500 µl HL5C-

filtered. To reduce clumping, *M. marinum* was syringed 10 times with a blunt-gauge needle. Then, the bacteria were added to the attached host cells and centrifuged twice (each round with 3500 RPM, RT, 10 min). The plates were incubated at RT for 20 min to let *D. discoideum* phagocytise the bacteria. Extracellular bacteria were removed by 3–8 washings with HL5C-filtered. Finally, the infected cells were resuspended in HL5C-filtered with 5 µg/ml streptomycin, 5 U/ml penicillin and sphingolipid inhibitors and transferred to a white 96-well plate with a lid. In each well, sphingolipid inhibitors (Myriocin, FB1 and AbA) and vehicle controls were supplied as indicated. Between 0.5 – 2.0 x 10^5 of infected cells were plated on non-treated 96-well plates (X50 LumiNunc, Nunc) and covered with a gas permeable moisture barrier seal (4Ti). Luminescence was recorded every hour at 25 °C for around 70 hours using an Infinite 200 Pro M-plex plate reader (Tecan).

RESULTS

Reconstruction of the sphingolipid biosynthetic pathway in *D. discoideum*

Sphingolipids are ubiquitous among eukaryotes; however, the sphingolipid synthetic pathway of *D. discoideum* is not well characterised. Here, a comprehensive BLAST search using sphingolipid enzymes from *A. thaliana* (Mamode Cassim *et al.*, 2020), *S. cerevisiae* (Körner and Fröhlich, 2022) and human (Snider et al., 2019) as baits was performed (Fig. 12, Supplementary Table 1). The search revealed putative homologues of enzymes from the sphingolipid pathway in *D. discoideum* (Table 2). The first committed and rate-limiting step of the pathway is the generation of 3-KDS (ketodihydrosphingosine) by the condensation of serine and palmitoyl-CoA by SPT. In eukaryotes, SPTs are composed of a core heterodimer of two large catalytic subunits and two accessory small subunits (ssSPT). Two large catalytic subunits (SptA and SptB; Table 2) are present in *D. discoideum*, while no ssSPT homologue is detected. A recent work showed the cryo-EM structure of the Cer-bound SPOTS complex in yeast and provided evidence for the presence of a Sac1-containing SPOTS complex in *D. discoideum* (Schäfer et al., 2023). SPT generates 3-KDS, which is then converted to sphinganine (dihydropshingosine) by 3-keto-sphinganine reductase (Ksr). In *D. discoideum*, there are two identical copies of this enzyme in AX3 and AX4

Table 2. Sphingolipid enzymes in *D. discoideum*, *A. thaliana*, *S. cerevisiae* and *H. sapiens.*

Enzyme	*D. discoideum*	*A. thaliana*	*S. cerevisiae*	*H. sapiens*
serine palmitoyltransferase (large subunit)	SptA (DDB_G0268056), SptB (DDB_G0291283)	LCB1, LCB2a, LCB2b	Lcb1, Lcb2	SPTLC1, SPTLC2, SPTLC3
3-ketodihydrosphingosine reductase	KsrA-1 (DDB_G0274015), KsrA-2 (DDB_G0272883)	KSR1, KSR2	Tsc10	KDSR
sphingolipid desaturase	DesA (DDB_G0269738)	SLD1, SLD2, DES1	non-existent	DEGS1
Cer synthase	CrsA (DDB_G0282607)	LOH1, LOH2, LOH3	Lac1, Lag1, Lip1	CERS1, CERS2, CERS3, CERS4, CERS5, CERS6
sphingolipid hydroxylase	LhsA (DDB_G0269788), LhsB (DDB_G0270946), LhsC (DDB_G0279611)	SBH1, SBH2	Sur2	DES2
Cer acyl hydroxylase	LhsD (DDB_G0269908)*	FAH1, FAH2	Scs7	non-existent

Putative sphingolipid biosynthetic enzymes from *D. discoideum* identified by BLAST search analysis using sequences of *A. thaliana*, *S. cerevisiae* and *H. sapiens* as bait. The putative lipid hydroxylases are not yet annotated at dictybase (www.dictybase.org) and were named here LhsA (DDB_G0269788), LhsB (DDB_G0270946), LhsC (DDB_G0279611) and LhsD (DDB_G0269908). For more information, please see Supplementary Table 1.

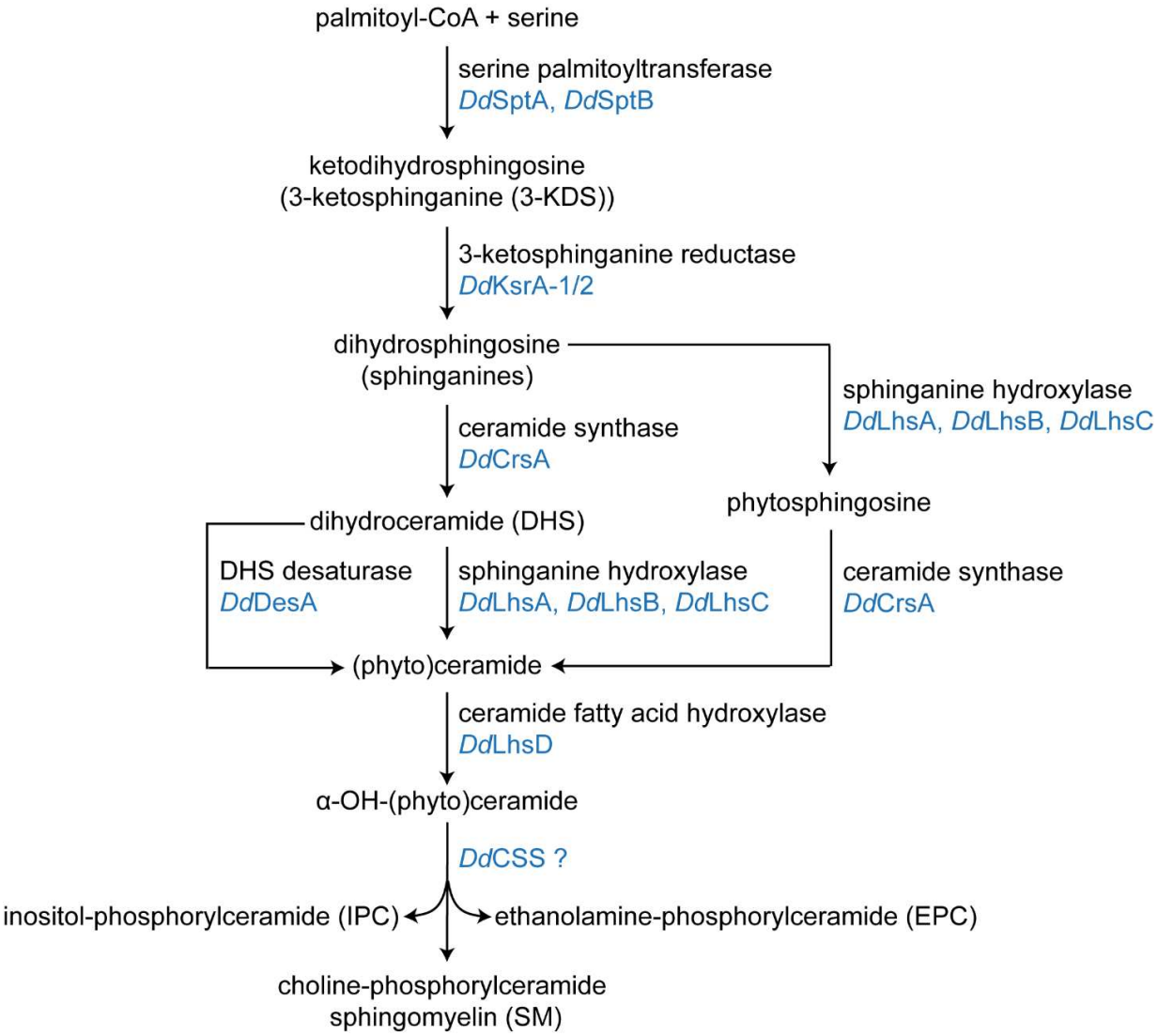

Fig. 12. The sphingolipid biosynthetic pathway in *D. discoideum*. The pathway was reconstructed based on BLAST searches for *D. discoideum* homologues (marked in blue) of key sphingolipid biosynthetic enzymes identified in *S. cerevisiae*, *A. thaliana* and *H. sapiens* (Supplementary Table 1). Note that this approach did not yield any *D. discoideum* homologues of CSS responsible for the production of IPC, EPC or SM in fungi, plants or animals.

(but not AX2), known as KsrA-1 and KsrA-2. Cer synthases (CerS) transform sphinganine into dihydroceramides by adding fatty acid moieties. Mammals, plants and yeast each contain three to six CerS isoforms that generate dihydroceramides with different acyl chain lengths (Cingolani et al., 2016; Kageyama-Yahara and Riezman, 2006; Luttgeharm et al., 2015). This is in sharp contrast to *D. discoideum,* which contains only one CerS homologue (CrsA) (Pathak et al., 2018). Generally, dihydrosphingosines and dihydroceramides are further modified by desaturases and hydroxylases. A BLAST search for *D. discoideum* homologues of the yeast sphinganine C4-hydroxylase Sur2 yielded three hits, which I refer to as lipid hydroxylase LhsA, LhsB and LhsC.

Sphingolipid desaturases are present in human (Rahmaniyan et al., 2011) and *A. thaliana* (Chen *et al.*, 2012; Michaelson et al., 2009) but absent in *S. cerevisiae* (Eisenberg and Büttner, 2014). In *D. discoideum,* I discovered one dihydroceramide desaturase homologue (DesA). The amide-linked acyl chain in sphingolipids normally undergoes hydroxylations. A search for *D. discoideum* homologues of the *S. cerevisiae* Cer fatty acid hydroxylase Scs7 and the *A. thaliana* Cer fatty acid hydroxylases FAH1 and FAH2 in each case yielded one hit, namely LhsD.

These finding suggest that *D. discoideum* are able to produce Cer with a desaturated LCB and hydroxyl groups in both the LCB and amide-linked acyl chain. Cer might be further derivatized by the addition of a headgroup at C1 to generate complex sphingolipids such as GlcCer, the precursor of complex glycosphingolipids that contain multiple sugar residues. Alternatively, the C1 of Cer might receive phospho-alcohol to generate SM, EPC or IPC. A search for *D. discoideum* homologues of GlcCer synthases in *Homo sapiens* (*Hs*CEGT), *Candida albicans* (*Ca*CEGT) or *A. thaliana* (*At*CEGT) did not yield any hits. Likewise, BLAST searches using sequences of the enzymes responsible for the production of SM (*Hs*SMS1), EPC (*Hs*SMSr) or IPC (*Sc*Aur1, *At*IPCS1) resulted in no *D. discoideum* homologues. As a result, my homology searches did not yield further insights into the nature of the complex sphingolipids produced by *D. discoideum*.

Phosphatidylethanolamine is the most abundant glycerophospholipid in *D. discoideum*

Eukaryotic organisms evolved different head group dominances regarding their glycerophospholipid and sphingolipid production. Mammals have more PC than PE or PI and predominantly synthesize phosphocholine-containing SM (Sampaio et al., 2011a). In contrast, yeast contains PI as its most abundant glycerophospholipid and produce phosphoinositol-containing sphingolipids (Ejsing *et al.*, 2009) whereas insects synthesize phosphoethanol-based glycerophospholipids and sphingolipids (Rietveld et al., 1999a; Vacaru *et al.*, 2013). Thus, the insect lipidome appears to be mainly ethanolamine-centric, in contrast to choline-centric mammals and inositol-centric yeast. To determine the head group dominance in *D. discoideum*, I performed an untargeted LC-MS/MS analysis of total lipid extracts from *D. discoideum* cultured in defined medium (SIH, Formedium). I found that PE is by far the most prevalent lipid class in *D. discoideum*, representing ~ 70 mol % of all lipids analysed, with PC and PI representing ~ 10 mol

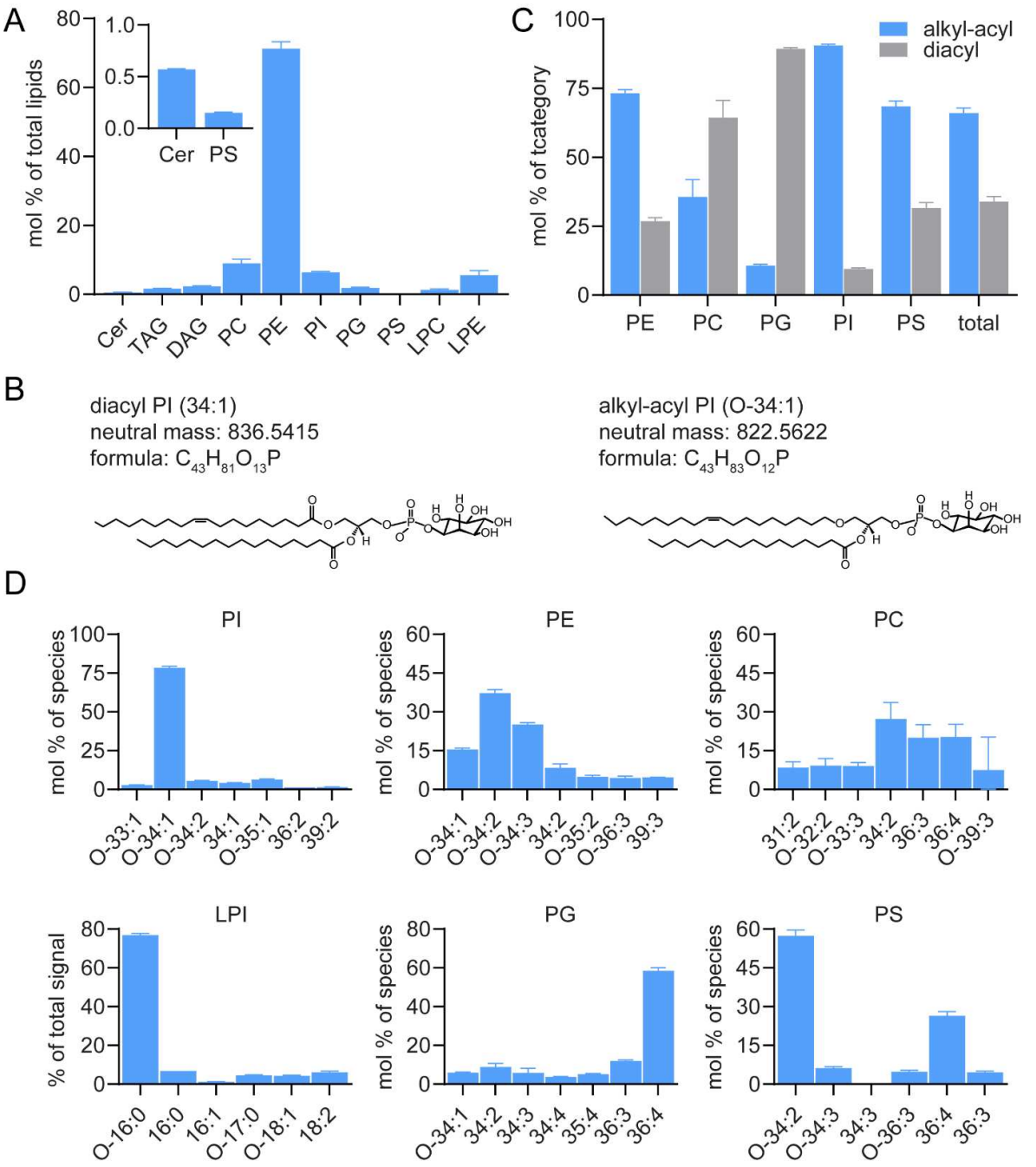

Fig. 13. Quantitative analysis of the main lipid classes in *D. discoideum*. **A:** Levels of indicated lipid classes in total lipid extracts from *D. discoideum* were determined by LC-MS/MS and expressed as mol % of total lipid analysed. Note that PE is the dominant glycerophospholipid in *D. discoideum*. Inset shows a close-up of Cer and PS levels. **B:** Molecular structures of ester (diacyl) PI (34:1) and ether (alkyl-acyl) PI (O-34:1). **C:** Quantification of the distribution of alkyl-acyl species (blue) and diacyl species (grey) within each glycerophospholipid class**. D:** Lipid molecular species composition within each glycerophospholipid class. Shown are the seven most abundant species of each category, except for PS and Lyso-phosphatidyl Inositol (LPI) where only six lipid species were detected. Lipids were quantified as mol % of total lipids analysed, except for LPI. LPI was quantified as % of total signal due to the absence of an LPI standard. *D. discoideum* was grown for six days in SIH (defined) medium prior to lipid extraction. Lipids were extracted following (Folch *et al.*, 1957). Data are means ± SD (n=3).

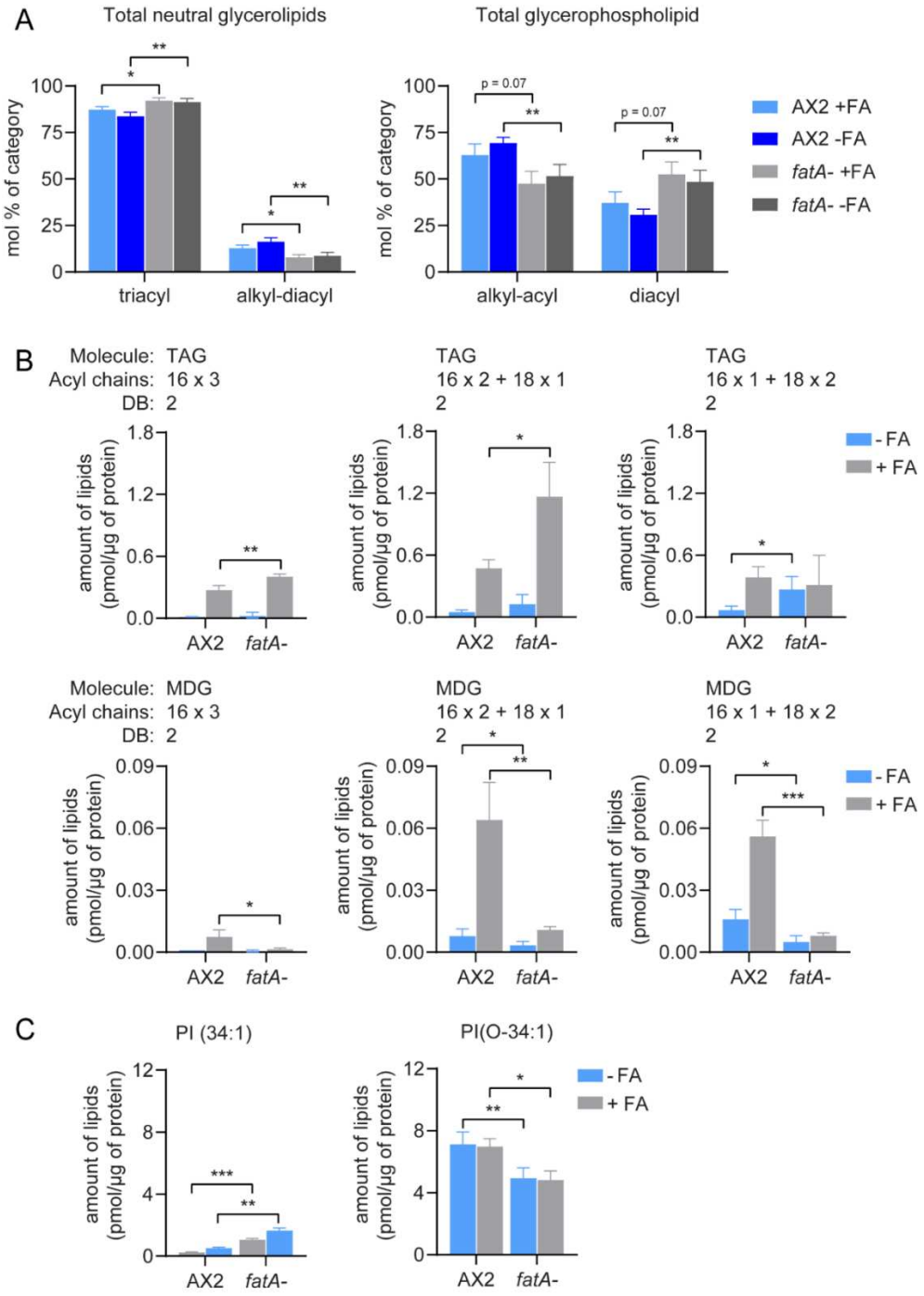

Fig. 14. *D. discoideum fatA-* produces less ether lipids and more ester lipids. **A:** The composition of alkyl ether lipids MDGs and alkyl-acyl glycerophospholipids) in *fatA-* cells is less than wild-type (AX2). The composition of ether (alkyl) and ester isoforms of neutral and glycerophospholipids were displayed in mol % of category. **B:** When fed with palmitic acid (FA), the *fatA-* cells produces more TAGs and less MDGs with C16 fatty acids per µg of protein relative to AX2. DB refers to double bonds. **C:** More ester PI (34:1) and less ether PI (O-34:1) (per µg of protein) were found in *fatA-* cells. *D. discoideum* was grown for in HL5C medium. To stimulate the formation of glycerolipids with C16 fatty acids, cells were fed with 200 µM of FA for three hours before harvesting. Methanol was used as vehicle control. Lipids were extracted following (Folch *et al.*, 1957) and quantified with Lipidsearch (A) or Skyline (B,C). Statistical differences were calculated with an paired t-test. Error bars indicate ±SD (N=4).

% and ~ 7 mol %, respectively (Fig. 13). These data are consistent with findings reported previously by others (Ellingson, 1974; Kappelt *et al.*, 2020; Weeks and Herring, 1980). Besides, diacylphospholipids (~ 88.7 mol %), *D. discoideum* contains substantial amounts of lysophospholipids (~ 6.8 mol %), notably LPE, Cer (~ 0.6 mol %), DAG (~ 2.3 mol %) and TAG (~ 1.6 mol %) (Fig. 13A).

Glycerophospholipids have either an ester or an ether bond at the *sn*-1 position. Figure 13B shows an example of the molecular structures of both an ester (diacyl PI) and an ether lipid (alkyl-acyl PI). Recently, it was described that in *D. discoideum*, the majority of inositol glycerophospolipids are ether lipids with a plasmanyl-O-34:1 structure (the "O" indicates that one of the carbon chains is ether-linked) (Clark et al., 2014). Strikingly, this also accounts for all *D. discoideum* glycerophospholipids except for PC and PG, in which diacyl bonds are more abundant (Fig. 13C). In addition, we found that the composition of PI species was highly similar to what has been reported previously (Fig. 13D) (Clark *et al.*, 2014). In the same study, Clark *et al*. demonstrated that PI (O-34:1) is comprised of an ether-linked C16:0 fatty acid at its *sn*-1 position. This is consistent with the fact that in our hands, LPI (O-16:0) is the predominant LPI species (Fig. 13D). Finally, I also noticed the presence of odd-chain glycerophospholipids and found that all of the most abundant glycerophospholipid species contain double bonds (Fig. 13D).

Recently it was shown that the ablation of FARAT (*fatA*-) leads to severe reduction of MDGs and an apparent reduction of ether gylcerophospholipids (Kappelt *et al.*, 2020). To support this claim, I performed lipidomics with *fatA*- cells, fed or not fed with palmitic acid (FA). The palmitic acid supplementation was done to induce the formation of glycerolipids with C16 fatty acids (Du *et al.*, 2014). The *fatA*- cells shows a significant compositional reduction of alkyl ether glycerolipids, both in neutral and glycerophospholipids (Fig. 14A). Consequently, in palmitic acid supplied *fatA*- cells, the amount of (ester) TAGs with C16 fatty acids (per μg of protein) were increased, while its (ether) MDG counterparts were decreased (Fig. 14B). As for glycerophospholipids, PI (34:1) and PI (O-34:1) were selected as representatives. A significant decrease of PI (O-34:1) was observed in *fatA*- cells, irrespective of palmitic acid supplementation. Conversely, PI (34:1) was increased in *fatA*- cells, especially when palmitic acid is added. Altogether, my lipidomics showed that the deletion of FARAT leads to the reduction and increase of ether and ester glycerolipids, respectively. Of note, under the present experimental condition, some alkyl ether lipids were still detected in *fatA*- cells, particularly PI (O-34:1).

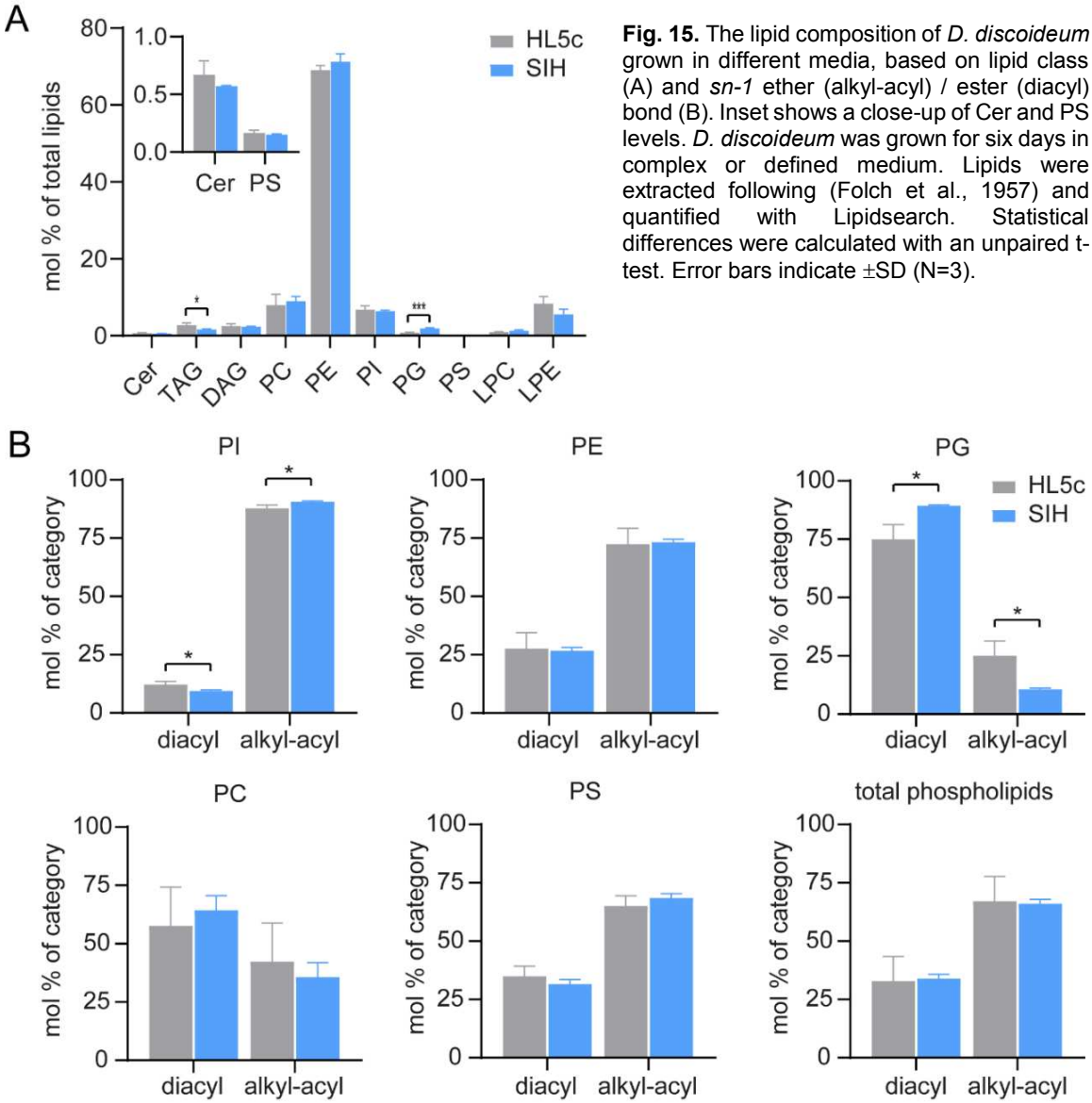

Fig. 15. The lipid composition of *D. discoideum* grown in different media, based on lipid class (A) and *sn-1* ether (alkyl-acyl) / ester (diacyl) bond (B). Inset shows a close-up of Cer and PS levels. *D. discoideum* was grown for six days in complex or defined medium. Lipids were extracted following (Folch et al., 1957) and quantified with Lipidsearch. Statistical differences were calculated with an unpaired t-test. Error bars indicate ±SD (N=3).

In response to nutritional changes, cells might adapt their lipid composition. For instance, in *S. cerevisiae*, cells changed their lipid composition when different carbon sources are supplied (Klose et al., 2012). Such variation in lipid composition may happen in multiple structural layers: (i) lipid class, (ii) *sn-1* ether/ester bond, (iii) lipid species, (iv) desaturation and others. Consequently, to test if the lipid profile of *D. discoideum* is dependent on the growth medium, I passed *D. discoideum* for six days in either SIH (defined) or HL5c (complex) medium. This showed that changing HL5c to SIH had only minor effects on the lipid composition. In cells grown in HL5c, significantly more TAGs and fewer PGs were observed (Fig. 15A). Also, changing the growth medium appeared to have little effect on the lipid composition based on *sn-1* ether-ester bond (Fig. 15B). In contrast, the species composition of *D. discoideum* in cells grown in HL5C and SIH appear different (Fig. 16).

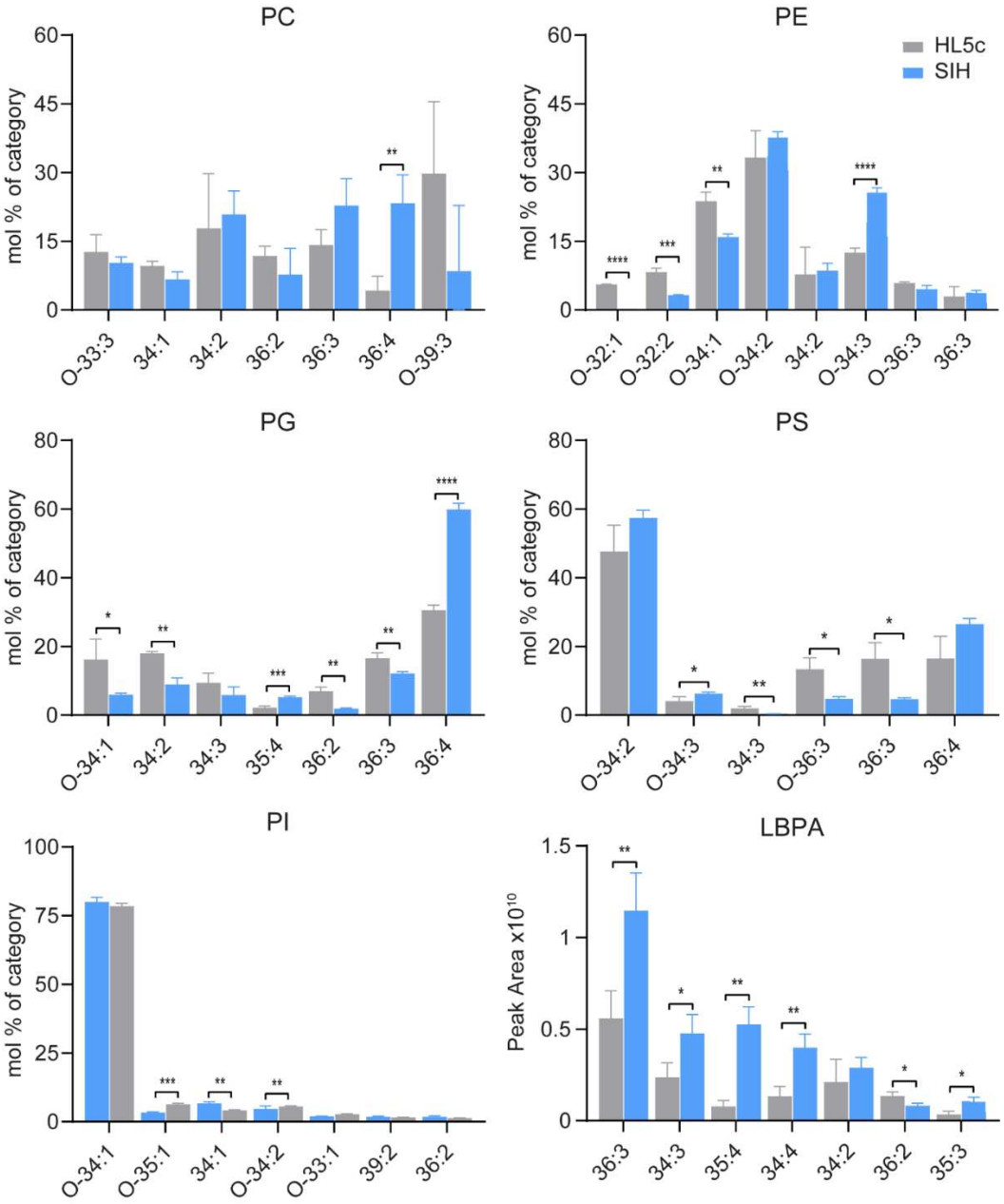

Fig. 16. Lipid species composition of *D. discoideum* glycerophospholipids under different media condition. *D. discoideum* was grown for six days in complex or defined medium. Shown are the seven prevalent glycerophospholipid species, with the exception of PS and LPI in which only six species were detected. Lipids were extracted following (Folch *et al.*, 1957) and quantified with Lipidsearch. Statistical differences were calculated with an unpaired t-test. Error bars indicate ±SD (N=3).

It is also observed that PEs and PIs from SIH grown cells have slightly but significantly more double bonds than those grown in HL5c (Fig. 17). In sum, changing the media from HL5c to SIH largely does not change the lipid composition in class level, however in species level, more apparent changes is observed.

In conclusion, our findings indicate that (i) PE is the most abundant glycerophospholipid in *D. discoideum*, (ii) the majority of *D. discoideum* glycerophospholipids are ether lipids that contain alkyl-acyl bonds, (iii) the deletion of FARAT leads to the reduction of ether glycerolipids and (iv) changing media from HL5c to SIH induced a mild alteration in lipid composition. The identity of glycerophospholipids in Figure 13D and Figure 16 was validated by checking the presence of class-specific glycerophospholipid MS2 fragments (Hsu and Turk, 2001; Pi et al., 2016).

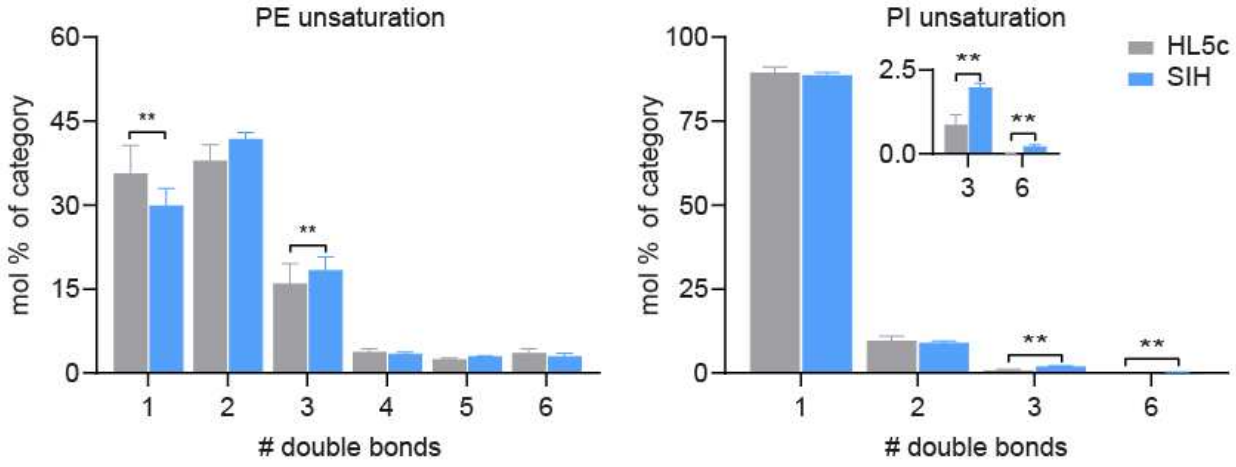

Fig. 17. Comparative analysis of lipid unsaturation in PE and PI under different media conditions. *D. discoideum* was grown for six days in complex or defined medium. Lipids were extracted following (Folch *et al.*, 1957) and quantified with Lipidsearch. Statistical differences were calculated with an unpaired t-test. Error bars indicate ±SD (N=3).

D. discoideum produces phospoinositol containing sphingolipids

The high abundance of PE implies that *D. discoideum* might use PE as headgroup donor to synthesis EPC as previously demonstrated in *Drosophila* and other insects (Carvalho et al., 2012; Vacaru *et al.*, 2013). To test this hypothesis and to characterise complex phosposphingolipids by lipidomics, I used an extraction protocol that has been adapted for the purification of sphingolipids (Sullards *et al.*, 2011). In brief, lipids are extracted with dichloromethane/methanol followed by an alkaline hydrolysis to deacylate glycerophospholipids and eliminate isobaric overlaps between sphingolipids and glycerophospholipids. The absence of PI (O-34:1) after alkaline hydrolysis reflects the efficiency of this protocol (Fig. 18). Moreover, to look for complex phosposphingolipids, I performed a targeted search using the LipidCreator workbench from Skyline, which allows user-friendly detection, curation and quantification of lipids (Peng *et al.*, 2020). Strikingly, instead of EPC, I observed that *D. discoideum* generates IPC (Fig. 19). IPC (38:0;4) was the predominant IPC species in the MS1 chromatogram (Fig. 19A-B), and its identity was supported by MS2 fragments (product ions) characteristic for IPC (inositol-1,2-cyclic phosphate anion and inositol monophosphate anion at *m/z* 241 and 259, respectively) (Fig. 19A, inset). In addition, the product ion at $[M-H-180]^-$ represents the loss of the inositol residue and

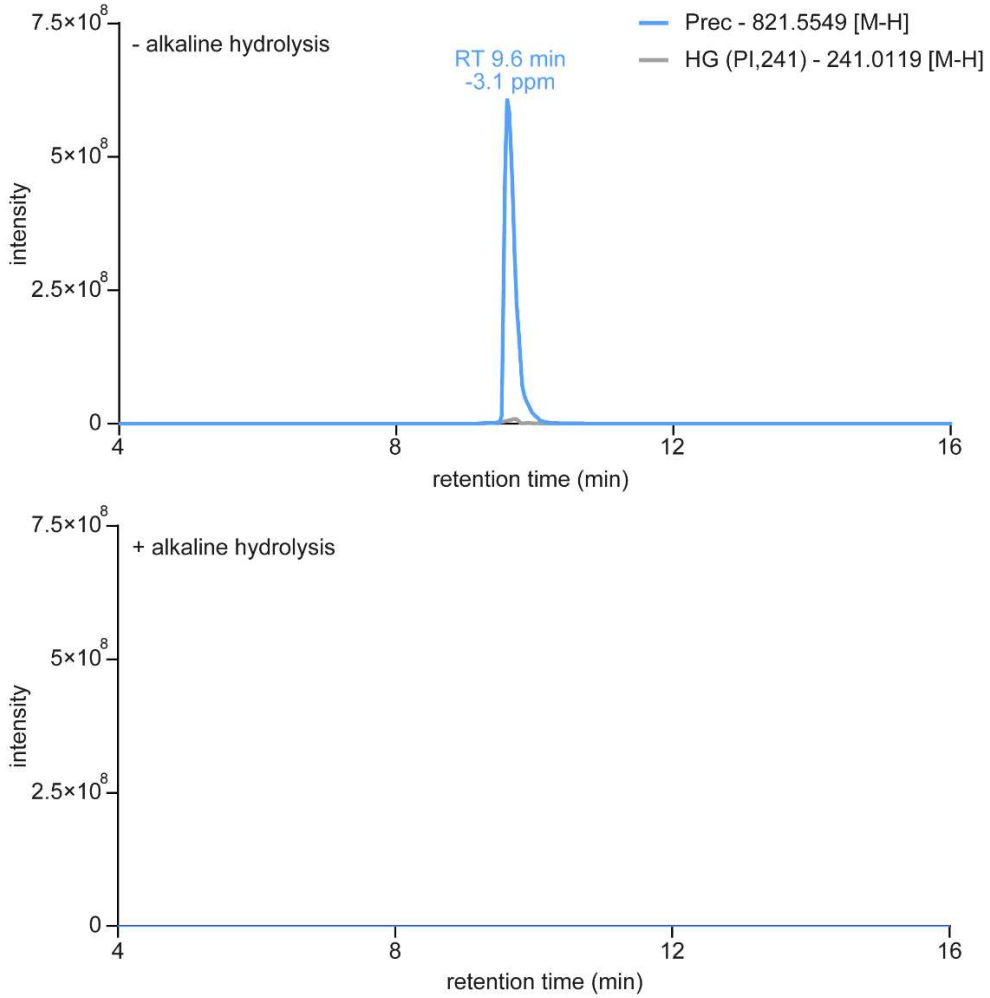

Fig. 18. Deacylation of the glycerophospholipids by alkaline hydrolysis. Intensity plots of PI (O-34:1) of samples subjected (+) or not (-) subjected to alkaline hydrolysis. *D. discoideum* was grown in HL5c (complex) medium. Lipids were extracted following (Sullards *et al.*, 2011) (+ alkaline hydrolysis) and (Folch *et al.*, 1957) (- alkaline hydrolysis).

corroborates the claim that the lipid described in Figure 19A is indeed IPC. However, with our current approach, I was unable to conclusively resolve the length of the acyl chains and the LCB from the peaks of IPC (38:0;4). To this end, I analysed the product ion fragmentation of Cer (38:0;4), which I presume to be the precursor of IPC (38:0;4) (Fig. 20). The product ions representing LCB (18:0;3) and LCB (20:0;3) were both detected in the precursor peak of Cer (38:0;4) (Fig 20). However, the intensity of LCB (18:0;3) was much higher than that of LCB (20:0;3) (Fig 20B). This strongly suggest that Cer (18:0;3/20:0;1) constitutes the major proportion of Cer (38:0;4), while Cer (20:0;3/18:0;1) account for the minority of fraction. Taken together, this suggest that the most abundant IPC species in *D. discoideum* is IPC (18:0;3/20:0;1).

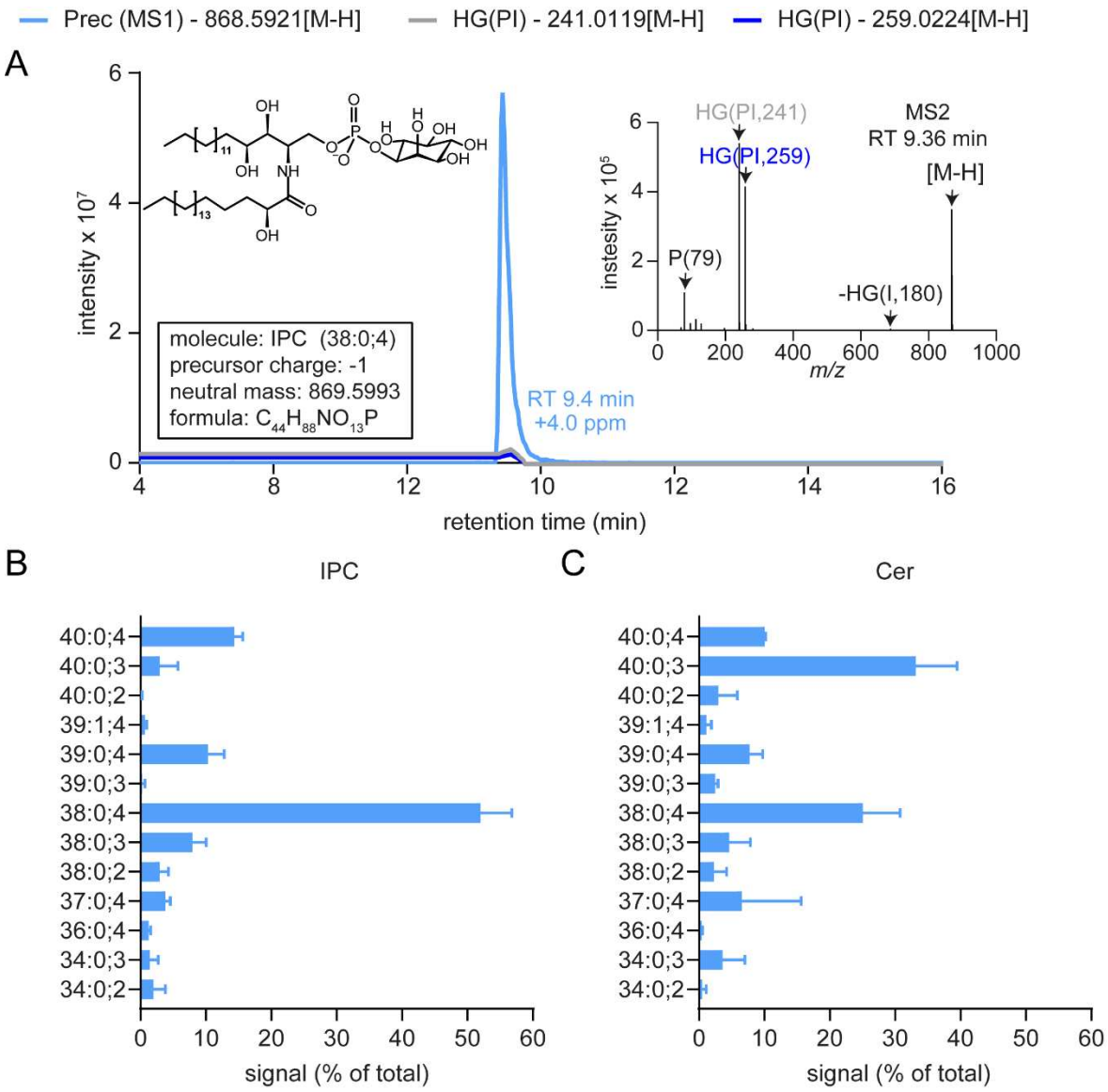

Fig. 19. Profiling of IPC and Cer species in *D. discoideum*. **A:** Detection of IPC (38:0;4) by LC-MS/MS. The inset shows the product ion fragmentation of IPC (38:0;4) at RT 9.36 min. **B:** LC-MS/MS analysis of the main IPC species in *D. discoideum.* **C:** LC-MS/MS analysis of the Cer species in *D. discoideum* that correspond to the IPC species shown in (B) with respect to chain length, hydroxylation status and saturation level. *D. discoideum* was grown in HL5c (complex) medium and then subjected to total lipid extraction according to (Sullards *et al.*, 2011). The peak area of the precursor ions ([M-H]) from each IPC and Cer species was quantified and normalized with the total peak area from all IPC/Cer species using Skyline. Data are means ±SD (n=3).

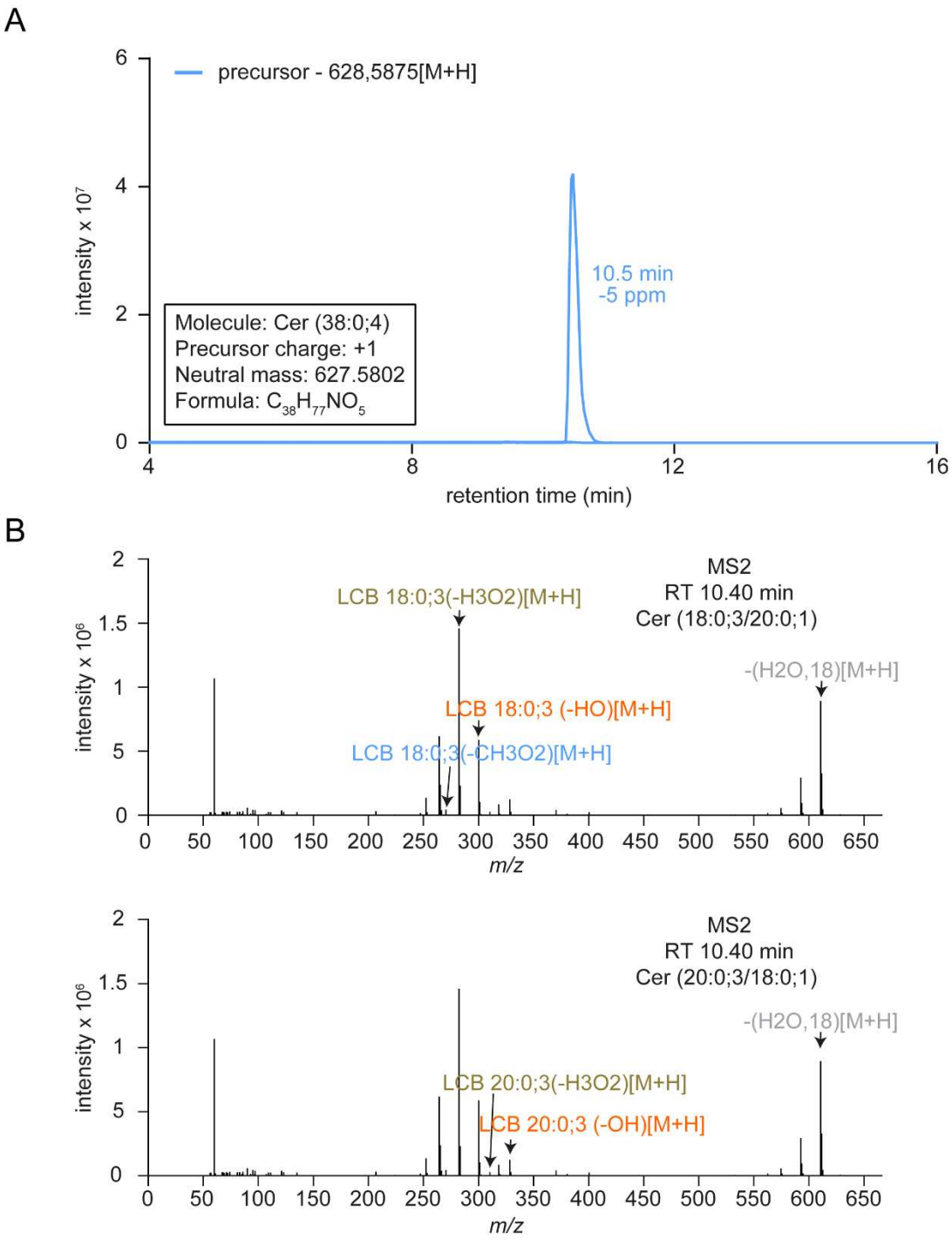

Fig. 20. Resolving the LCB chain length of Cer. **A:** Precursor chromatogram of Cer (38:0;4). **B:** Product ion fragmentation pattern of Cer (38:0;4) including annotations of Cer (18:0;3/20:0;1) (top) and Cer (20:0;3/18:0;1) (bottom) fragments. *D. discoideum* was grown in HL5c (complex) medium. Lipids were extracted following (Sullards *et al.*, 2011) with alkaline hydrolysis.

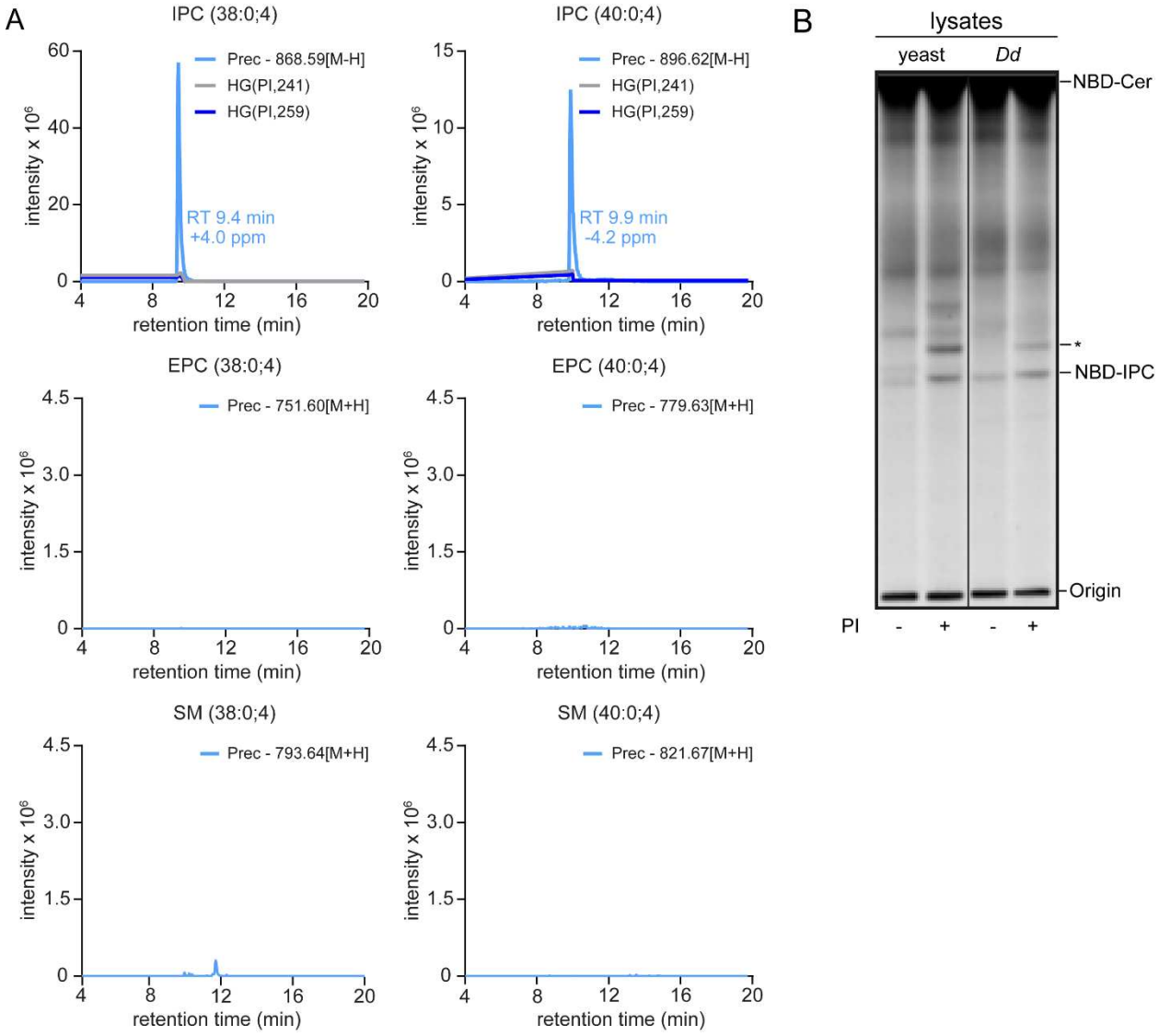

Fig. 21. *D. discoideum* exclusively produces inositol-containing phosphosphingolipids. **A:** Detection of IPC (38:0;4) and IPC (40:0;4) but not their SM or EPC counterparts by LC-MS/MS analysis in alkaline-treated lipid extracts from *D. discoideum*. *D. discoideum* was grown in HL5c (complex) medium. Lipids were extracted following (Sullards *et al.*, 2011). Data shown are representative of three independent experiments (n=3). **B:** *D. discoideum* lysates possess PI:Cer cholinephosphotransferase activity. NBD-Cer turnover assay with lysates of *D. discoideum* and yeast were treated with PI (62.5 µg/ml) as indicated. Asterisk indicates an unidentified band.

Besides IPC (38:0;4) (~ 52 % of total IPC), *D. discoideum* synthesises IPC (40:0;4) (~14.3 %), IPC (39:0;4) (~10.2 %) and IPC (38:0;3) (~7.9 %) (Fig. 19B). Inversely, the most abundant Cer species are Cer (40:0;3) (~35.9 % of total Cer species), followed by Cer (38:0;4) (~27.3 %), Cer (40:0;4) (~11.0 %) and Cer (39:0;4) (~8.5 %) (Fig. 19C). This displayed that, like in fungi and plants, *D. discoideum* contains mainly "phyto" sphingolipid species with three or more hydroxyl groups. Also, I saw a minimal presence of unsaturated IPC and Cer species, as well as odd chain IPCs and Cers. Notably, NBD-Cer fed lysate of *D. discoideum* and yeast producing the same TLC band suggest that *D. discoideum* lysate convert Cer to IPC (Fig. 21B).

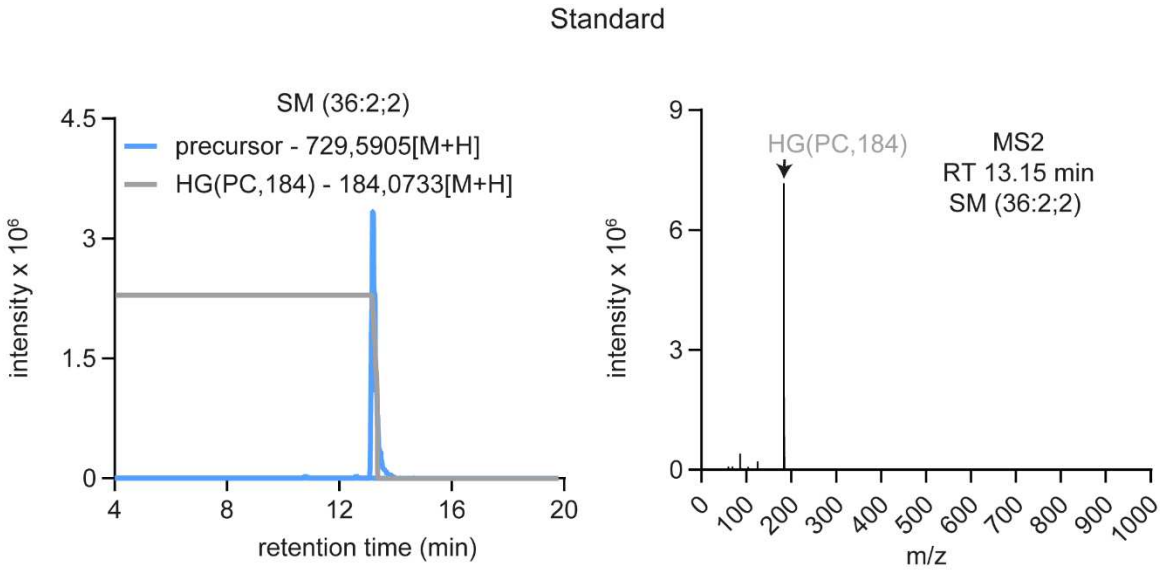

Fig. 22. Intensity plot of SM. SM (36:2;2) from a commercial standard (Avanti Polar Lipids) served as positive control for SM detection.

Given that *D. discoideum* contains more PE than PC or PI (Fig. 13A), I attempted to look for EPC and SM from the alkaline-hydrolised lipid extract (Fig. 21A). However, I did not find EPC and SM counterpart of the most abundant IPC species. As a positive control, I displayed the peak representing SM (36:2;2) from a commercial standard (Fig. 22).

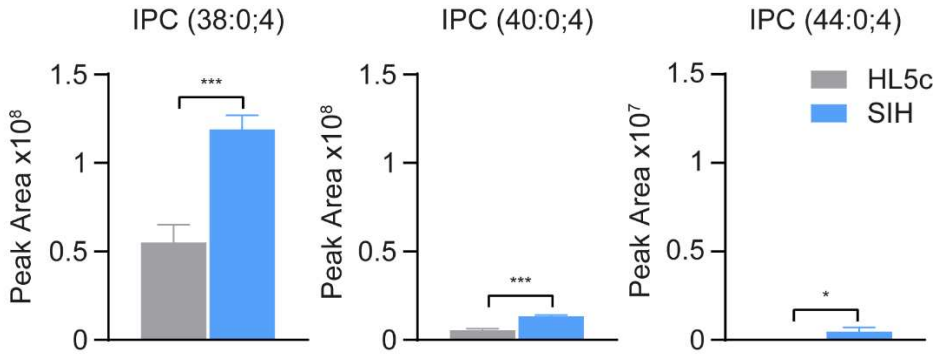

Fig. 23. IPC is not derived from the media as IPC is still detectable in cells grown in media lacking yeast extract (SIH). IPC (44:0;4), predominant in yeast, is not found in SIH samples. *D. discoideum* was passed in HL5c or SIH medium for six days. Lipids were extracted following (Folch *et al.*, 1957). The peak area of the precursor ions ([M-H]) from each IPC (B) and Cer (C) species was quantified and normalized with the total peak area from all Cer/IPC species using Skyline and Freestyle. Statistical differences were calculated with an unpaired t-test. Graphs show mean and ±SD (N=3).

To confirm that the measured IPC is not originating from the yeast extract, I passed *D. discoideum* cells in SIH media (no added yeast extract) and measured the IPC content (Fig. 23). IPC (38:0;4) and IPC (40:0;4), are still detected in SIH samples, suggesting *D. discoideum* produces IPC de-novo (Fig. 23). It is also noticeable that in SIH samples, IPCs were more abundant. The IPC

(44:0;4), predominant in yeast, is not detected in SIH samples but is detected in a trace amount in HL5c samples (Fig. 23).

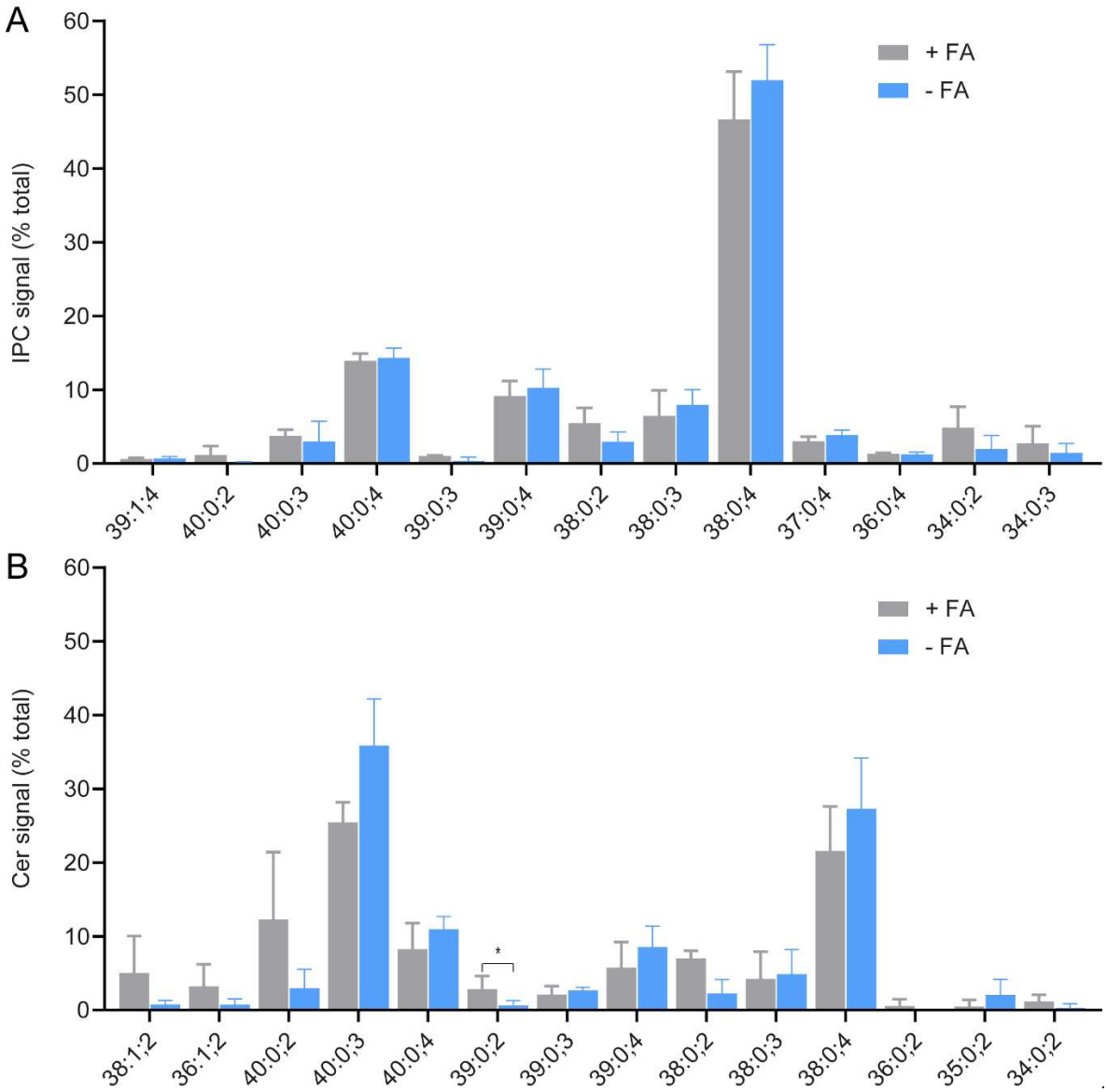

Fig. 24. Palmitic acid (FA) feeding has little effect on Cer and IPC composition. Molecular composition of IPC (A) and Cer (B) in *D. discoideum* under the presence and absence of palmitic acid treatment. Cells were fed with 200 μM of palmitic acid or vehicle for three hours before harvesting. The peak area of the precursor ions ([M-H]) from each IPC (A) and Cer (B) species was quantified and normalized with the total peak area from all Cer/IPC species using Skyline. Lipids were extracted following (Sullards *et al.*, 2011). Statistical differences were calculated with an unpaired t-test. Graphs show mean and ±SD (N=3).

As stated previously, feeding *D. discoideum* with palmitic acid induces the formation of glycerolipids with C16 fatty acids (Fig. 14) (Du *et al.*, 2014). I asked if the palmitic acid fed to *D. discoideum* is incorporated into Cer or IPC and if this feeding would change the lipid composition of *D. discoideum*. The molecular species composition of IPC and Cer was relatively unchanged by the palmitic acid feeding (Fig. 24). Only Cer (39:0;2) was significantly increased after palmitic

acid feeding (Fig. 24). This suggests that, palmitic acid is largely not incorporated into Cer and IPC.

A bioinformatics-based search for IPC synthase in *D. discoideum*

As BLAST search of the *D. discoideum* proteome did not yield structural homologues of the IPC synthases from plants and yeast, we pursued a bioinformatics and functional cloning strategy to identify the IPC synthase(s) in *D. discoideum*. Figure 25 shows an outline of the bioinformatics strategy used to identify IPC synthases in the *D. discoideum* proteome. A similar approach has been used previously to identify human *Hs*SMS1 and *Hs*SMS2 (Huitema *et al.*, 2004). CSS were identified based on the following criteria: (1) presence of a simplified sequence motif (H-X3-D-X3-[GA]-X3-[GSTA]) found in LPPs and Aur1 homologues; (2) presence of multiple (>3) transmembrane domains, since all known CCSs have six and eight predicted transmembrane spans, respectively; (3) biochemical function unknown; (4) and the domain architecture should be similar to known CSS (2 hits). Of the 12,734 protein sequences analysed, seven candidates have both the LPP motif and more than three TMDs (Table. 3). Out of the seven candidates, two met

Table 3. Seven CSS candidates with more than > 3 TMDs.

Gene ID	Gene Name	Predicted function	# of TMDs	homologue in yeast	Comment
DDB_G0284367 (*Dd*CSS1)	n.a.	PA-phosphatase related-family protein	6	Dpp1 (bifunctional DAG diphosphate phosphatase)	not annotated
DDB_G0268928 (*Dd*CSS2)	n.a.	PA-phosphatase related-family protein	7-8	-	not annotated
DDB_G0274591	*dolpp1*	dolichyldiphosphatase 1	4	Cax4 (Dolichyl pyrophosphate phosphatase)	annotated
DDB_G0292564	*iplA*	inositol 1,4,5-trisphosphate receptor-like protein A	5	-	(Lusche et al., 2012)
DDB_G0281669	*lmbd2B*	LMBR1 domain-containing protein 2 homolog B	8	-	(Kelsey et al., 2012)
DDB_G0272260	*sppA*	sphingosine-1-phosphate phosphatase	9	Lcb3 (dihydrosphingosine-1-phosphate phosphatase)	annotated
DDB_G0269332	*zntC*	zinc transporter	6	Zrc1 (zinc transporter)	(Barisch *et al.*, 2018)

Numbers of TMDs were predicted using TMHMM - 2.0 (https://services.healthtech.dtu.dk/services /TMHMM-2.0/) and Membranefold (https://ku.biolib.com/MembraneFold/). Homologues in yeast were identified by BLAST search analysis. Annotations were checked at www.dictybase.org; PA: phosphatidate.

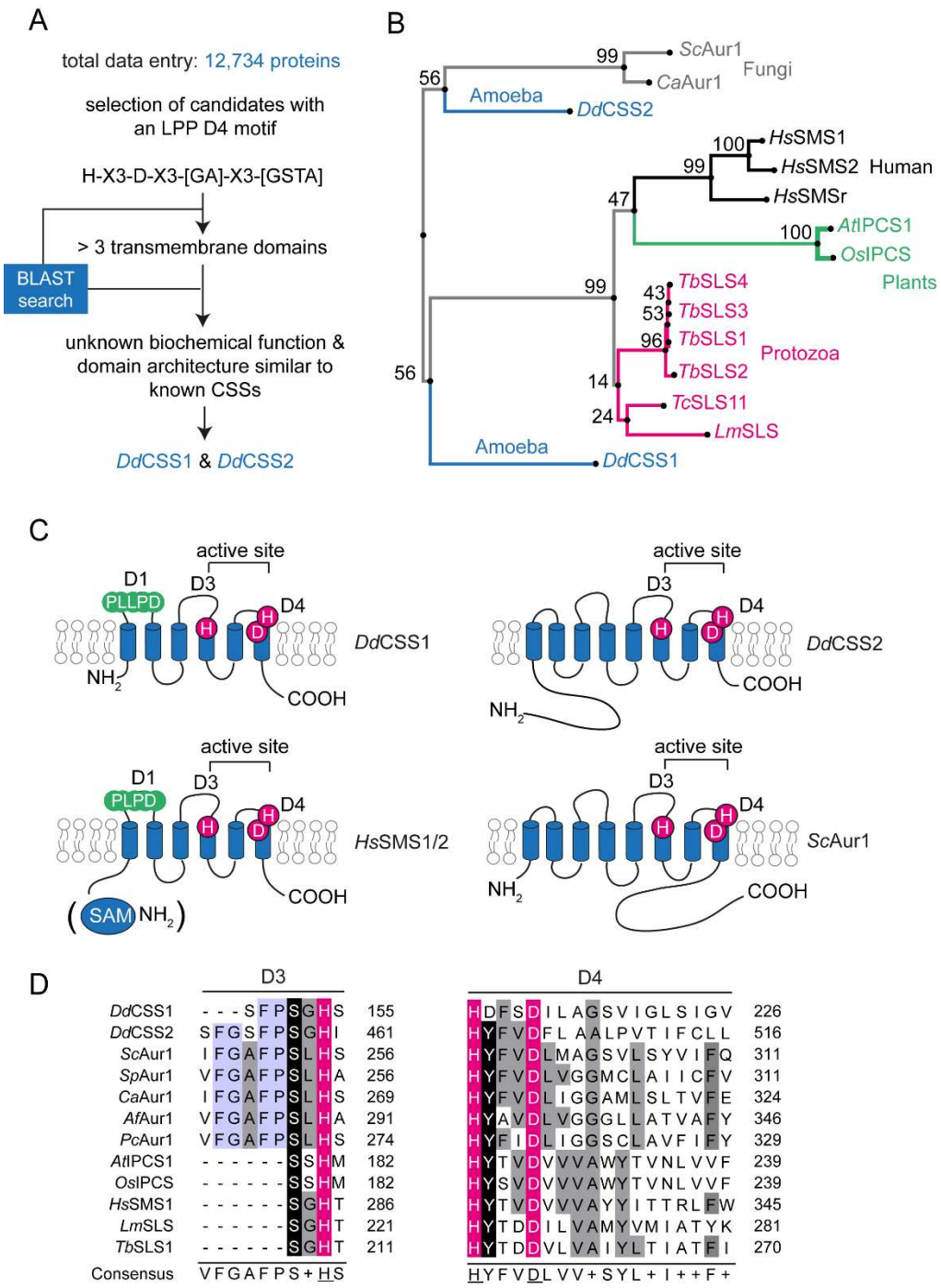

Fig. 25. Selection and phylogenetic analysis of candidate IPC synthases in *D. discoideum*. **A:** Search of the *D. discoideum* proteome for polytopic membrane proteins that contain the LPP-like sequence motif H-X3-D-X3-[GA]-X3-[GSTA] and meet additional selection criteria as indicated yielded two candidate CSSs: *Dd*CSS1 (DDB_G0284367) and *Dd*CSS2 (DDB_G0268928). **B:** Phylogenetic tree of *Dd*CSS1, *Dd*CSS2 and IPC/SM synthases from different species: *Sc*Aur1 from *Saccharomyces cerevisiae* (UniProt accession: P36107); *Ca*Aur1 from *Candida albicans* (O13332); *At*IPCS1 (Q9M325) from *Arabidopsis thaliana*; *Os*IPCS1 from *Oryza sativa* (Q5N7A7); *Hs*SMS1, *Hs*SMS2 and *Hs*SMSr (Q86VZ5, Q8NHU3 and Q96LT4) from *Homo sapiens*; *Lm*SLS (E9AFX2) from *Leishmania*; *Tb*SLS1-4 (Q38E54, Q38E56, Q38E53 and Q38E55) from *T. brucei; Tc*SLS11 from *Trypanosoma cruzi* (UniProt accession: Q4E4I4). Protein sequences were aligned with MAFFT (https://mafft.cbrc.jp) using the G-INS-i strategy, unalignlevel 0.0 and "try to align gappy regions away" to generate a phylogenetic tree in phylo.ilo using NJ conserved sites and the JTT substitution model. Numbers on the branches indicate bootstrap support for nodes from 100 bootstrap replicates.

C: Membrane topology of *Dd*CSS1 and *Dd*CSS2 reconstructed by AlphaFold (https://alphafold.ebi.ac.uk/). **D:** Alignment of D3 and D4 sequence motifs in *Dd*CSS1, *Dd*CSS2 and known IPC/SM synthases from different organisms. *Sp*Aur1 (Q10142) from *Schizosaccharomyces pombe*; *Af*Aur1 (Q9Y745) from *Aspergillus fumigatus*; *Pc*Aur1 (Q9Y745) from *Pneumocystis carinii* (Q6AHV1). Alignment was performed with Jalview workbench (Waterhouse et al., 2009) using the in-built MAFFT alignment option (E-INS-i). Identical residues are shaded in black, conservative residue substitutions are shaded in grey and conserved residues that are part of the catalytic triad are shaded in magenta. Residues conserved among fungal IPC synthases, *Dd*CSS1 and *Dd*CSS2 are shaded in blue.

all four selection criteria and therefore qualified as candidates of *D. discoideum* IPC synthases: *Dd*CSS1 and *Dd*CSS2 (Fig. 25). A phylogenetic analysis of CSS sequences from humans, fungi, parasites, plants and *D. discoideum* showed that *Dd*CSS1 is more closely related to human SMS and IPCS from plants and protozoa, whereas *Dd*CSS2 is more closely related to fungal IPC synthases (Fig. 25B).

Two conserved sequence motifs that correspond to the D3 and D4 motifs in human SMS1/2 are found in *Dd*CSS1 and *Dd*CSS2 (Huitema *et al.*, 2004). The D3 (C-G-D-X3-S-G-H-T) and D4 (H-Y-T-X-D-V-X3-Y-X6-F-X2-Y-H) motifs are reminiscent of the C2 and C3 motifs in LPPs (Waggoner et al., 1999) and include the histidine and aspartate residues (magenta) that form the catalytic triad mediating the nucleophilic attack on the lipid phosphate ester bond (Fig. 25C-D) (Neuwald, 1997). In addition, in the first exomembrane loop, *Dd*CSS1 contains a D1 (P-L-P-D)-like domain ("P-L-L-P-D") (Fig. 25D, Fig. 26A). The D1 domain is present in *Hs*SMS (Huitema *et al.*, 2004) and protozoan IPCS (Denny *et al.*, 2006). Together, this agrees with the fact that *Dd*CSS1 is more closely related to SMS proteins and protozoan IPCS (Fig. 25B). The D2 (R-R-X8-Y-X2-R-X6-T) domain, believed to be exclusive to SMS proteins, was neither detected in *Dd*CSS1 nor *Dd*CSS2. In addition, two unique domains are present in fungal Aur1 (Heidler and Radding, 2000): D-h-h-n-W-X2-Y-X3-H-X3-P (here referred to as "IPC1") and Y-X3-G-X3-G-L-X-R-X-D ("IPC2"). After aligning these two fungal Aur1 domains with *Dd*CSS1 and *Dd*CSS2, we discovered that the tyrosine residue at position 254 (Y) in the IPC1 domain and the R-I-D motif at positions 444-446 in the IPC2 domain are especially well conserved in *Dd*CSS2 and not in *Dd*CSS1 (Fig. 26B).

Protein analysis with MembraneFold combines structural information (AlphaFold) with the topology of TMDs (DeepTMHMM) (Gutierrez *et al.*, 2022). Using MembraneFold (Fig. 26A-C), I am able to predict the topology and TMD spans of *Dd*CSS1 and *Dd*CSS2 (Fig. 25C, Fig. 26A). *Dd*CSS1 contains six TMDs, similar to human SMSs and plant IPCS. In contrast, eight TMDs were predicted for *Dd*CSS2, comparable to *Sc*Aur1. The median span of the TMDs for both

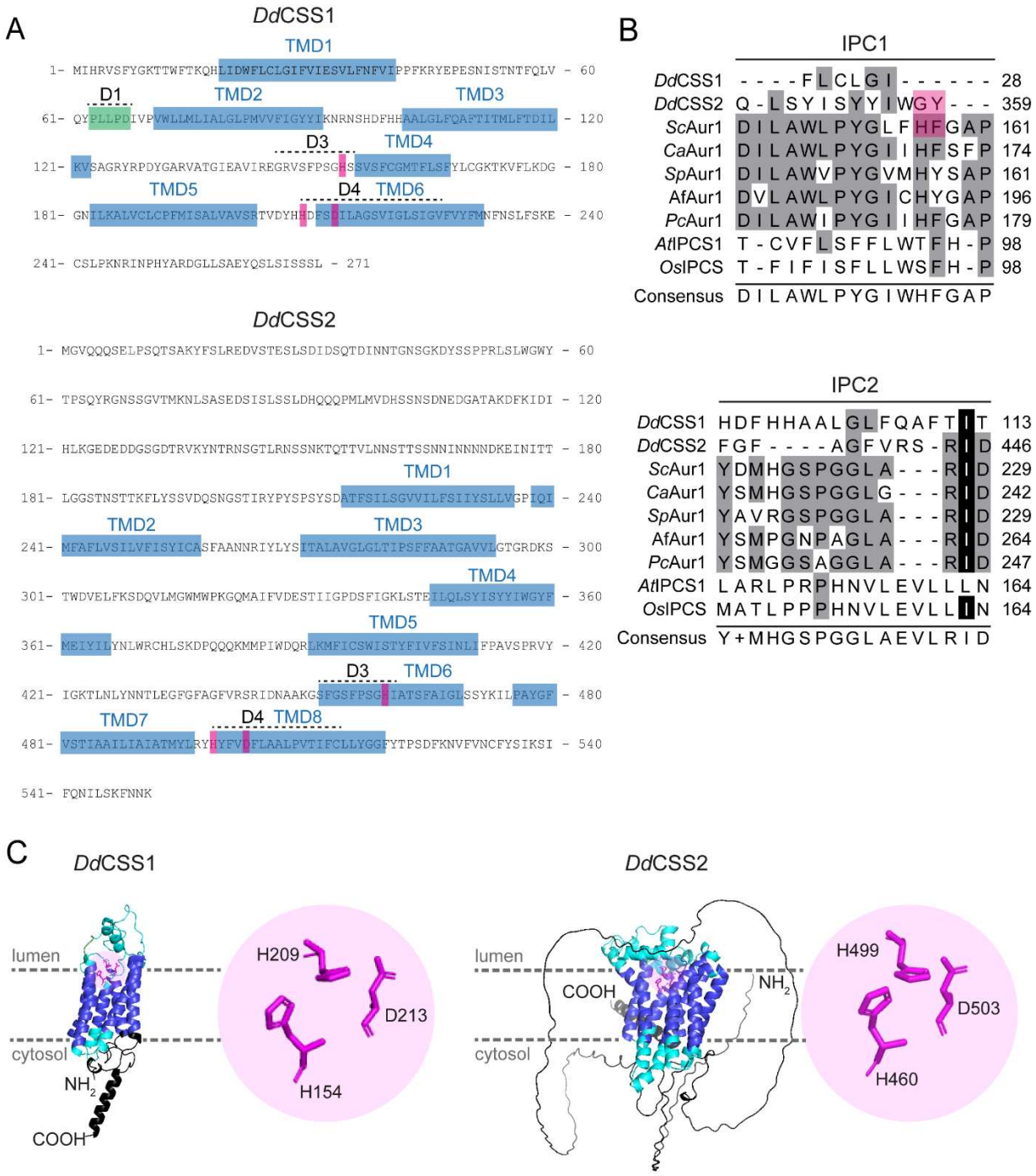

Fig. 26. Conserved sequence motifs in *Dd*CSS1 and *Dd*CSS2. **A:** Amino acid sequences of *Dd*CSS1 and *Dd*CSS2. Regions predicted to form TMDs (TMD1-TMD8) are highlighted in blue. Amino acids of the catalytic triad are marked in magenta, a potential SMS D1 motif is labelled in green. The sequences that are highly similar to D1, D3 and D4 motifs from human SM synthases are indicated. **B:** Alignment of two domains conserved in fungal IPC synthases (named IPC1 and IPC2). Black indicates identical amino acids, grey conservative amino acid substitutions. Residues that confer AbA resistance in *Sc*Aur1 and the corresponding amino acids in *Dd*CSS2 are highlighted in magenta. Alignment was performed with Jalview workbench (Waterhouse *et al.*, 2009), using the in-built MAFFT alignment option (G-INS-i). **C:** AlphaFold-derived structures of *Dd*CSS1 and *Dd*CSS2. The inset shows the amino acids composing the catalytic triad (magenta). Luminal- and cytosolic-exposed regions are indicated in cyan, TMDs are presented in violet.

*Dd*CSS1 and *Dd*CSS2 is 20 amino acids, which is, again, very similar to *Sc*Aur1 (19.5 amino acids) (Quiroga et al., 2013; Sharpe et al., 2010). Moreover, MembraneFold predicted that the N- and C-termini of both candidates are cytosolic, while their active site is situated in the exoplasmic leaflet (Fig. 25C, Fig. 26C). Notably, using models derived from Alphafold, I note that the catalytic triad of *Dd*CSS1 and *Dd*CSS2 are in close proximity to each other (Fig. 26C).
In conclusion, the membrane topology and location of the catalytic triad are preserved in *Dd*CSS1 and *Dd*CSS2, suggesting that both could be CSS. Moreover, *Dd*CSS2 showed features shared with Aur1 proteins from fungi, indicating that it might have IPCS activity.

_Dd_CSS2 displays IPC synthase activity

To test if *Dd*CSS1 and *Dd*CSS2 possess IPC synthase activity, the mRNA of the corresponding proteins were translated in WGE in the presence of unilamelar liposomes prepared from a mixture of PC, PE and PI (Fig. 27A). This approach allows the CFE of catalytically active *Hs*SMS1/2 (Kol *et al.*, 2017) and protozoan IPC synthases (Sevova *et al.*, 2010). Hence, I cloned the cDNAs of *Dd*CSS1 and *Dd*CSS2 into the pEU Flexi-vector pFLx (Goren *et al.*, 2009) with the V5 epitope at the C-termini to facilitate detection. Following a previously established protocol, the mRNAs of both proteins and of *Hs*SMS2 (positive control) were synthesized by *in vitro* transcription and translated into proteins in a WGE (Fig. 27A) (Goren *et al.*, 2009; Kol *et al.*, 2017). In all cases, the correct size of the translated proteins were confirmed and no protein was detected in the Western Blot (WB) when no mRNA was added (Fig. 27B, top).
Next, the fluorescent NBD-C6-Cer (NBD-Cer) was added to the proteoliposome and the formation of NDB-labelled complex phosposphingolipids was monitored by TLC (Fig. 27A). As previously observed, CFE-produced *Hs*SMS2 displayed SM-synthase activity (Fig. 27B, bottom) (Kol *et al.*, 2017). *Dd*CSS1 did not yield any obvious NBD-labelled reaction product. However, conversion of NBD-Cer was observed for *Dd*CSS2 and resulted in a band that runs below NBD-SM (Fig. 27B, bottom). Importantly, the omission of PI from the proteoliposome abolished the production of NBD-labelled lipids, while the omission of PC and PE did not (Fig. 27C, bottom). In contrast, omission of PC from *Hs*SMS2 proteoliposomes reduced but did not entirely eliminate production of NBD-SM, probably because the WGE contain a residual amount of PC (Fig. 28C). Unfortunately, in this study, I did not succeed in generating the *css2* knockout. In addition, the extensive restriction-enzyme-mediated insertional mutagenesis (REMI) library of *D. discoideum*

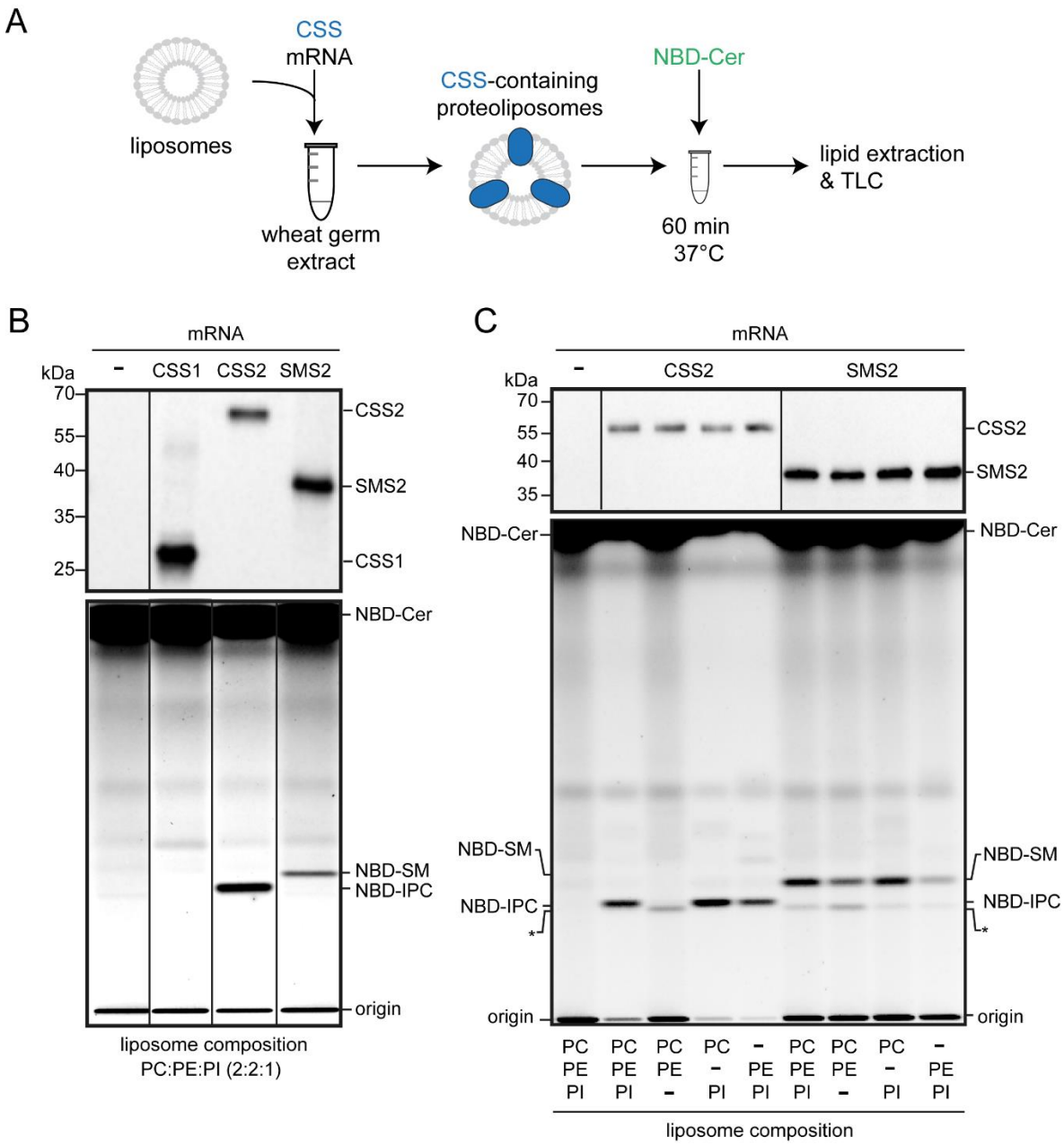

Fig. 27. CFE and functional analysis of *Dd*CSS1 and *Dd*CSS2. **A:** Schematic outline of the wheat germ-based cell-free translation of CSS mRNA. Unless indicated otherwise, translation reactions were carried out in the presence of liposomes with defined lipid compositions. The resulting proteoliposomes were incubated with NBD-Cer and NBD-labeled reaction products were analysed by TLC. **B:** Top panel: translation reactions with or without mRNA encoding V5-tagged *Dd*CSS1, *Dd*CSS2 and *Hs*SMS2 carried out in the presence of liposomes with the indicated lipid composition were subjected to western blot analysis using anti-V5 antibody. Bottom panel: TLC analysis of reaction products formed when *Dd*CSS1, *Dd*CSS2 and *Hs*SMS2 produced in the presence of liposomes containing PC:PE:PI (2:2:1) were incubated with NBD-Cer for 60 min at 37°C. **C:** Top panel: translation reactions with or without mRNA encoding V5-tagged *Dd*CSS2 or *Hs*SMS2 carried out in the presence of liposomes with the indicated lipid composition were subjected to western blot analysis using anti-V5 antibody. Bottom panel: TLC analysis of reaction products formed when *Dd*CSS2 and *Hs*SMS2 produced in the presence of liposomes with the indicated lipid composition were incubated with NBD-Cer for 60 min at 37°C. Migration of an unidentified fluorescent lipid that was present in reactions irrespective of the presence of *Dd*CSS2 or *Hs*SMS2 is marked by an asterisk. Credit: Matthijs Kol.

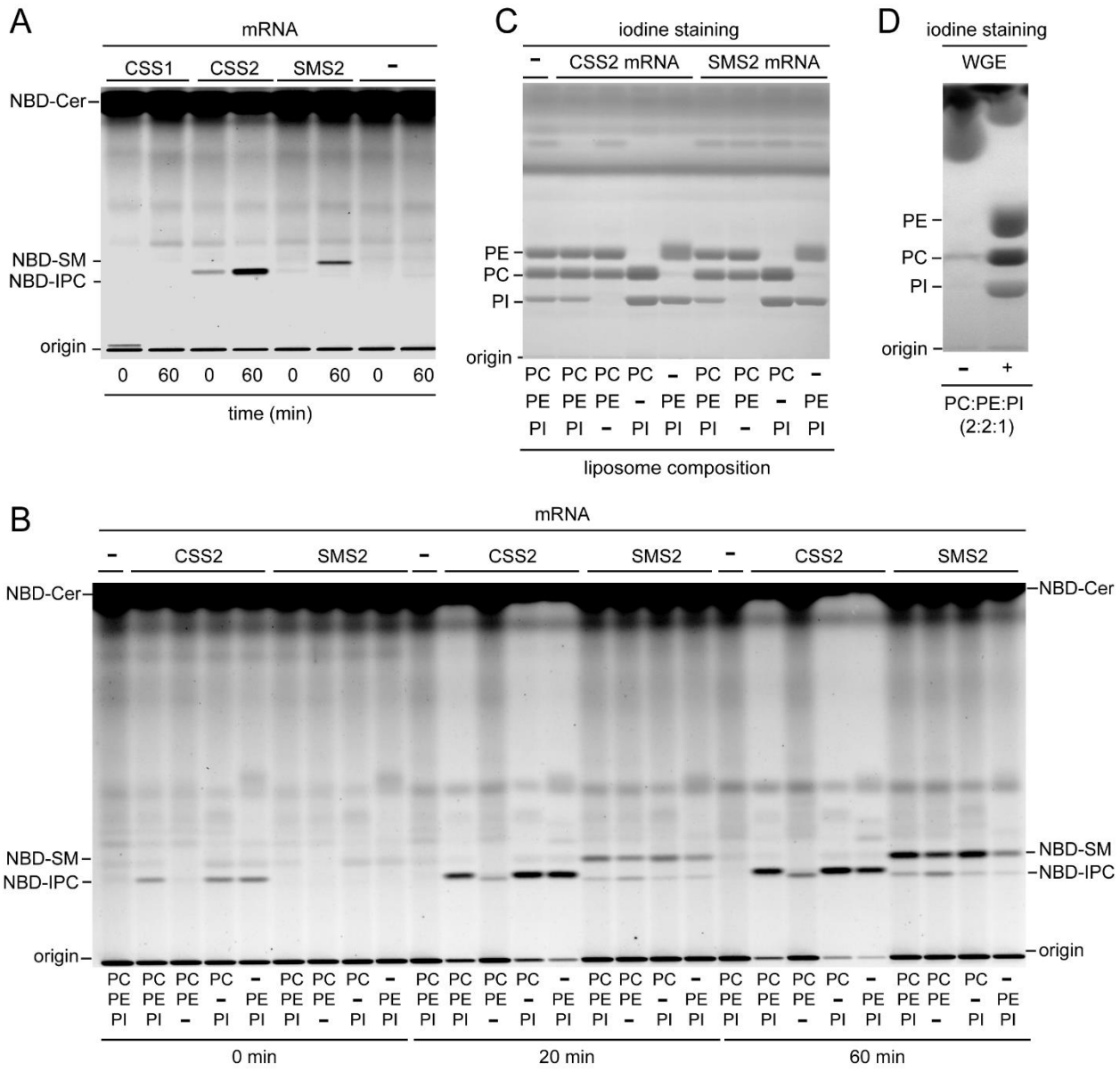

Fig. 28. Complete TLCs and iodine staining. **A:** TLC analysis of reaction products formed when the translational reactions of *Hs*SMS2, *Dd*CSS1 and *Dd*CSS2 were incubated with liposomes containing PC:PE:PI (2:2:1). **B:** TLC analysis of reaction products of *Hs*SMS2 and *Dd*CSS2 that were incubated with liposomes of varying glycerophospholipid composition. The reaction was stopped at the indicated time points. **C:** Iodine staining of B. Shown are the reaction products after 60 min incubation. D: Iodine staining of the WGE with and without the addition of liposomes (PC:PE:PI; 2:2:1). Credit: Matthijs Kol.

does not contain any *css2* mutants (Gruenheit et al., 2021). This suggests the essentiality of *Dd*CSS2, like the IPC synthase from yeast (*Sc*Aur1) (Sato et al., 2009). The cyclic depsipeptide antibiotic AbA is a potent inhibitor of IPC synthase from fungi (Heidler and Radding, 1995; Takesako et al., 1993). The addition of AbA (50 µM) to yeast lysates co-incubated with NBD-Cer and exogenously added PI effectively blocked the formation of NBD-IPC (Fig. 29A). Moreover, the NBD-IPC synthase activity of cell-free-produced *Dd*CSS2 was resistant to even a high amount

of AbA (500 µM). Also, extended treatment of *D. discoideum* with AbA had no impact on steady state IPC levels (Fig. 29B).

In sum, our results show that *Dd*CSS2 functions as an IPC synthase that lacks the AbA sensitivity typical for IPC synthases from fungi. Whether *Dd*CSS2 is needed for IPC production in *D. discoideum* remains to be answered.

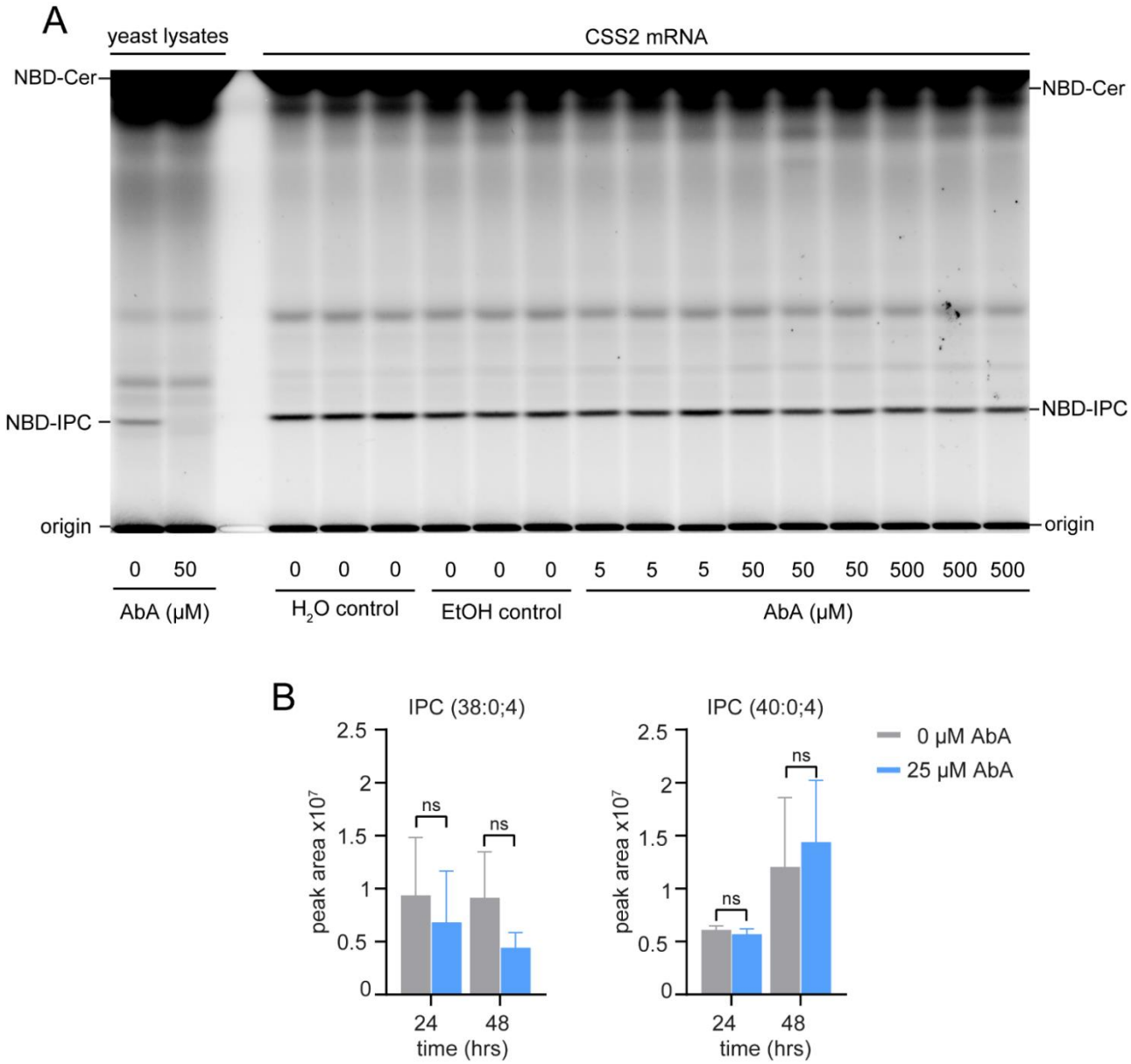

Fig. 29. Analysis of IPC synthesis by AbA. **A:** TLC analysis of reaction products of *Dd*CSS2 that were incubated with AbA. Yeast lysates incubated with AbA served as a positive control. **B:** LC/MS-MS analysis of IPC(38:0,4) and IPC(40:0,4) after treatment with AbA. HL5c grown-*D. discoideum* was treated with or without 25 µM of AbA for 24 or 48 hrs, prior to extraction by (Folch *et al.*, 1957). Graph shows mean and ±SD (n=4). Statistics were assessed with a paired t-test. ns: not significant. Credit; A: Matthijs Kol.

*Dd*CSS2 localises to the Golgi apparatus, the CV and the MCV

The enzymes responsible for bulk production of IPC, EPC and SM mostly localise at the Golgi complex (Huitema *et al.*, 2004; Levine *et al.*, 2000; Vacaru *et al.*, 2013). To confirm the subcellular localisation of *Dd*CSS2, *Dd*CSS2 was tagged with mCherry at either end using extrachromosomal plasmids and the expected size of both fusion was confirmed by WB (Fig. 31A). As expected, when cells expressing CSS2-mCherry as well as mCherry-CSS2 showed partial co-localisation with ZntD-GFP, a zinc transporter that is present at the juxtanuclear region that is characteristic for the Golgi complex/recycling endosomes in *D. discoideum* was observed (Barisch *et al.*, 2018) (Fig. 30A-B). The localisation of *Dd*CSS2 at the Golgi apparatus was further confirmed by immunostaining with the Golgi marker AK426 (Fig. 30C-D) (Gräf et al., 1999; Lima, 2019; Merlot et al., 2003). Moreover, we did not observe any co-localisation of mCherry-CSS2 or CSS2-mCherry with the ER marker protein disulfide isomerase (PDI) (Fig. 31B). In addition, both fusion proteins were present at membrane structures resembling bladders of the

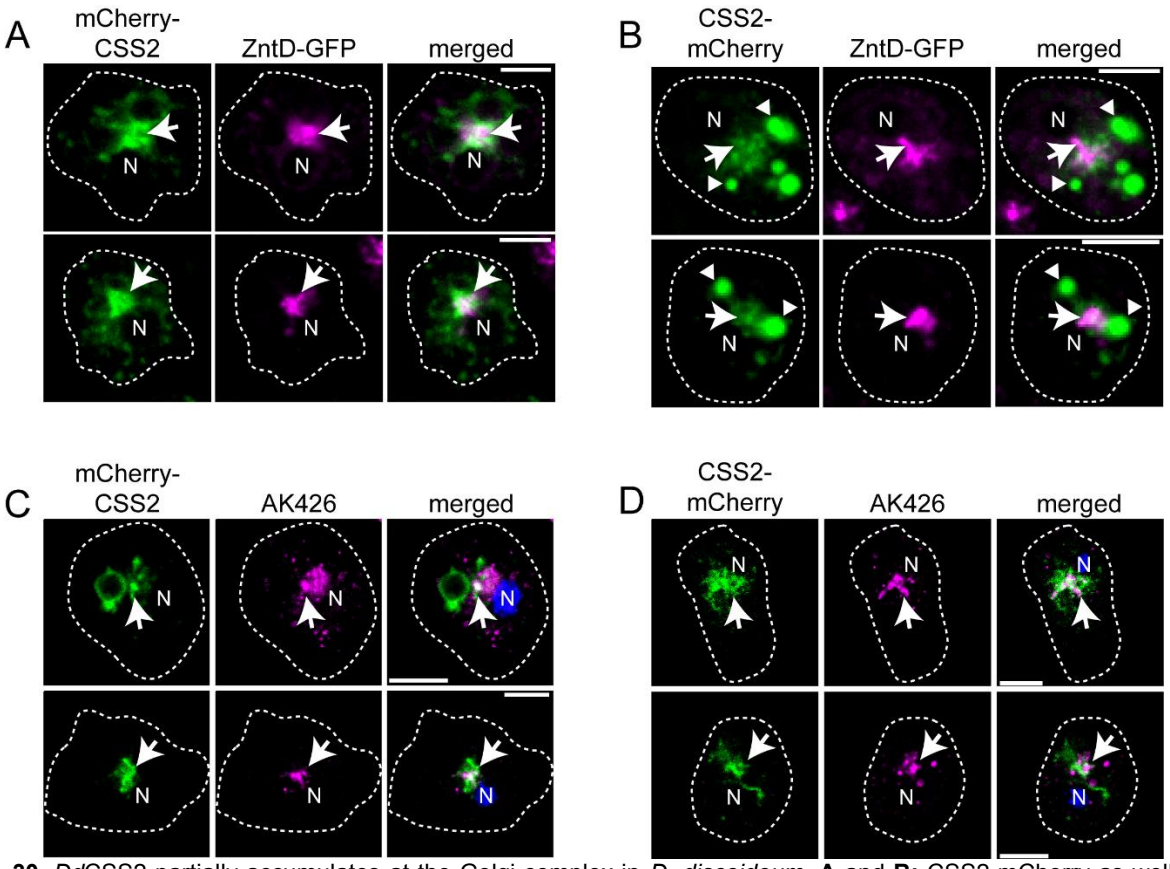

Fig. 30. *Dd*CSS2 partially accumulates at the Golgi complex in *D. discoideum*. **A** and **B:** CSS2-mCherry as well as mCherry-CSS2 co-localise with ZntD-GFP, a zinc transporter that is located at the Golgi apparatus/recycling endosomes. **C** and **D:** CSS2-mCherry as well as mCherry-CSS2 co-localise with the Golgi marker AK426 (Gräf *et al.*, 1999). Cells were either imaged live using SD microscopy (A, B) or fixed with MeOH, stained with the AK426 antibody and imaged using confocal laser scanning microscopy (CLSM) (C, D). Arrows indicate co-localisation, arrowheads point to CSS2-mCherry-positive vesicles. N: nucleus. Scale bars, 5 µm. Credit; B: Edwin Ufelmann.

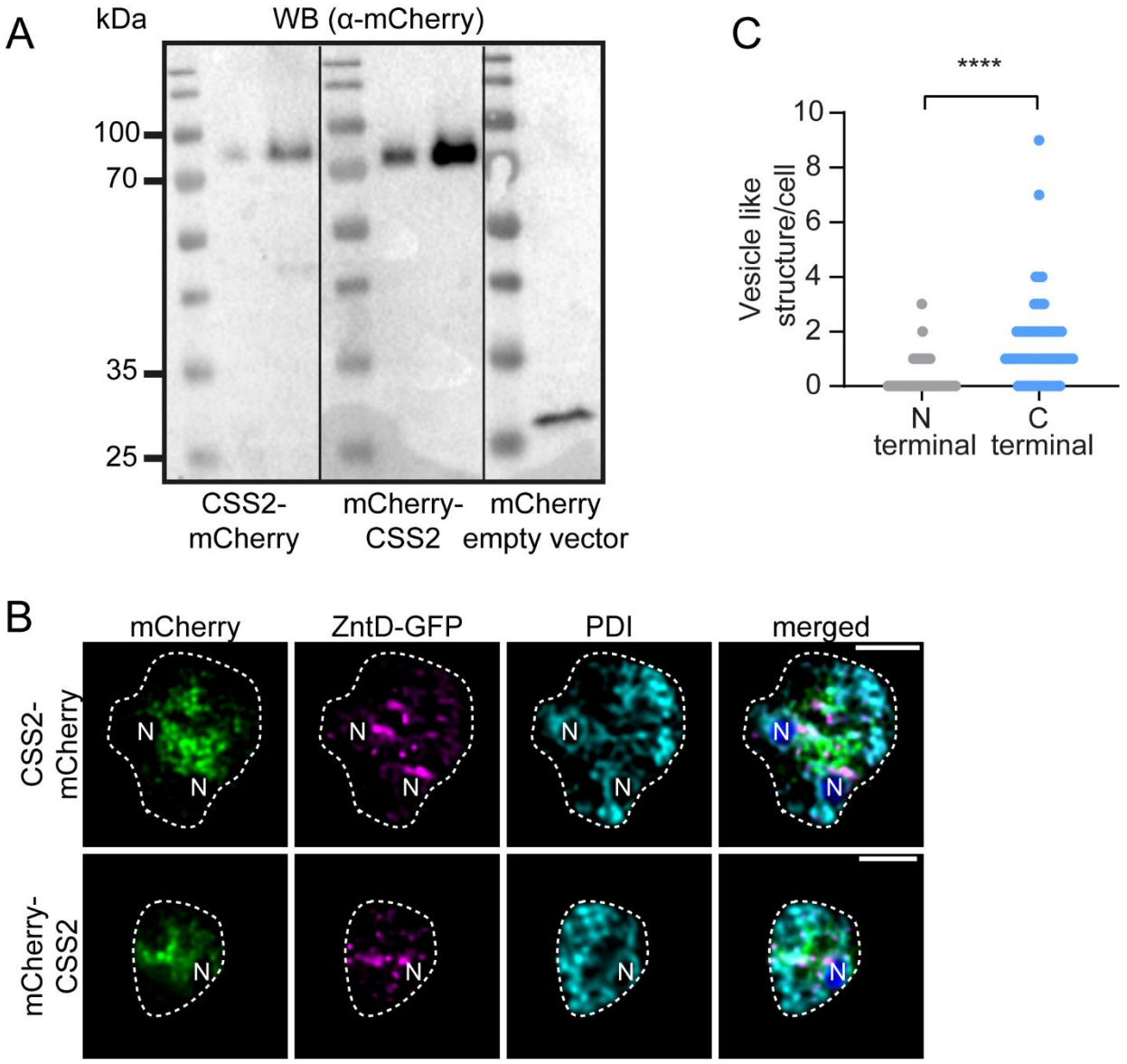

Fig. 31. Expression of fusion constructs and localisation analysis. **A:** Western blot of mCherry-CSS2 and CSS2-mCherry with untagged mCherry as a control. $2x10^4$ and $10x10^5$ cells were used for the first and second lanes, respectively. **B:** CSS2-mCherry and mCherry-CSS2 do not co-localise with the ER-marker PDI. Cells were fixed with MeOH, stained for PDI and imaged by CLSM. Images were deconvolved. N: nucleus. Scale bars, 5 µm. **C:** Quantification of CSS2-mCherry and mCherry-positive vesicles. Statistical differences were calculated with an unpaired t-test (**** $p < 0.0001$). Error bars indicate ±SD (n=3; number of cells = 60). Credit; B,C: Edwin Ufelmann.

CV system prior to water discharge, as well as on vesicle-like structures that were more prevalent in CSS2-mCherry expressing cells (Fig. 30C; Fig. 32A-B, arrow heads).

To confirm the localisation of *Dd*CSS2 on CV bladders, cells expressing the CSS2 fusions were fed with latex beads and fixed and stained with anti-VatA, a subunit of the vATPase that is present in both lysosomes and membranes of the CV network (Fig. 32A-B, arrowheads) (Neuhaus et al., 1998). To distinguish between the CV and lysosomes, cells were additionally labelled with p80, a copper transporter that labels all endosomes in *D. discoideum* but is absent at the CV (Ravanel

et al., 2001). Indeed, the presence of both mCherry at VatA-positive, p80-negative compartments (Fig. 33A-B, arrowheads), and their absence at VatA-positive bead-containing phagosomes (BCPs) (Fig. 33A-B, asterisks) suggests that *Dd*CSS2 is confined to the CV and not present on lysosomes. Moreover, we did not observe any co-localisation of CSS2-mCherry or mCherry-CSS2 on Vacuolin positive BCPs (Fig. 33C-D). In summary, while the Golgi localisation of IPC synthase is conserved in *D. discoideum*, our findings demonstrate that *Dd*CSS2 is also localised at the CV.

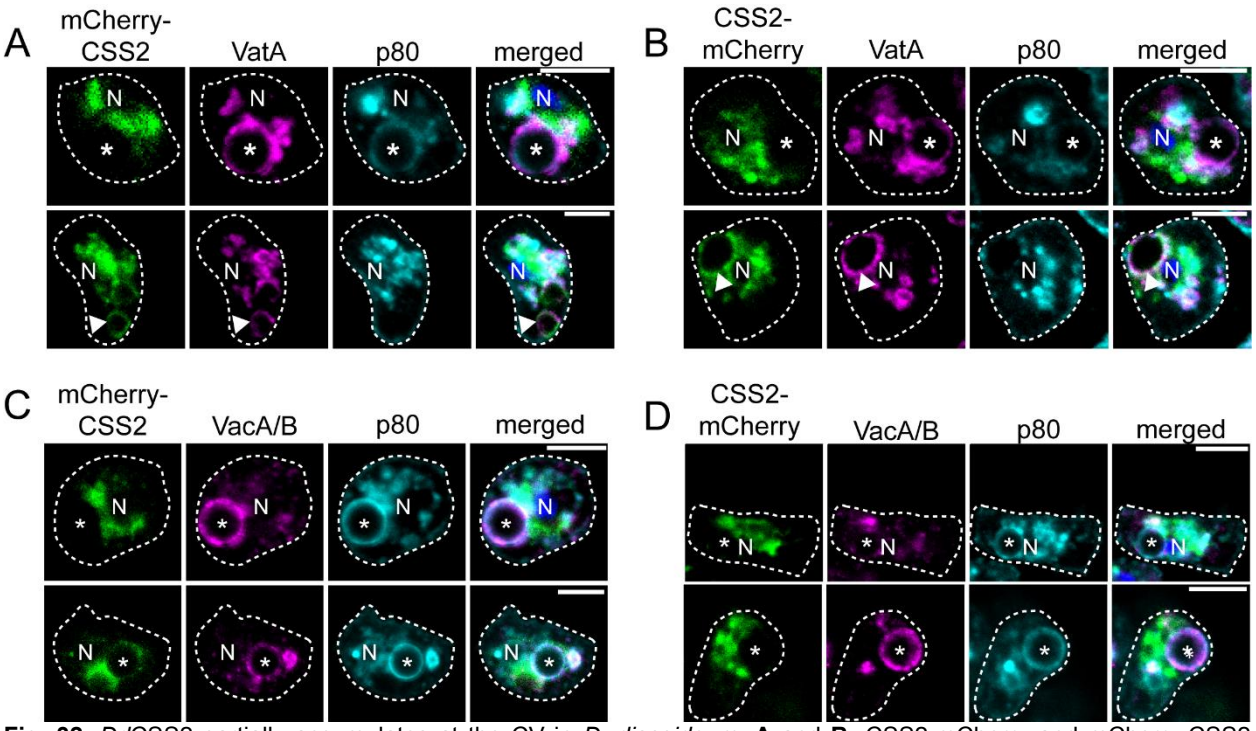

Fig. 32. *Dd*CSS2 partially accumulates at the CV in *D. discoideum*. **A** and **B:** CSS2-mCherry and mCherry-CSS2 partially co-localises with H^+-vATPase-positive, p80-negative structures, indicative of the CV. **C** and **D:** CSS2-mCherry and mCherry-CSS2 do not accumulate on BCPs. CSS2-Cherry and mCherry-CSS2 expressing cells were incubated with 3 µm latex beads, fixed with PFA/picric acid (A, B) or MeOH (C, D) and stained with either anti-VatA (A, B) or anti-VacA/B (C, D) and anti-p80 antibodies. Images were generated by CLSM. Asterisks label BCPs. Arrowheads label CSS2-positive CV bladders. N: nucleus. Scale bars, 5 µm. Credit: Edwin Ufelmann.

D. discoideum is an established host cell to investigate mycobacterial pathogenesis. When *D. discoideum* is infected with *M. marinum*, the MCV undergoes proteomic remodeling (Cardenal-Muñoz *et al.*, 2017; Hagedorn and Soldati, 2007). As an endosomal compartment, the MCV has special characteristics: it accumulates vacuolins and the vATPase is nearly undetectable at later infection stages (Hagedorn and Soldati, 2007). Importantly, some proteins are exclusively recruited to the MCV and not to the endosome, like the zinc transporter *Dd*ZntA and the lipid transport protein OSBP8 (Anand *et al.*, 2023; Hanna et al., 2021). To determine if *D. discoideum* MCV recruits *Dd*CSS2, we infect *D. discoideum* with BFP-expressing *M. marinum*. Strikingly, it

was observed that, throughout the *M. marinum* infection course, *Dd*CSS2 is recruited to the MCV (Fig. 33).

In summary, while the Golgi localisation of IPC synthase is conserved in *D. discoideum*, our findings demonstrate that *Dd*CSS2 is also localised at the CV and the MCV.

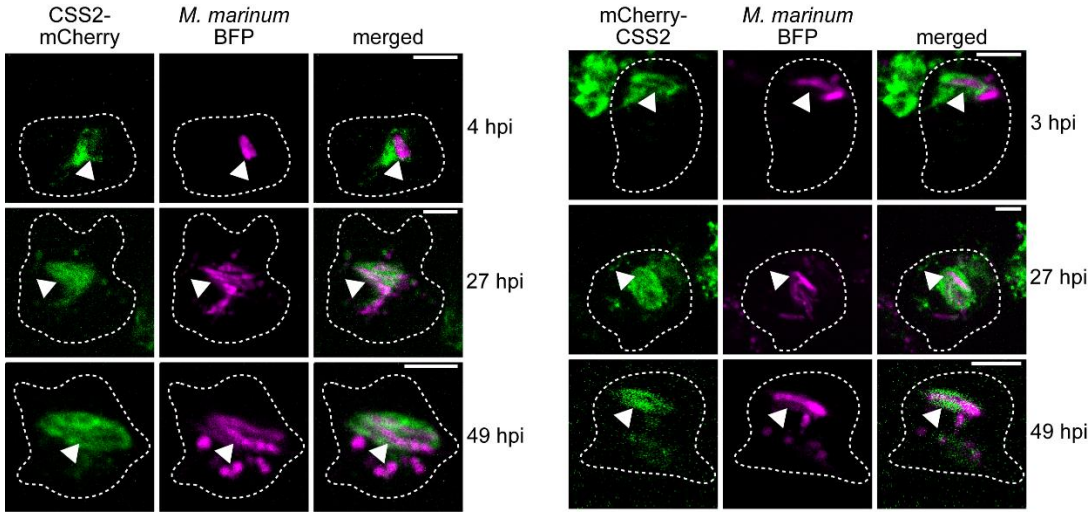

Fig. 33. *Dd*CSS2 localises at the MCV. Cells were infected with BFP-expressing *M. marinum* wt. Samples were collected at the indicated time points an imaged using SD microscopy. Arrowheads label CSS2-positive MCV. Scale bars, 5 µm. Credit: Edwin Ufelmann.

Sterols is enriched in *D. discoideum* endosome

Sterols and sphingolipids are tightly associated. For example within synthetic membranes they cluster to form microdomains (Risselada and Marrink, 2008). Consequently, I reasoned that it might be informative to showcase in which membrane in *D. discoideum* does the sterol localised. D4H is a sterol probe, which binds to mammalian cholesterol when its membrane concentration is above 20 mol % (Maekawa and Fairn, 2015). The binding of D4H is specific to the cytosolic leaflet of the organelles (Maekawa and Fairn, 2015), and it has been useful in investigating the subcellular cholesterol organization in cells expressing pathogenic SMS2 variant (Sokoya *et al.*, 2022). The use of D4H probe in *Schizosaccharomyces pombe* (where ergosterol instead of cholesterol is present), shows that D4H is able to bind to other sterol species aside from cholesterol (Marek et al., 2020). Accordingly, D4H binds to free cholesterol in the membrane but not to the ones which are sequestered by sphingolipids (Das et al., 2014; Sokoya *et al.*, 2022). Filipin, is a fluorescent polyene macrolide that also binds to free sterols (Jin et al., 2008). In contrast to D4H, Filipin stains sterols indiscriminately, whether it is sitting on the luminal side or the cytosolic leaflet of organellar membranes (Zaremberg et al., 2005).

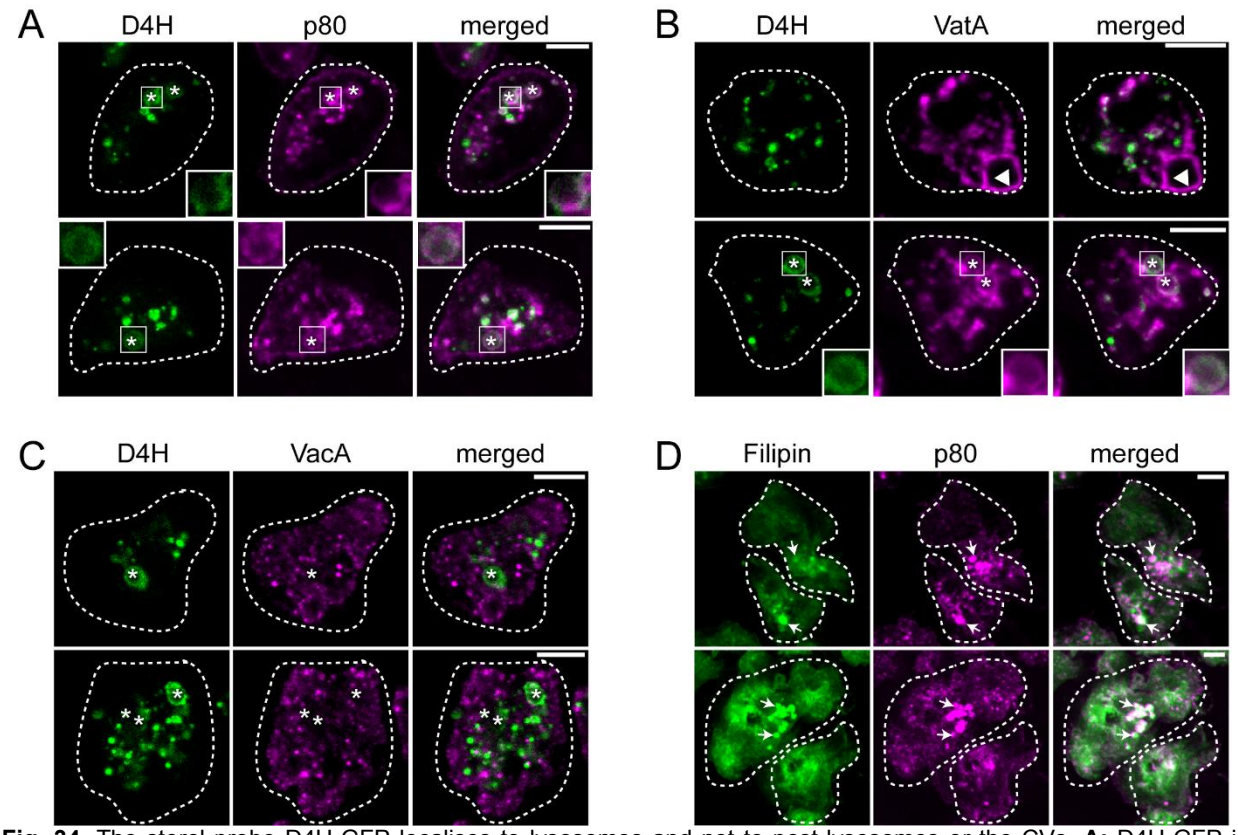

Fig. 34. The sterol probe D4H-GFP localises to lysosomes and not to post-lysosomes or the CVs. **A:** D4H-GFP is localised in p80-positive BCPs. **B:** D4H-GFP does not co-localise with VatA-positive CV-like structures (top), but instead, with VatA-positive BCPs (bottom). **C:** D4H-GFP-positive BCPs are VacA-negative. **D:** Ax2 cells were stained with Filipin and p80. D4H-GFP expressing and non-expressing cells were incubated with 3 µm latex beads and fixed with PFA/picric acid. Arrows label points of co-localisation. Arrowheads show a CV-like structure. Asterisks show BCPs. Scale bars, 5 µm.

Our microscopy data showed that D4H-GFP did not show co-localisation with VatA-positive CV-like structure (Fig. 34B, arrowhead), however, we saw that it co-localises with p80-positive BCPs (Fig. 34A) and VatA-positive BCPs (Fig. 34A-B, bottom). This suggests the enrichment of free sterols at the cytoplasmic leaflet of the lysosomal membrane. Furthermore, D4H-GFP-positive BCPs showing no Vacuolin (VacA) localisation indicate that the free sterols are not enriched at the cytoplasmic leaflet of the post-lysosome (Fig. 34C). Additionally, Filipin staining confirms the enrichment of free sterols at the endosome (Fig. 34D, arrows). Altogether, the microscopy data suggest that free sterols (unbound to sphingolipids) are enriched at the cytosolic leaflet of the lysosome.

The intracellular growth of *M. marinum* in *D. discoideum* in response to sphingolipid inhibitors

The intracellular replication of Zika virus is attenuated in the presence of sphingolipid inhibitors (Leier et al., 2020). In *M. tuberculosis,* when the sphingomyelinase *Mt*SpmT is deleted, the

intracellular growth in macrophage cells is reduced (Speer et al., 2015). Therefore, we asked if blocking the sphingolipid pathway in *D. discoideum* would impact the intracellular growth of *M. marinum*. Consequently, *D. discoideum* was infected with luciferase-expressing *M. marinum* and AbA, Fumonisin B1 (FB1), and Myriocin were added after the removal of the extracellular bacteria. FB1 and Myriocin block CerS and SPT, respectively. In the presence of AbA, intracellular growth of *M. marinum* was unaltered (Fig. 35). However, an indication for a growth increase was seen when FB1 and Myriocin were added to the infected cells (Fig. 35). All together, this suggests that FB1 or myriocin treatment may increase the intracellular growth of *M. marinum*. However, further replicates are necessary to validate the results of FB1 and myriocin.

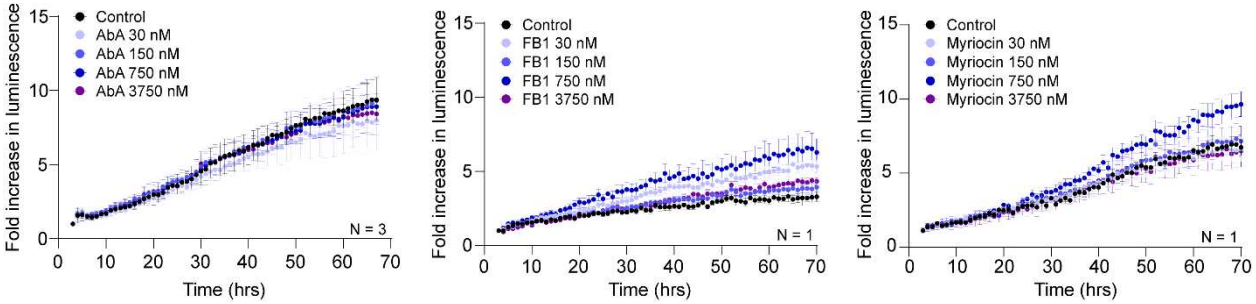

Fig. 35. Intracellular growth of *M. marinum* in the presence of sphingolipid inhibitors. AbA, FB1 and Myriocin were added at indicated concentrations. *D. discoideum* was infected with *M. marinum* expressing luciferase and the luminescence was measured with a microplate reader. Symbols and error bars shows mean and standard deviation of three biological replicates (AbA) and three technical replicates (FB1 and Myriocin). N = 3 (Aba); N = 1 (FB1 and myriocin). Credit: Edwin Ufelmann.

DISCUSSION

Although extensively used in cell and infection biology, information about the sphingolipidome and the sphingolipid biosynthetic pathway of *D. discoideum* remains scarce. Thus, in this work, a systematic BLAST search to hunt for *D. discoideum* sphingolipid enzymes and the reconstruction of the sphingolipid pathway were performed. Combining BLAST searches for homologs of sphingolipid biosynthetic enzymes with LC-MS/MS-based lipidomics and the functional characterization of cell-free expressed enzymes, I found that *D. discoideum* mainly synthesises phosphoinositol-containing sphingolipids with phytoceramide backbones. Identification of the corresponding IPC synthase, *Dd*CSS2, revealed a polytopic membrane protein that shares several sequence motifs with both yeast IPC synthases and human SM synthases. Interestingly, *Dd*CSS2 displays localisation in the Golgi apparatus and the organism's osmoregulatory vacuole (CV). Altogether, this study serves as the groundwork for utilising *D. discoideum* as a model organism to investigate the role of sphingolipid in phagocytosis and *M. marinum* infection.

Characterization of the *D. discoideum* lipidome and sphingolipidome

To characterise the lipidome of *D. discoideum,* I performed untargeted LC-MS/MS lipidomics. This revealed that, PE is the predominant glycerophospholipid in *D. discoideum* as previously described (Fig. 13A) (Ellingson, 1974; Kappelt *et al.*, 2020). The lipidome of *D. discoideum* presented in Figure 13A is very similar to that of *Drosophila* melanogaster and bacteria where PE predominates (Raetz and Dowhan, 1990; Goh and Guan, 2021) and in stark contrast to that of mammalian cells (where PC is the major glycerophospholipid) (Symons et al., 2021).

Here, I also confirmed that the glycerophospholipid pool of *D. discoideum* is mostly composed of ether lipids (Fig. 13C-D). *D. discoideum* has been suggested to be a good model organism to investigate the biological role of ether lipids due to its relative simplicity (Jiménez-Rojo and Riezman, 2019). Accordingly, it has been reported that the loss of peroxisomal fatty acid reductase acyl transferase (FARAT) in *D. discoideum* leads to (a) severely diminished MDG and (b) an impaired endocytosis (Kappelt *et al.*, 2020). I confirmed that the deletion of *fatA* leads to a significant reduction in MDGs and ether (alkyl-acyl) glycerophospholipids (Fig. 14). However, despite the reduction, both MDGs and alkyl-acyl glycerophospholipids were still detected (Fig. 14). *Dd*FARAT has been suggested to be responsible for the synthesis of monoalkyglycerol-3-phosphate (ether-LPA), the precursor of both MDGs and ether glycerophospholipids (Fig. 7). The detection of ether lipids in the *Dd*FARAT null mutant suggests the presence of an alternative pathway to synthesise ether lipids.

Another plausible implication of *D. discoideum* containing mostly ether glycerophospholipids is the possibility of using this organism to study GPI-anchored proteins. In mammalian cells, the GPI-anchored protein is mostly based on ether-linked (alkyl-acyl) PI, whereas in yeast, it is based on Cer (Jiménez-Rojo and Riezman, 2019; Kinoshita, 2020). Evidence suggests that the GPI-anchored protein *Dd*PsA in *D. discoideum* is based on IPC containing (18:0;3) phytoceramide (Haynes et al., 1993).

In addition, growing *D. discoideum* in different media (SIH versus HL5c) appears to have only a minor effect on the *D. discoideum* lipidome in the context of lipid classes (Fig. 15-17). As SIH and HL5c media differ in many nutritional variables (albeit the glucose concentration remains the same), I postulate that *D. discoideum* exerts efforts to maintain its membrane composition in spite of nutritional changes. Notably, LipidSearch was able to detect and profile LBPAs (Fig. 16). LBPA is a lipid found almost exclusively in the late endosomes of vertebrates, and plays a role in controlling endosomal cholesterol levels (Gruenberg, 2020). Interestingly, unlike other lower eukaryotes, *D. discoideum* and *Entamoeba histolytica* produce LBPA (Castellanos-Castro et al., 2016; Gruenberg, 2020; Rodriguez-Paris et al., 1993). I anticipate the use of *D. discoideum* to elucidate the LBPA synthesis pathway and to investigate the role of LBPA in phagocytosis.

Remarkably, despite PE is the most abundant glycerophospholipid, our findings reveal a very significant synthesis of IPC (18:0;3/20:0;1) which receives the headgroup from PI (Fig. 19A-B, Fig. 36). Eukaryotic organisms commonly use the most abundant glycerophospholipid as headgroup donor in the production of complex phosphosphingolipids, e.g. PC for the synthesis of SM in mammals (Sampaio et al., 2011b), PE for the synthesis of EPC in *D. melanogaster* (Rietveld et al., 1999b; Vacaru *et al.*, 2013), and PI for the synthesis of IPC in yeast (Ejsing *et al.*, 2009). Our finding that *D. discoideum* produces IPC in spite of having PE as most abundant glycerophospholipid class provides a significant break in this trend.

Similar to *S. cerevisiae* where IPC (18:0;3/26:0;1) is the major IPC species, *D. discoideum* predominately synthesises LCB (18:0;3). However, the fatty-acid moieties of its IPC species are shorter, ranging from 16 to 22 carbon atoms in length (Fig. 19B-C), thus highlighting species-specific variations in IPC composition. I also noticed a high abundance of "phyto" sphingolipids with three or more hydroxyl groups in the LCBs, which are prominent in yeast and plants (Marquês et al., 2018) (Fig. 19B-C, Fig. 36). Furthermore, our data shows that, under the current growth conditions, the species composition of Cer and IPC differs: While Cer (40:0;3) is the most abundant Cer, the levels of IPC (40:0;3) are relatively low (Fig. 19B-C, Fig. 36). Consequently, I propose that the enzyme mediating IPC synthesis in *D. discoideum* prefers substrates containing hydroxylated acyl chains.

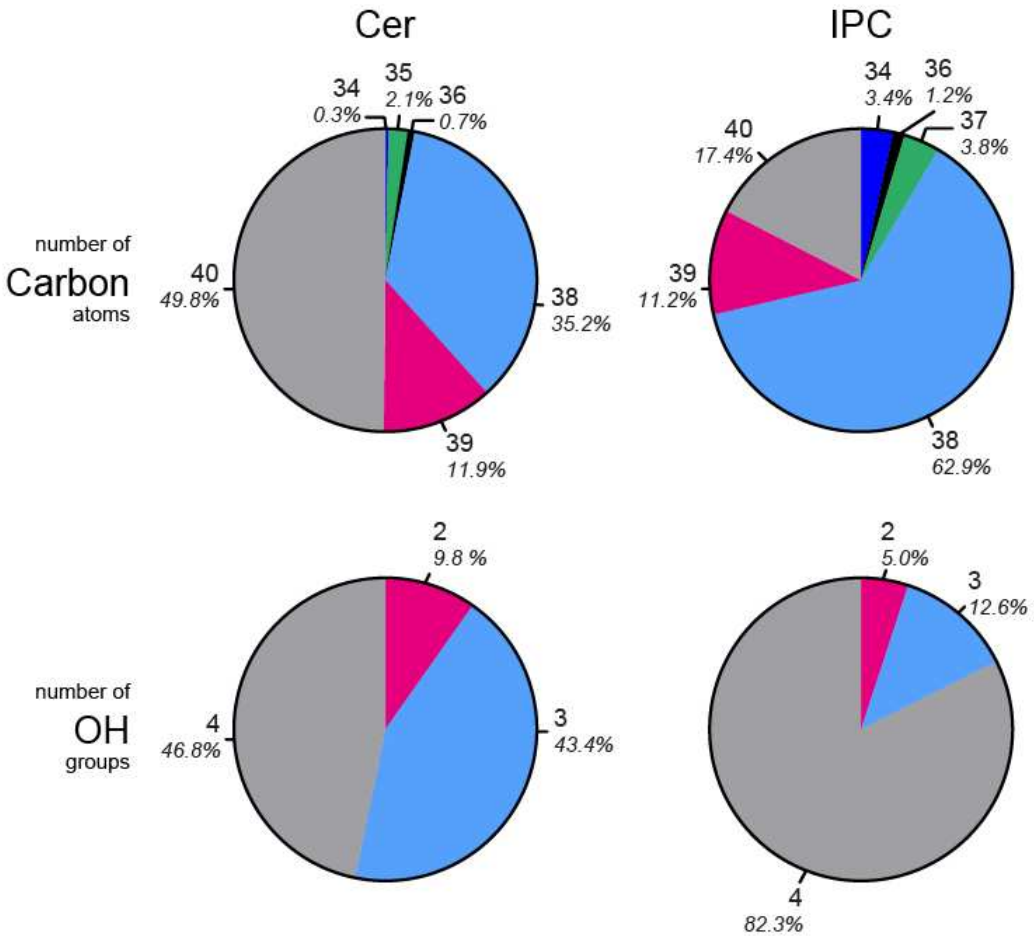

Fig. 36. The composition of Cer and IPC species based on the number of carbon atoms (within the Cer backbone) and the degree of hydroxylation as determined in this work (Fig. 19B-C).

IPCs in *D.* discoideum might undergo even further modifications similar to those of plants (glucuronosylation) or *S. cerevisiae* (mannosylation), leading to the synthesis of GIPC or MIPC, respectively (Mamode Cassim *et al.*, 2020; Megyeri *et al.*, 2016). The notion was reinforced by the discovery of one plant IPC glucuronosyl transferase 1 (IPUT1) homolog in *D. discoideum* (Supplementary Table 1) (Rennie et al., 2014). In dictybase, this protein is annotated as *Dd*Gtr3 (DDB_G0286945). However, here, I was unable to detect GIPC in *D. discoideum*.

Additionally, the IPC composition was significantly unaffected by palmitic acid feeding (Fig. 24). This suggests that palmitate is largely not incorporated into Cer or IPC. I also observed that the IPC levels are significantly increased when *D. discoideum* was grown in SIH medium (Fig. 23). This may be explained by the fact that SIH medium containes more free serine compared to HL5c. Serine is the precursor of sphingolipids, and the presence of exogenous serine influences sphingolipid metabolism (Esch et al., 2020).

Altogether, I conclude that the sphingolipidome of *D. discoideum* is unique and, if any, possesses more similarities to fungi and plants than to vertebrates.

The sphingolipid pathway in *D. discoideum* is largely conserved

Figure 12 describes the reconstruction of the *D. discoideum* sphingolipid pathway. The sphingolipid pathway in *D. discoideum* is largely conserved, as shown by the detection of homologs and *D. discoideum* most likely possesses the enzymes required to construct complex phosphosphingolipids, as well as the necessary modifications (acyl chains, double bonds and hydroxyl groups) (Fig. 12, Table 2). This section highlights some interesting findings throughout the *D. discoideum* sphingolipid pathway and its plausible biological implications.

One interesting aspect of the *D. discoideum* sphingolipid pathway is the presence of one Cer putative synthase homolog: *Dd*CrsA (DDB_G0282607) (Table 2). This is comparable to *D. melanogaster*, where also one CerS (*Dm*Schlank) is expressed (Sociale et al., 2018). As comparison, mammals and yeast have six and three CerS, respectively (Körner and Fröhlich, 2022; Snider *et al.*, 2019). *Dd*CrsA shares 100% conservation of the active site which is part of the Lag1P motif (Fig. 37) (Pathak *et al.*, 2018). Judging by the presence of multiple Cer species (Fig. 19C) and *Dd*CrsA being the sole CerS detected (Table 2, Supplementary Table 1), it is likely that *Dd*CrsA has a lower substrate specificity than its mammalian or yeast counterparts. *Dd*CrsA has never been cloned. Consequently, it would be interesting to test whether this protein is sensitive to the CerS inhibitor, FB1, and if inhibiting the synthesis of Cer is toxic to the cell. Of note, preliminary result showed that after 50 hours of 3.75 µM FB1 treatment, *D. discoideum* still exhibits growth (Edwin Ufelmann, Gross praktikum). Taken together, being the sole putative CerS, *Dd*CrsA might be essential for *D. discoideum*.

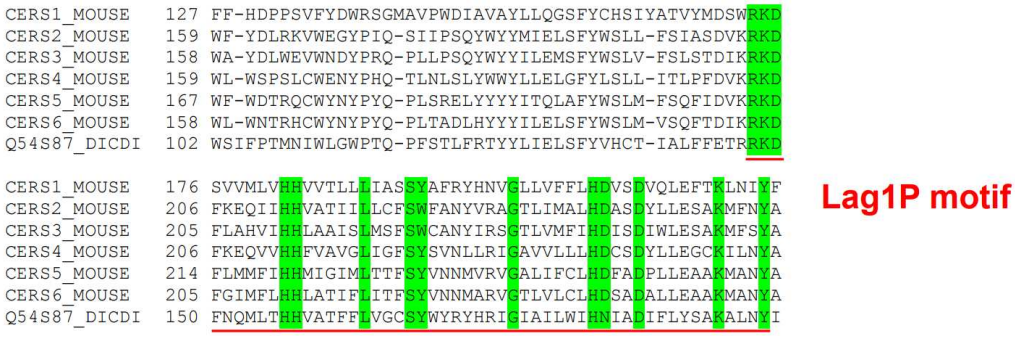

Fig. 37. Alignment of mouse CerS (CerS 1 – 6) with the one from *Dictyostelium discoideum* (*Dd*CrsA, DDB_G0282607). Green: catalytically relevant amino acids. Red line: Lag1P motif. Figure addapted from Pathak et al., (2018).

Because the presence of VLCFAs in *D. discoideum* sphingolipids was observed (Fig. 19, 20), I asked if fatty acid elongases are conserved in this organism. *Sc*Elo1, *Sc*Elo2 and *Sc*Elo3 are

required for fatty acid elongation in yeast, and deletion of each elongase results in a distinct complex phosposphingolipid species profile (Ejsing *et al.*, 2009). I looked for *Sc*Elo1, *Sc*Elo2 and *Sc*Elo3 homologues in *D. discoideum* and obtained 7-8 hits of highly similar proteins, two of which were annotated as *Dd*EloA (DDB_G0292896) and *Dd*EloB (DDB_G0281821) at dictybase (Supplementary Table 1). This suggests that *D. discoideum* is capable of producing VLCFAs.

In mammalian cells, Cer is transported from the ER to the Golgi by the START domain-containing Cer Transport (CERT) protein (Hanada et al., 2003) prior to the synthesis of SM at the Golgi (Huitema *et al.*, 2004). CERT has an FFAT motif that is recognised by ER-resident VAP-A and VAP-B and a PH domain that binds to PI(4)P at the Golgi membrane (Kumagai and Hanada, 2019). In *S. cerevisiae*, the ER-Golgi Cer transfer is less clear. In addition to lipid transport protein (LTP), vesicular trafficking has been proposed to play a role in ER-Golgi Cer transfer (Funato and Riezman, 2001; Limar et al., 2023; Liu et al., 2017). Recently, *Sc*Svf1 has been suggested to be an LTP that transports Cer from the ER to the Golgi in *S. cerevisiae* (Limar *et al.*, 2023). A direct BLAST search on the *D. discoideum* proteome did not yield any putative homolog of *Hs*CERT and *Sc*Svf1 in *D. discoideum* (Supplementary Table 1). However, I noted that in *D. discoideum*, there are two proteins that possess the a START domain: *Dd*FbxA (DDB_G0276887) and DDB_G0280895.

As previously mentioned*, S. cerevisiae* also generates more complex, mannosylated IPC (MIPC and M(IP)2C), in addition to IPC. There was no indication that the key enzymes (*Sc*Csg2, *Sc*Csh1, *Sc*Sur1 and *Sc*Ipt1) are conserved in *D. discoideum. A. thaliana,* on the other hand, converts IPC into GIPC (Mamode Cassim *et al.*, 2020; Markham et al., 2006). In *A. thaliana,* three GIPC enzymes have been identified: *At*IPUT1, *At*GMT1 and *At*GINT1 (Mamode Cassim *et al.*, 2020). A BLAST search of *At*GMT1 and *At*GINT1 did not yield any putative *D. discoideum* homologue, however, *At*IPUT1 yielded one hit (DDB_G0286945), as noted before.

Consequently, the sphingolipid pathway is largely conserved between plants, fungi and *D. discoideum*. The pathway conservation raises the possibility of that *D. discoideum* may be used as an alternative model system to study sphingolipid metabolism, especially in relation to phagocytosis and evolution.

Additional comments on the selection of CSS candidates

Figure 25 details the CSS candidate selection criteria as well as the information about the phylogeny, topology and conservation of *Dd*CSS1 and *Dd*CSS2. The main reason *Dd*CSS1 and *Dd*CSS2 were chosen for biochemical investigation is because their domain architecture is similar

to that of other known CSSs. Here, I explain why *Dd*CSS1 and *Dd*CSS2 were selected among the five other CSS candidates listed in Table 3.

Based on the assumptions that (i) the topology of the catalytic triad is essential for the synthesis of complex phosposphingolipids and that (ii) it is conserved among CSS across the eukaryotic kingdom, I reasoned that the catalytic amino acids from various CSS are conserved (would align together during sequence alignment). Hence, I performed a protein sequence alignment (MAFFT, G-INS) of the seven CSS candidates with 21 other CSSs from highly unrelated organisms and observed the alignment of the amino acids composing the catalytic triad (His-His-Asp) (Fig. 38). Only *Dd*CSS1, *Dd*CSS2 and *Dd*SppA contained an aligned catalytic triad, implying that these three proteins share similar active site topologies with other CSSs.

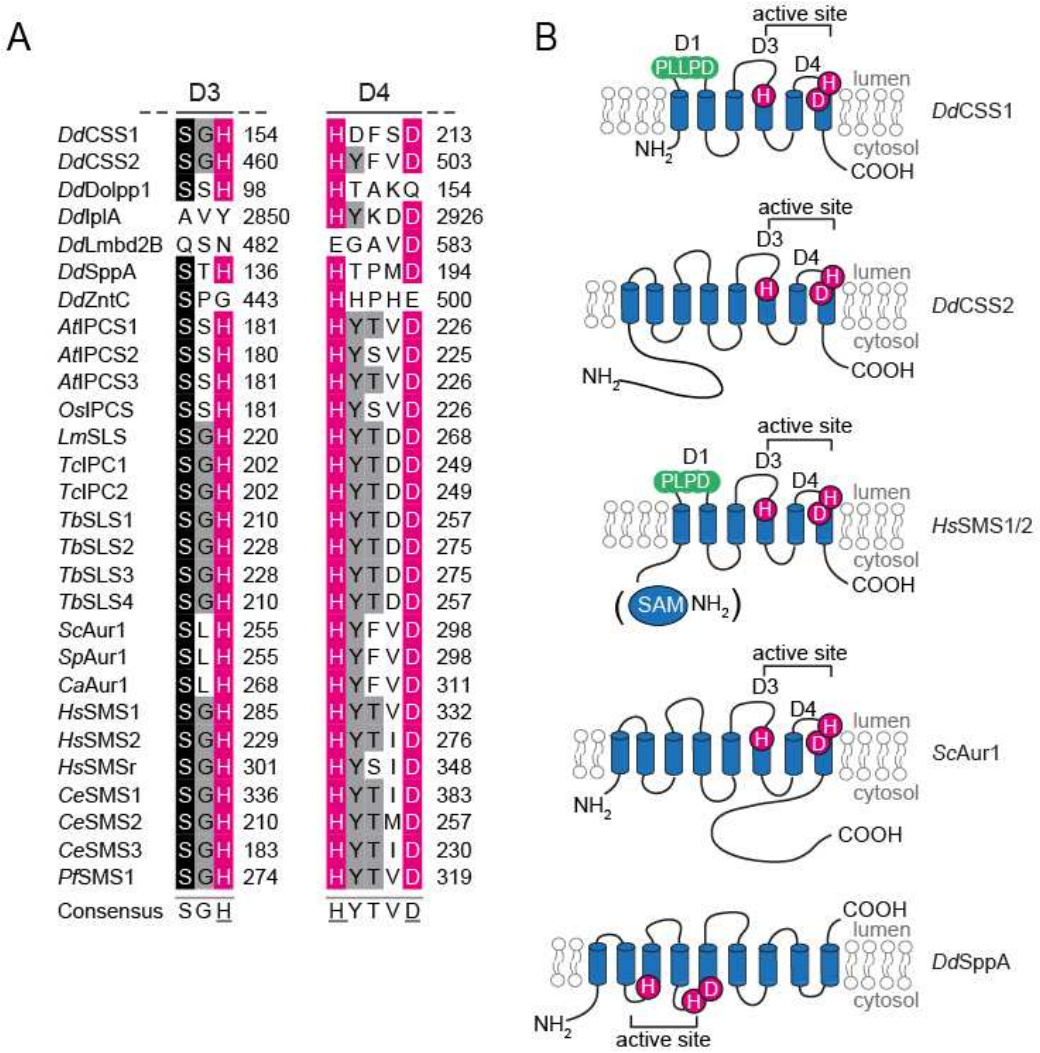

Fig. 38. *Dd*CSS1 and *Dd*CSS2, unlike other candidates, share a conserved protein topology with other known CSSs. **A:** Alignment of the D3 and D4 motifs of *Dd*CSS1, *Dd*CSS2, fungal, plant and human CSSs. **B:** Membrane topology of *Dd*CSS1 and *Dd*CSS2. The topology of *Dd*CSS1 and *Dd*CSS2 was reconstructed using MembraneFold (https://biolib.com/KU/MembraneFold/).

All complex phosphosphingolipid synthases discovered to date contain an active site that faces the lumen (Denny *et al.*, 2006; Huitema *et al.*, 2004; Levine *et al.*, 2000). To determine whether the active sites of the proteins face the lumen or the cytosol, MembraneFold (Gutierrez *et al.*, 2022) was used for prediction. As a result, it was found that the active site of *Dd*SppA faces the cytosol, unlike *Dd*CSS1, *Dd*CSS2 and other CSS, such as *Hs*SMS1 or ScAur1 (Fig. 38B). Consequently, this protein was excluded also because of the fact that *Dd*SppA is most likely a homolog of sphingosine-1-phosphate phosphatase. It has been annotated at dictybase, and the direct BLAST search of *Hs*SGPP1 (human sphingosine-1-phosphate phosphatase) yielded only *Dd*SppA.

_Dd_CSS2/_Dd_IPCS1 is an IPC synthase and shared many features with its yeast homologue

Bio-IT analysis reveals two promising CSS candidates: *Dd*CSS1 and *Dd*CSS2 (Fig. 25). *Dd*CSS2, on the other hand, qualified as an IPC synthase based on the following criteria: (i) cell-free expressed *Dd*CSS2 produces IPC when Cer and PI as the headgroup donors are added; (ii) *Dd*CSS2 shares conserved sequence motifs containing active site residues with known IPC synthases in plants and yeast; (iii) *Dd*CSS2 is predicted to adopt a membrane topology similar to that of IPC synthases in plants and yeast, whereby the active site residues are facing the exoplasmic leaflet, hence the side of the membrane where IPC production is believed to occur; (iv) *Dd*CSS2 localises to the Golgi apparatus, the organelle previously established as the site of IPC production in plants and yeast (Levine *et al.*, 2000; Wang *et al.*, 2008). We propose to rename *Dd*CSS2 as *Dd*IPCS1 for IPC synthase 1.

Bio-IT analysis reveals two promising CSS candidates: *Dd*CSS1 and *Dd*CSS2 (Fig. 25). *Dd*CSS2, on the other hand, qualified as IPC synthase based on the following criteria: (i) cell-free expressed *Dd*CSS2 produces IPC when Cer and PI as the headgroup donor were added; (ii) *Dd*CSS2 shares conserved sequence motifs containing active site residues with known IPC synthases in plants and fungi; (iii) *Dd*CSS2 is predicted to adopt a membrane topology similar to that of IPC synthases in plants and fungi whereby the active site residues are facing the exoplasmic leaflet, hence the side of the membrane where IPC production is believed to occur; (iv) *Dd*CSS2 localises to the Golgi apparatus, the organelle previously established as the site of IPC production in plants and fungi (Levine *et al.*, 2000; Wang *et al.*, 2008).

In terms of *Dd*CSS1, our current experimental setup produced no obvious CSS activities (Fig. 27B). The lack of NBD-Cer turnover does not rule out the possibility that *Dd*CSS1 is a CSS, however, a BLAST search revealed the similarities between *Dd*CSS1 and the yeast DAG pyrophosphate phosphatase 1 (*Sc*Dpp1). *Sc*Dpp1 is an enzyme that dephosphorylates DAG

pyrophosphate to generate phosphatidate (PA) and subsequently dephosphorylates PA to release DAG. Whether *Dd*CSS1 mediates dephosphorylation of PA remains to be established.

Another striking characteristic of *Dd*CSS2/*Dd*IPCS1 is that, unlike *Sc*Aur1 (Berchtold *et al.*, 2012; Nagiec *et al.*, 1997; Sevova *et al.*, 2010), it appears to be highly resistant to AbA. This was demonstrated by both the CFE assay (Fig. 29A) and the addition of AbA to living cells (Fig. 29B). In yeast, the inhibition of *Sc*Aur1 by AbA is dependent on the amino acid residues 137, 157 and 158 (Hashida-Okado *et al.*, 1996; Heidler and Radding, 1995). These amino acid residues are partially part of the IPC1 domain and are not conserved in *Dd*CSS2/*Dd*IPCS1 (Fig. 26B). *Dd*CSS2/*Dd*IPCS1 resistance to AbA suggests that despite its close relation to fungal Aur1, this protein might have undergone natural selection to develop unique resistance mechanisms. AbA was originally isolated from *Aureobasidium pullulans*, a yeast-like fungus found in *D. discoideum*'s natural habitat (Di Francesco et al., 2023). Aside from AbA, there are alternative IPC synthase inhibitors such as khafrefungin and rustmicin (Aeed et al., 2009). Because khafrefungin and rustmicin have been shown to inhibit IPC synthase differently than AbA (reversible versus irreversible), it is possible that these compounds have inhibitory properties against *Dd*CSS2/*Dd*IPCS1 (Aeed *et al.*, 2009). However, this needs experimental validation.

Our findings raise the question of whether *Dd*IPCS1 is the sole IPC synthase in *D. discoideum*. Interestingly, all of our attempts to generate *Dd*IPCS1 knockouts by homologous recombination failed, indicating that *Dd*IPCS1 might have non-redundant functions. Similar observations have been made in *A. thaliana* and *S. cerevisiae,* where IPC synthesising enzymes are essential (Heidler and Radding, 1995; Rennie et al., 2014), while in *T. brucei*, the complete RNAi knock-down of the entire gene locus encoding *Tb*SLS1-4 is lethal (Sutterwala *et al.*, 2008). Thus, generating conditional *Dd*IPCS1 knockouts might provide valuable insights about the essentiality of IPC synthesis in *D. discoideum* and would allow us to identify the specific substrates and mechanisms of *Dd*IPCS1.

The compartmentalisation of *D. discoideum* sphingolipid metabolism

Here, we report that *Dd*CSS2/*Dd*IPCS1, expressed by an extrachromosomal expression vector, displays localisation at the Golgi (Fig. 30) and the CV (Fig. 32). The Golgi localisation of *Dd*CSS2/*Dd*IPCS1 was expected because most complex phosphosphingolipid synthases localise to this organelle (Denny *et al.*, 2006; Huitema *et al.*, 2004; Levine *et al.*, 2000; Wang *et al.*, 2008), with some exceptions such as *Hs*SMSr, which resides at the ER (Vacaru *et al.*, 2009), and *Hs*SMS2 which has dual localisation (plasma membrane and the Golgi) (Tafesse et al., 2007). Strikingly, *Dd*CSS2/*Dd*IPCS1 is also localised at the CV (Fig. 32). The CV mediates

osmoregulation and the discharge of excess water and toxic ions (Barisch *et al.*, 2018; Gabriel *et al.*, 1999). This discharge is carried out by a giant kiss-and-run event where two membranes, the plasma membrane and the CV membranes, only transiently fuse but do not completely merge (Essid *et al.*, 2012).

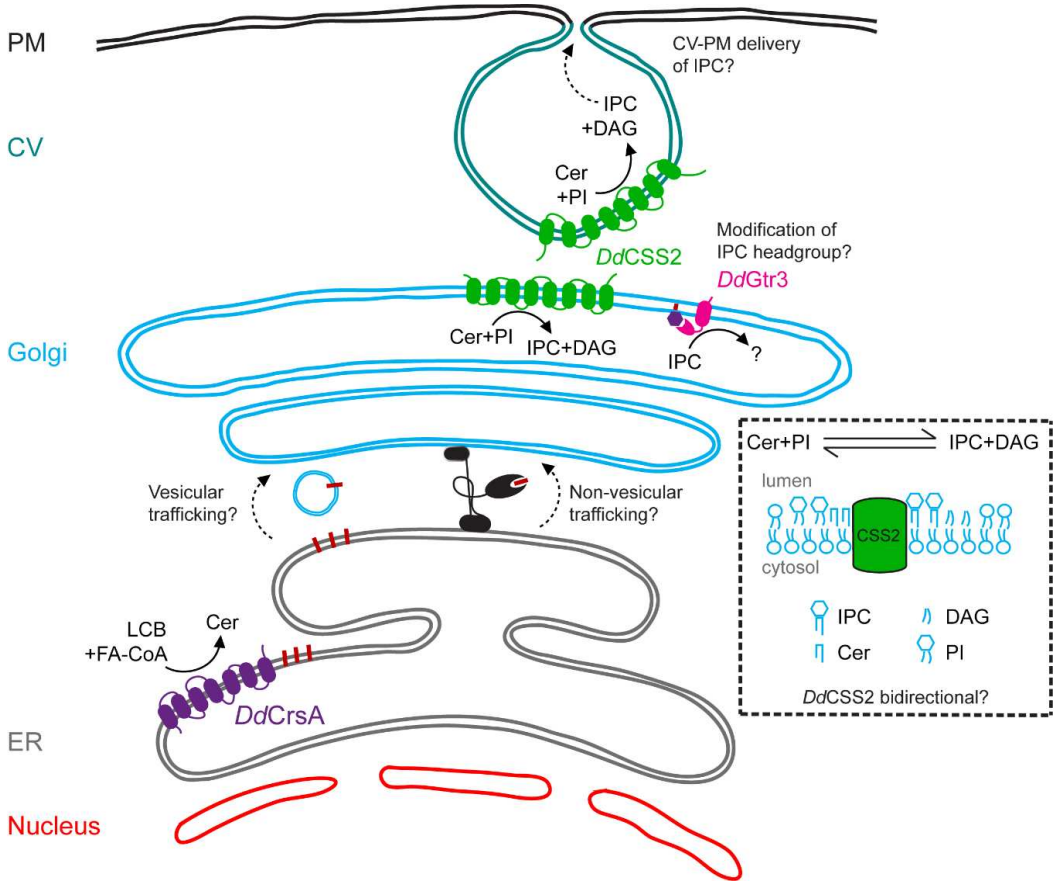

Fig. 39. *Dd*CSS2/*Dd*IPCS1 converts Cer to IPC at the Golgi and the CV. The model includes some open questions regarding *D. discoideum*'s sphingolipid metabolism. Cer are likely synthesized at the ER by *Dd*CrsA. It is not clear how Cer are transported to the Golgi. Some possible mechanisms are vesicular or non-vesicular trafficking (or both). At the Golgi, Cer are presumably converted to IPC by *Dd*CSS2/*Dd*IPCS1 which transfers the phosphoinositol headgroup from PI, yielding DAG as side product. *Dd*CSS2/*Dd*IPCS1, is also localised at the CV, where the conversion of Cer to IPC probably also happens. I speculated that the localisation of *Dd*CSS2/*Dd*IPCS1 contributes to the transfer of IPC (or its derivatives) to the outer leaflet of the plasma membrane. In addition, the directionality of IPC synthase reaction has not yet been deterermined.

I speculate that *Dd*CSS2/*Dd*IPCS1 might be involved in delivering IPC to the plasma membrane by CV discharge (Fig. 39). In mammalian cells, the gradient of complex phosposphingolipid is maintained by the localisation of *Hs*SMS2, and its mislocalisation to the ER perturbs the gradient (Sokoya *et al.*, 2022). Such a gradient pathway most likely does exist in *D. discoideum*; however, this needs experimental validation, for example, by combining lipidomics with organellar purifications (Sokoya *et al.*, 2022). Furthermore, it is also interesting to ask if the mislocalisation

of *Dd*CSS2/*Dd*IPCS1, for instance, by organellar targeting (John Peter et al., 2022) alters the sphingolipid gradient in *D. discoideum*.

Another speculation is that the *Dd*CSS2/*Dd*IPCS1 localisation at the CV is important to maintain the membrane lipid homeostasis of the organelle. The catalytic activity of *Hs*SMS1 and *Hs*SMS2 is bidirectional (Huitema *et al.*, 2004). This bidirectionality might be important to maintain the homeostasis of the lipid composition of the organellar membrane and, in turn, may influence the recruitment of proteins regulating the CV discharge cycle, such as *Dd*Rab11a-GTPase (Du *et al.*, 2008). By engineering a conditional knockout of *Dd*CSS2/*Dd*IPCS1, one could explore the link between *Dd*CSS2/*Dd*IPCS1 localisation and CV function. The model in Figure 39 describes some unexplained questions regarding the sphingolipid metabolism in *D. discoideum* as well as the compartmentalization of IPC synthesis.

Ergosterol and complex phosphosphingolipids (IPC, MIPC, and M(IP)2C) clusters within the *S. cerevisiae* membranes to generate the highly debated lipid-raft microdomains (Dickson et al., 2006). I reason that the same is true for *D. discoideum*. The free sterol-binding D4H probe binds to *Dd*V-ATPase-positive lysosomes but not to *Dd*vacuolin-positive post-lysosomes (Fig. 34). This suggests that the sterols/sphingolipids ratio in the cytoplasmic leaflet of the lysosome is high enough for D4H to bind, whereas it is not in the post-lysosome. In other words, as the phagosome matures, the concentration of sphingolipids may increase, quenching the sterols and rendering them inaccessible for the D4H probe. This is consistent with previous findings that sterols and sphingolipids are enriched in both *D. discoideum* and mammalian cells during the latter phases of the phagosome (Pathak *et al.*, 2018).

D. discoideum – *M. marinum* model system for investigating the role of sphingolipids during mycobacterial infection

Host glycerolipids and sphingolipids are relevant for mycobacteria infection. Mycobacteria secrete a plethora of lipid-modifying enzymes and import host sterols, fatty acids and Cer for its own metabolism (Barisch and Soldati, 2017; Foulon *et al.*, 2022; Nazarova et al., 2017; Pandey and Sassetti, 2008; Speer *et al.*, 2015). For sphingolipids in particular, the deletion of *M. tuberculosis* sphingomyelinase, *Mt*SpmT, attenuates intracellular growth inside macrophages (Speer *et al.*, 2015). To investigate if the sphingolipid metabolism is altered during infection, I looked at the transcriptomics analysis from *M. marinum*-infected *D. discoideum* (Hanna et al., 2019). Interestingly, enzymes of the sphingolipid metabolic pathway are differentially expressed,

particularly during the later stages of infection, where the vacuole escapes likely occurs (Fig. 40). Also during later stages, an upregulation of *Dd*CSS2/*Dd*IPCS1 was observed (Fig. 40).

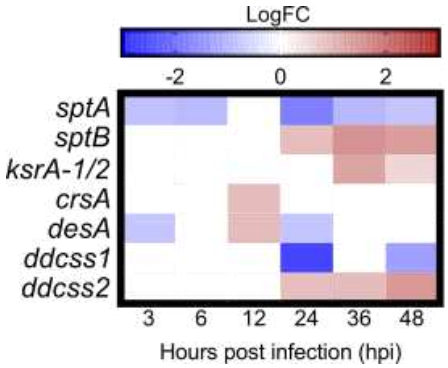

Annotation	Dictybase ID	Ortholog of
sptA	DDB_G0268056	Serine palmitoyltransferase
sptB	DDB_G0291283	
ksrA-1/2	DDB_G0272883	Sphingosine reductase
crsA	DDB_G0282607	Ceramide synthase
desA	DDB_G0269738	Sphingolipid desaturase
ddcss1	DDB_G0284367	Complex sphingolipid synthase
ddcss2	DDB_G0268928	

Fig. 40. *D. discoideum* sphingolipid enzymes are differentially expressed during the late stages of *M. marinum* infection. *D. discoideum* was infected with *M. marinum* prior to RNAseq analysis. The up- and down- regulation of the sphingolipid genes is expressed in LogFC. Transcriptomics data obtained from Hanna et al., (2019). Figure editing by Edwin Ufelmann.

*Dd*CSS2/*Dd*IPCS1 is recruited to the MCV (Fig. 33), however, no apparent accumulation on the phagosomes was observed (Fig. 32). This might be explained by the fact that the MCV recruits CV proteins to some extend. For instance, the CV resident zinc transporter, *Dd*ZntA, is localised to the MCV during *M. marinum* infection (Hanna *et al.*, 2021), but not to p80-positive endosomes (Barisch *et al.*, 2018). *Dd*Rab11a and *Dd*Rab11c and other CV proteins have also been shown to localise to the MCV, both by microscopy and proteomics (Guého et al., 2023; Hanna *et al.*, 2021). In addition, although the inhibitory properties of FB1 and myrioicin on *D. discoideum* cells have not been validated, preliminary evidence (N =1) suggests that blocking SPTs and CerS in D. discoideum by adding these inhibitors accelerated mycobacteria growth (Fig. 35). The growth increase seems to be more apparent for FB1 treatment (Fig. 35). This suggests that *M. marinum* growth favours lower concentration of Cer. One hypothesis is that Cer promotes autophagy, which is detrimental for intracellular persistence (Pattingre et al., 2009).

Additionally, sphingolipids may also impact phagocytosis. Knocking-out mammalian SPTLC2 and SMS2 greatly reduced the uptake of *M. tuberculosis.* This is linked with the failed segregation of the regulatory phosphatase CD45 from the phagocytic cup, highlighting the role of sphingolipids in signalling at the cell surface (Niekamp et al., 2021). With this in mind, one could ask if the reduction of bacterial uptake through the disruption of the sphingolipid pathway is evolutionary conserved in *D. discoideum*. As *D. discoideum* is a well-established model organism to investigate phagocytosis and pinocytosis (Vines and King, 2019), protocols for the phagocytosis assay are well established. In conclusion, studying the role of sphingolipids in mycobacteria infection using the *D. discoideum* – *M. marinum* model system is feasible and might contribute to the development of novel tuberculosis therapeutics.

CONCLUSION

This work provides an extensive characterization of the *D. discoideum* lipidome and sphingolipidome. I showed that the sphingolipid pathway is conserved in *D. discoideum* and demonstrated that *D. discoideum* produces IPC, like plants and yeast. The protein *Dd*CSS2/*Dd*IPCS1 has been identified as an IPC synthase. Through localisation studies, it was found that *Dd*CSS2/*Dd*IPCS1 is localised at the Golgi, the CV and the MCV. Collectively, this study laid the groundwork for the investigation of *D. discoideum* sphingolipids.

OUTLOOK

The limitations of this study can be are addressed through a number of experiments: One suggestion is to construct a conditional knock-out of *Dd*CSS2/*Dd*IPCS1. This is achieved through RNA interference or by utilizing drug-inducible expression. The conditional knockout would confirm the lethality of *Dd*CSS2/*Dd*IPCS1 ablation and may provide important insights regarding how IPC synthesis influences cell function and organellar morphology. Another crucial investigation is to confirm the endogenous localisation of *Dd*CSS2/*Dd*IPCS1, either by knock-in using homologous recombination or by performing organellar purification coupled with biochemical assays. Such experiments will further strengthen the claim that *Dd*CSS2 is localised at the CV and the Golgi. Also, performing sphingolipidomics with a synthetic IPC standard would be of an advantage, as the composition of the IPC in mol % has not been determined in this study. To investigate how *M. marinum* remodels the MCVs membrane, one endeavor is to perform lipidomics on purified endosomes and MCV of *D. discoideum* to observe how the lipid composition of the organelle develops over time. Alternatively, investigating the lipidomics and sphingolipidomics of *D. discoideum* in response to mycobacterial infection may provide an answer on which lipids are up- or down-regulated during infection. I anticipate future studies to elucidate the role of sphingolipids in phagocytosis and infection biology, using *D. discoideum* as the model organism.

REFERENCES

Aeed, P.A., Young, C.L., Nagiec, M.M., and Elhammer, A.P. (2009). Inhibition of inositol phosphorylceramide synthase by the cyclic peptide aureobasidin A. *Antimicrob Agents Chemother 53*, 496-504. 10.1128/aac.00633-08.

Anand, A., Mazur, A.-C., Rosell-Arevalo, P., Franzkoch, R., Breitsprecher, L., Listian, S.A., Hüttel, S.V., Müller, D., Schäfer, D.G., Vormittag, S., et al. (2023). ER-dependent membrane repair of mycobacteria-induced vacuole damage. *bioRxiv*, 2023.2004.2017.537276. 10.1101/2023.04.17.537276.

Barisch, C., Kalinina, V., Lefrançois, L.H., Appiah, J., López-Jiménez, A.T., and Soldati, T. (2018). Localization of all four ZnT zinc transporters in *Dictyostelium* and impact of ZntA and ZntB knockout on bacteria killing. *J Cell Sci 131*. 10.1242/jcs.222000.

Barisch, C., Paschke, P., Hagedorn, M., Maniak, M., and Soldati, T. (2015). Lipid droplet dynamics at early stages of *Mycobacterium marinum* infection in *Dictyostelium*. *Cell Microbiol 17*, 1332-1349. 10.1111/cmi.12437.

Barisch, C., and Soldati, T. (2017). *Mycobacterium marinum* Degrades Both Triacylglycerols and Phospholipids from Its *Dictyostelium* Host to Synthesise Its Own Triacylglycerols and Generate Lipid Inclusions. *PLoS Pathog 13*, e1006095. 10.1371/journal.ppat.1006095.

Barry, N.P., and Bretscher, M.S. (2010). *Dictyostelium* amoebae and neutrophils can swim. *Proc Natl Acad Sci U S A 107*, 11376-11380. 10.1073/pnas.1006327107.

Bartlett, E.M., and Lewis, D.H. (1970). Spectrophotometric determination of phosphate esters in the presence and absence of orthophosphate. *Anal Biochem 36*, 159-167. 10.1016/0003-2697(70)90343-x.

Beeler, T.J., Fu, D., Rivera, J., Monaghan, E., Gable, K., and Dunn, T.M. (1997). SUR1 (CSG1/BCL21), a gene necessary for growth of *Saccharomyces cerevisiae* in the presence of high Ca2+ concentrations at 37 degrees C, is required for mannosylation of inositolphosphorylceramide. *Mol Gen Genet* 255, 570-579. 10.1007/s004380050530.

Berchtold, D., Piccolis, M., Chiaruttini, N., Riezman, I., Riezman, H., Roux, A., Walther, T.C., and Loewith, R. (2012). Plasma membrane stress induces relocalization of Slm proteins and activation of TORC2 to promote sphingolipid synthesis. *Nat Cell Biol 14*, 542-547. 10.1038/ncb2480.

Bligh, E.G., and Dyer, W.J. (1959). A rapid method of total lipid extraction and purification. *Can J Biochem Physiol 37*, 911-917.

Bosmani, C., Leuba, F., Hanna, N., Bach, F., Burdet, F., Pagni, M., Hagedorn, M., and Soldati, T. (2020). Vacuolins and myosin VII are required for phagocytic uptake and phagosomal membrane recycling in *Dictyostelium discoideum*. *J Cell Sci 133*. 10.1242/jcs.242974.

Boulais, J., Trost, M., Landry, C.R., Dieckmann, R., Levy, E.D., Soldati, T., Michnick, S.W., Thibault, P., and Desjardins, M. (2010). Molecular characterization of the evolution of phagosomes. *Mol Syst Biol 6*, 423. 10.1038/msb.2010.80.

Braverman, N.E., and Moser, A.B. (2012). Functions of plasmalogen lipids in health and disease. *Biochim Biophys Acta 1822*, 1442-1452. 10.1016/j.bbadis.2012.05.008.

Cardenal-Muñoz, E., Barisch, C., Lefrançois, L.H., López-Jiménez, A.T., and Soldati, T. (2017). When Dicty Met Myco, a (Not So) Romantic Story about One Amoeba and Its Intracellular Pathogen. *Front Cell Infect Microbiol 7*, 529. 10.3389/fcimb.2017.00529.

Carvalho, M., Sampaio, J.L., Palm, W., Brankatschk, M., Eaton, S., and Shevchenko, A. (2012). Effects of diet and development on the *Drosophila* lipidome. *Mol Syst Biol 8*, 600. 10.1038/msb.2012.29.

Castellanos-Castro, S., Cerda-García-Rojas, C.M., Javier-Reyna, R., Pais-Morales, J., Chávez-Munguía, B., and Orozco, E. (2016). Identification of the phospholipid lysobisphosphatidic acid in the protozoan *Entamoeba histolytica*: An active molecule in endocytosis. *Biochem Biophys Rep 5*, 224-236. 10.1016/j.bbrep.2015.12.010.

Chen, M., Markham, J.E., and Cahoon, E.B. (2012). Sphingolipid Δ8 unsaturation is important for glucosylceramide biosynthesis and low-temperature performance in *Arabidopsis*. Plant J *69*, 769-781. 10.1111/j.1365-313X.2011.04829.x.

Chen, M., Markham, J.E., Dietrich, C.R., Jaworski, J.G., and Cahoon, E.B. (2008). Sphingolipid long-chain base hydroxylation is important for growth and regulation of sphingolipid content and composition in *Arabidopsis*. *Plant Cell 20*, 1862-1878. 10.1105/tpc.107.057851.

Cingolani, F., Futerman, A.H., and Casas, J. (2016). Ceramide synthases in biomedical research. *Chem Phys Lipids 197*, 25-32. 10.1016/j.chemphyslip.2015.07.026.

Clark, J., Kay, R.R., Kielkowska, A., Niewczas, I., Fets, L., Oxley, D., Stephens, L.R., and Hawkins, P.T. (2014). Dictyostelium uses ether-linked inositol phospholipids for intracellular signalling. *Embo j 33*, 2188-2200. 10.15252/embj.201488677.

Clarke, M., Maddera, L., Engel, U., and Gerisch, G. (2010). Retrieval of the vacuolar H-ATPase from phagosomes revealed by live cell imaging. *PLoS One 5*, e8585. 10.1371/journal.pone.0008585.

da Silva, T.F., Eira, J., Lopes, A.T., Malheiro, A.R., Sousa, V., Luoma, A., Avila, R.L., Wanders, R.J., Just, W.W., Kirschner, D.A., et al. (2014). Peripheral nervous system plasmalogens regulate Schwann cell differentiation and myelination. *J Clin Invest 124*, 2560-2570. 10.1172/jci72063.

da Silva, T.F., Sousa, V.F., Malheiro, A.R., and Brites, P. (2012). The importance of ether-phospholipids: a view from the perspective of mouse models. *Biochim Biophys Acta 1822*, 1501-1508. 10.1016/j.bbadis.2012.05.014.

Das, A., Brown, M.S., Anderson, D.D., Goldstein, J.L., and Radhakrishnan, A. (2014). Three pools of plasma membrane cholesterol and their relation to cholesterol homeostasis. *Elife 3*. 10.7554/eLife.02882.

Dean, J.M., and Lodhi, I.J. (2018). Structural and functional roles of ether lipids. *Protein Cell 9*, 196-206. 10.1007/s13238-017-0423-5.

Denny, P.W., Shams-Eldin, H., Price, H.P., Smith, D.F., and Schwarz, R.T. (2006). The protozoan inositol phosphorylceramide synthase: a novel drug target that defines a new class of sphingolipid synthase. *J Biol Chem 281*, 28200-28209. 10.1074/jbc.M600796200.

Di Francesco, A., Zajc, J., and Stenberg, J.A. (2023). *Aureobasidium* spp.: Diversity, Versatility, and Agricultural Utility. Horticulturae *9*, 59.

Dickson, R.C., Sumanasekera, C., and Lester, R.L. (2006). Functions and metabolism of sphingolipids in *Saccharomyces cerevisiae*. *Prog Lipid Res 45*, 447-465. 10.1016/j.plipres.2006.03.004.

Du, F., Edwards, K., Shen, Z., Sun, B., De Lozanne, A., Briggs, S., and Firtel, R.A. (2008). Regulation of contractile vacuole formation and activity in *Dictyostelium*. *Embo j 27*, 2064-2076. 10.1038/emboj.2008.131.

Du, X., Herrfurth, C., Gottlieb, T., Kawelke, S., Feussner, K., Rühling, H., Feussner, I., and Maniak, M. (2014). *Dictyostelium discoideum* Dgat2 can substitute for the essential function of Dgat1 in triglyceride production but not in ether lipid synthesis. *Eukaryot Cell 13*, 517-526. 10.1128/ec.00327-13.

Dunn, J.D., Bosmani, C., Barisch, C., Raykov, L., Lefrançois, L.H., Cardenal-Muñoz, E., López-Jiménez, A.T., and Soldati, T. (2017). Eat Prey, Live: *Dictyostelium discoideum* As a Model for Cell-Autonomous Defenses. *Front Immunol 8*, 1906. 10.3389/fimmu.2017.01906.

Eichinger, L., Pachebat, J.A., Glöckner, G., Rajandream, M.A., Sucgang, R., Berriman, M., Song, J., Olsen, R., Szafranski, K., Xu, Q., et al. (2005). The genome of the social amoeba *Dictyostelium discoideum*. *Nature 435*, 43-57. 10.1038/nature03481.

Eisenberg, T., and Büttner, S. (2014). Lipids and cell death in yeast. *FEMS Yeast Res 14*, 179-197. 10.1111/1567-1364.12105.

Eising, S., Thiele, L., and Fröhlich, F. (2019). A systematic approach to identify recycling endocytic cargo depending on the GARP complex. *Elife 8*. 10.7554/eLife.42837.

Ejsing, C.S., Sampaio, J.L., Surendranath, V., Duchoslav, E., Ekroos, K., Klemm, R.W., Simons, K., and Shevchenko, A. (2009). Global analysis of the yeast lipidome by quantitative shotgun mass spectrometry. *Proc Natl Acad Sci U S A 106*, 2136-2141. 10.1073/pnas.0811700106.

Ellingson, J.S. (1974). Changes in the phospholipid composition in the differentiating cellular slime mold, *Dictyostelium discoideum*. *Biochim Biophys Acta 337*, 60-67. 10.1016/0005-2760(74)90040-x.

Esch, B.M., Limar, S., Bogdanowski, A., Gournas, C., More, T., Sundag, C., Walter, S., Heinisch, J.J., Ejsing, C.S., André, B., and Fröhlich, F. (2020). Uptake of exogenous serine is important to maintain sphingolipid homeostasis in *Saccharomyces cerevisiae*. *PLoS Genet 16*, e1008745. 10.1371/journal.pgen.1008745.

Essid, M., Gopaldass, N., Yoshida, K., Merrifield, C., and Soldati, T. (2012). Rab8a regulates the exocyst-mediated kiss-and-run discharge of the *Dictyostelium* contractile vacuole. *Mol Biol Cell 23*, 1267-1282. 10.1091/mbc.E11-06-0576.

Folch, J., Lees, M., and Sloane Stanley, G.H. (1957). A simple method for the isolation and purification of total lipides from animal tissues. *J Biol Chem 226*, 497-509.

Foulon, M., Listian, S.A., Soldati, T., and Barisch, C. (2022). Chapter 6 - Conserved mechanisms drive host-lipid access, import, and utilization in *Mycobacterium tuberculosis* and *M. marinum*. In Biology of Mycobacterial Lipids, Z. Fatima, and S. Canaan, eds. (Academic Press), pp. 133-161. https://doi.org/10.1016/B978-0-323-91948-7.00011-7.

Fröhlich, F., Petit, C., Kory, N., Christiano, R., Hannibal-Bach, H.K., Graham, M., Liu, X., Ejsing, C.S., Farese, R.V., and Walther, T.C. (2015). The GARP complex is required for cellular sphingolipid homeostasis. *Elife 4*. 10.7554/eLife.08712.

Funato, K., and Riezman, H. (2001). Vesicular and nonvesicular transport of ceramide from ER to the Golgi apparatus in yeast. *J Cell Biol 155*, 949-959. 10.1083/jcb.200105033.

Gabriel, D., Hacker, U., Köhler, J., Müller-Taubenberger, A., Schwartz, J.M., Westphal, M., and Gerisch, G. (1999). The contractile vacuole network of *Dictyostelium* as a distinct organelle: its dynamics visualized by a GFP marker protein. *J Cell Sci 112 (Pt 22)*, 3995-4005. 10.1242/jcs.112.22.3995.

Gaudet, R.G., Bradfield, C.J., and MacMicking, J.D. (2016). Evolution of Cell-Autonomous Effector Mechanisms in Macrophages versus Non-Immune Cells. *Microbiol Spectr 4*. 10.1128/microbiolspec.MCHD-0050-2016.

Glöckner, G., Lawal, H.M., Felder, M., Singh, R., Singer, G., Weijer, C.J., and Schaap, P. (2016). The multicellularity genes of dictyostelid social amoebas. *Nat Commun 7*, 12085. 10.1038/ncomms12085.

Goh, E.X.Y., and Guan, X.L. (2021). Targeted Lipidomics of *Drosophila* melanogaster During Development. *Methods Mol Biol 2306*, 187-213. 10.1007/978-1-0716-1410-5_13.

Goldfine, H. (2010). The appearance, disappearance and reappearance of plasmalogens in evolution. *Prog Lipid Res 49*, 493-498. 10.1016/j.plipres.2010.07.003.

Goren, M.A., Nozawa, A., Makino, S., Wrobel, R.L., and Fox, B.G. (2009). Cell-free translation of integral membrane proteins into unilamelar liposomes. *Methods Enzymol 463*, 647-673. 10.1016/s0076-6879(09)63037-8.

Gräf, R., Daunderer, C., and Schliwa, M. (1999). Cell cycle-dependent localization of monoclonal antibodies raised against isolated *Dictyostelium* centrosomes. *Biol Cell 91*, 471-477. 10.1111/j.1768-322x.1999.tb01102.x.

Gröschel, M.I., Sayes, F., Simeone, R., Majlessi, L., and Brosch, R. (2016). ESX secretion systems: mycobacterial evolution to counter host immunity. *Nat Rev Microbiol 14*, 677-691. 10.1038/nrmicro.2016.131.

Gruenberg, J. (2020). Life in the lumen: The multivesicular endosome. *Traffic 21*, 76-93. 10.1111/tra.12715.

Gruenheit, N., Baldwin, A., Stewart, B., Jaques, S., Keller, T., Parkinson, K., Salvidge, W., Baines, R., Brimson, C., Wolf, J.B., et al. (2021). Mutant resources for functional genomics in *Dictyostelium discoideum* using REMI-seq technology. *BMC Biol 19*, 172. 10.1186/s12915-021-01108-y.

Guého, A., Bosmani, C., Nitschke, J., and Soldati, T. (2023). Proteomic characterization of the *Mycobacterium marinum*-containing vacuole in *Dictyostelium discoideum*. *bioRxiv*, 592717. 10.1101/592717.

Gutierrez, S., Tyczynski, W., Boomsma, W., Teufel, F., and Winther, O. (2022). MembraneFold: Visualising transmembrane protein structure and topology. *bioRxiv*.

Hagedorn, M., Neuhaus, E.M., and Soldati, T. (2006). Optimized fixation and immunofluorescence staining methods for *Dictyostelium* cells. *Methods Mol Biol 346*, 327-338. 10.1385/1-59745-144-4:327.

Hagedorn, M., and Soldati, T. (2007). Flotillin and RacH modulate the intracellular immunity of *Dictyostelium* to *Mycobacterium marinum* infection. *Cell Microbiol 9*, 2716-2733. 10.1111/j.1462-5822.2007.00993.x.

Hallgren, J., Tsirigos, K.D., Pedersen, M.D., Almagro Armenteros, J.J., Marcatili, P., Nielsen, H., Krogh, A., and Winther, O. (2022). DeepTMHMM predicts alpha and beta transmembrane proteins using deep neural networks. *bioRxiv*, 2022.2004.2008.487609. 10.1101/2022.04.08.487609.

Hama, H. (2010). Fatty acid 2-Hydroxylation in mammalian sphingolipid biology. *Biochim Biophys Acta 1801*, 405-414. 10.1016/j.bbalip.2009.12.004.

Han, X. (2016). Fragmentation Patterns of Sphingolipids. In Lipidomics: Comprehensive Mass Spectrometry of Lipids, (Willey). 10.1002/9781119085263.

Hanada, K., Kumagai, K., Yasuda, S., Miura, Y., Kawano, M., Fukasawa, M., and Nishijima, M. (2003). Molecular machinery for non-vesicular trafficking of ceramide. *Nature 426*, 803-809. 10.1038/nature02188.

Hanna, N., Burdet, F., Melotti, A., Bosmani, C., Kicka, S., Hilbi, H., Cosson, P., Pagni, M., and Soldati, T. (2019). Time-resolved RNA-seq profiling of the infection of *Dictyostelium discoideum* by *Mycobacterium marinum* reveals an integrated host response to damage and stress. *bioRxiv*, 590810. 10.1101/590810.

Hanna, N., Koliwer-Brandl, H., Lefrançois, L.H., Kalinina, V., Cardenal-Muñoz, E., Appiah, J., Leuba, F., Gueho, A., Hilbi, H., Soldati, T., and Barisch, C. (2021). Zn(2+) Intoxication of *Mycobacterium marinum* during *Dictyostelium discoideum* Infection Is Counteracted by Induction of the Pathogen Zn(2+) Exporter CtpC. *mBio 12*. 10.1128/mBio.01313-20.

Hannun, Y.A., and Obeid, L.M. (2018). Sphingolipids and their metabolism in physiology and disease. *Nat Rev Mol Cell Biol 19*, 175-191. 10.1038/nrm.2017.107.

Harayama, T., and Riezman, H. (2018). Understanding the diversity of membrane lipid composition. *Nat Rev Mol Cell Biol 19*, 281-296. 10.1038/nrm.2017.138.

Hashida-Okado, T., Ogawa, A., Endo, M., Yasumoto, R., Takesako, K., and Kato, I. (1996). AUR1, a novel gene conferring aureobasidin resistance on *Saccharomyces cerevisiae*: a study of defective morphologies in Aur1p-depleted cells. *Mol Gen Genet 251*, 236-244. 10.1007/bf02172923.

Haynes, P.A., Gooley, A.A., Ferguson, M.A., Redmond, J.W., and Williams, K.L. (1993). Post-translational modifications of the *Dictyostelium discoideum* glycoprotein PsA. Glycosylphosphatidylinositol membrane anchor and composition of O-linked oligosaccharides. *Eur J Biochem 216*, 729-737. 10.1111/j.1432-1033.1993.tb18192.x.

Heidler, S.A., and Radding, J.A. (1995). The AUR1 gene in *Saccharomyces cerevisiae* encodes dominant resistance to the antifungal agent aureobasidin A (LY295337). *Antimicrob Agents Chemother 39*, 2765-2769. 10.1128/aac.39.12.2765.

Heidler, S.A., and Radding, J.A. (2000). Inositol phosphoryl transferases from human pathogenic fungi. *Biochimica et Biophysica Acta (BBA) - Molecular Basis of Disease 1500*, 147-152. https://doi.org/10.1016/S0925-4439(99)00097-6.

Heuser, J., Zhu, Q., and Clarke, M. (1993). Proton pumps populate the contractile vacuoles of *Dictyostelium* amoebae. *J Cell Biol 121*, 1311-1327. 10.1083/jcb.121.6.1311.

Hilbi, H., Weber, S.S., Ragaz, C., Nyfeler, Y., and Urwyler, S. (2007). Environmental predators as models for bacterial pathogenesis. *Environ Microbiol 9*, 563-575. 10.1111/j.1462-2920.2007.01238.x.

Hornemann, T., Penno, A., Rütti, M.F., Ernst, D., Kivrak-Pfiffner, F., Rohrer, L., and von Eckardstein, A. (2009). The SPTLC3 subunit of serine palmitoyltransferase generates short chain sphingoid bases. *J Biol Chem 284*, 26322-26330. 10.1074/jbc.M109.023192.

Hsu, F.-F., and Turk, J. (2001). Studies on phosphatidylglycerol with triple quadrupole tandem mass spectrometry with electrospray ionization: fragmentation processes and structural characterization. *Journal of the American Society for Mass Spectrometry 12*, 1036-1043. https://doi.org/10.1016/S1044-0305(01)00285-9.

Huitema, K., van den Dikkenberg, J., Brouwers, J.F., and Holthuis, J.C. (2004). Identification of a family of animal sphingomyelin synthases. *Embo j 23*, 33-44. 10.1038/sj.emboj.7600034.

Jiménez-Rojo, N., and Riezman, H. (2019). On the road to unraveling the molecular functions of ether lipids. *FEBS Lett 593*, 2378-2389. 10.1002/1873-3468.13465.

Jin, H., McCaffery, J.M., and Grote, E. (2008). Ergosterol promotes pheromone signaling and plasma membrane fusion in mating yeast. *J Cell Biol 180*, 813-826. 10.1083/jcb.200705076.

John Peter, A.T., Petrungaro, C., Peter, M., and Kornmann, B. (2022). METALIC reveals interorganelle lipid flux in live cells by enzymatic mass tagging. *Nat Cell Biol 24*, 996-1004. 10.1038/s41556-022-00917-9.

Jumper, J., Evans, R., Pritzel, A., Green, T., Figurnov, M., Ronneberger, O., Tunyasuvunakool, K., Bates, R., Žídek, A., Potapenko, A., et al. (2021). Highly accurate protein structure prediction with AlphaFold. *Nature 596*, 583-589. 10.1038/s41586-021-03819-2.

Kageyama-Yahara, N., and Riezman, H. (2006). Transmembrane topology of ceramide synthase in yeast. *Biochem J 398*, 585-593. 10.1042/bj20060697.

Kappelt, F., Du Ma, X., Abou Hasna, B., Kornke, J.M., and Maniak, M. (2020). Phospholipids containing ether-bound hydrocarbon-chains are essential for efficient phagocytosis and neutral lipids of the ester-type perturb development in *Dictyostelium*. *Biol Open 9*. 10.1242/bio.052126.

Katoh, K., Rozewicki, J., and Yamada, K.D. (2019). MAFFT online service: multiple sequence alignment, interactive sequence choice and visualization. *Brief Bioinform 20*, 1160-1166. 10.1093/bib/bbx108.

Kelsey, J.S., Fastman, N.M., and Blumberg, D.D. (2012). Evidence of an evolutionarily conserved LMBR1 domain-containing protein that associates with endocytic cups and plays a role in cell migration in *Dictyostelium discoideum*. *Eukaryot Cell 11*, 401-416. 10.1128/ec.05186-11.

Kinoshita, T. (2020). Biosynthesis and biology of mammalian GPI-anchored proteins. *Open Biol 10*, 190290. 10.1098/rsob.190290.

Kinoshita, T., and Fujita, M. (2016). Biosynthesis of GPI-anchored proteins: special emphasis on GPI lipid remodeling. *J Lipid Res 57*, 6-24. 10.1194/jlr.R063313.

Klose, C., Surma, M.A., Gerl, M.J., Meyenhofer, F., Shevchenko, A., and Simons, K. (2012). Flexibility of a eukaryotic lipidome--insights from yeast lipidomics. *PLoS One 7*, e35063. 10.1371/journal.pone.0035063.

Kol, M., Panatala, R., Nordmann, M., Swart, L., van Suijlekom, L., Cabukusta, B., Hilderink, A., Grabietz, T., Mina, J.G.M., Somerharju, P., et al. (2017). Switching head group selectivity in mammalian sphingolipid biosynthesis by active-site-engineering of sphingomyelin synthases. *J Lipid Res 58*, 962-973. 10.1194/jlr.M076133.

Körner, C., and Fröhlich, F. (2022). Compartmentation and functions of sphingolipids. *Curr Opin Cell Biol 74*, 104-111. 10.1016/j.ceb.2022.01.006.

Krogh, A., Larsson, B., von Heijne, G., and Sonnhammer, E.L. (2001). Predicting transmembrane protein topology with a hidden Markov model: application to complete genomes. *J Mol Biol 305*, 567-580. 10.1006/jmbi.2000.4315.

Kumagai, K., and Hanada, K. (2019). Structure, functions and regulation of CERT, a lipid-transfer protein for the delivery of ceramide at the ER-Golgi membrane contact sites. *FEBS Lett 593*, 2366-2377. 10.1002/1873-3468.13511.

Kuspa, A., and Loomis, W.F. (1992). Tagging developmental genes in *Dictyostelium* by restriction enzyme-mediated integration of plasmid DNA. *Proc Natl Acad Sci U S A 89*, 8803-8807. 10.1073/pnas.89.18.8803.

References

Leier, H.C., Weinstein, J.B., Kyle, J.E., Lee, J.Y., Bramer, L.M., Stratton, K.G., Kempthorne, D., Navratil, A.R., Tafesse, E.G., Hornemann, T., et al. (2020). A global lipid map defines a network essential for Zika virus replication. *Nat Commun 11*, 3652. 10.1038/s41467-020-17433-9.

Levine, T.P., Wiggins, C.A., and Munro, S. (2000). Inositol phosphorylceramide synthase is located in the Golgi apparatus of *Saccharomyces cerevisiae*. *Mol Biol Cell 11*, 2267-2281. 10.1091/mbc.11.7.2267.

Lima, W.C. (2019). The AK426 antibody recognizes the Golgi apparatus in *Dictyostelium* cells by immunofluorescence. Antibody Reports *2*, e59. 10.24450/journals/abrep.2019.e59.

Limar, S., Körner, C., Martínez-Montañés, F., Stancheva, V.G., Wolf, V.N., Walter, S., Miller, E.A., Ejsing, C.S., Galassi, V.V., and Fröhlich, F. (2023). Yeast Svf1 binds ceramides and contributes to sphingolipid metabolism at the ER cis-Golgi interface. *J Cell Biol 222*. 10.1083/jcb.202109162.

Lisman, Q., Pomorski, T., Vogelzangs, C., Urli-Stam, D., de Cocq van Delwijnen, W., and Holthuis, J.C. (2004). Protein sorting in the late Golgi of *Saccharomyces cerevisiae* does not require mannosylated sphingolipids. *J Biol Chem 279*, 1020-1029. 10.1074/jbc.M306119200.

Listian, S.A., Kol, M., Ufelmann, E., Eising, S., Froehlich, F., Walter, S., Holthuis, J.C.M., and Barisch, C. (2023). Complex Sphingolipid Profiling and Identification of an Inositol Phosphorylceramide Synthase in *Dictyostelium discoideum*. bioRxiv, 2023.2007.2007.548115. 10.1101/2023.07.07.548115.

Liu, L.K., Choudhary, V., Toulmay, A., and Prinz, W.A. (2017). An inducible ER-Golgi tether facilitates ceramide transport to alleviate lipotoxicity. *J Cell Biol 216*, 131-147. 10.1083/jcb.201606059.

Loomis, W.F. (2014). Cell signaling during development of *Dictyostelium*. Dev Biol *391*, 1-16. 10.1016/j.ydbio.2014.04.001.

López-Jiménez, A.T., Cardenal-Muñoz, E., Leuba, F., Gerstenmaier, L., Barisch, C., Hagedorn, M., King, J.S., and Soldati, T. (2018). The ESCRT and autophagy machineries cooperate to repair ESX-1-dependent damage at the *Mycobacterium*-containing vacuole but have opposite impact on containing the infection. *PLoS Pathog 14*, e1007501. 10.1371/journal.ppat.1007501.

Lusche, D.F., Wessels, D., Scherer, A., Daniels, K., Kuhl, S., and Soll, D.R. (2012). The IplA Ca2+ channel of *Dictyostelium discoideum* is necessary for chemotaxis mediated through Ca2+, but not through cAMP, and has a fundamental role in natural aggregation. *J Cell Sci 125*, 1770-1783. 10.1242/jcs.098301.

Luttgeharm, K.D., Chen, M., Mehra, A., Cahoon, R.E., Markham, J.E., and Cahoon, E.B. (2015). Overexpression of Arabidopsis Ceramide Synthases Differentially Affects Growth, Sphingolipid Metabolism, Programmed Cell Death, and Mycotoxin Resistance *Plant Physiology 169*, 1108-1117. 10.1104/pp.15.00987.

MacLean, B., Tomazela, D.M., Shulman, N., Chambers, M., Finney, G.L., Frewen, B., Kern, R., Tabb, D.L., Liebler, D.C., and MacCoss, M.J. (2010). Skyline: an open source document editor for creating and analyzing targeted proteomics experiments. *Bioinformatics 26*, 966-968. 10.1093/bioinformatics/btq054.

Maekawa, M., and Fairn, G.D. (2015). Complementary probes reveal that phosphatidylserine is required for the proper transbilayer distribution of cholesterol. *J Cell Sci 128*, 1422-1433. 10.1242/jcs.164715.

Mamode Cassim, A., Grison, M., Ito, Y., Simon-Plas, F., Mongrand, S., and Boutté, Y. (2020). Sphingolipids in plants: a guidebook on their function in membrane architecture, cellular processes, and environmental or developmental responses. *FEBS Lett 594*, 3719-3738. 10.1002/1873-3468.13987.

Maniak, M. (2003). Fusion and fission events in the endocytic pathway of *Dictyostelium*. *Traffic 4*, 1-5. 10.1034/j.1600-0854.2003.40101.x.

Marek, M., Vincenzetti, V., and Martin, S.G. (2020). Sterol biosensor reveals LAM-family Ltc1-dependent sterol flow to endosomes upon Arp2/3 inhibition. *J Cell Biol 219*. 10.1083/jcb.202001147.

Markham, J.E., Li, J., Cahoon, E.B., and Jaworski, J.G. (2006). Separation and identification of major plant sphingolipid classes from leaves. *J Biol Chem 281*, 22684-22694. 10.1074/jbc.M604050200.

Marquês, J.T., Marinho, H.S., and de Almeida, R.F.M. (2018). Sphingolipid hydroxylation in mammals, yeast and plants - An integrated view. *Prog Lipid Res 71*, 18-42. 10.1016/j.plipres.2018.05.001.

Matsuzawa, Y., and Hostetler, K.Y. (1979). Degradation of bis(monoacylglycero)phosphate by an acid phosphodiesterase in rat liver lysosomes. *J Biol Chem 254*, 5997-6001.

Megyeri, M., Riezman, H., Schuldiner, M., and Futerman, A.H. (2016). Making Sense of the Yeast Sphingolipid Pathway. *J Mol Biol 428*, 4765-4775. 10.1016/j.jmb.2016.09.010.

Merlot, S., Meili, R., Pagliarini, D.J., Maehama, T., Dixon, J.E., and Firtel, R.A. (2003). A PTEN-related 5-phosphatidylinositol phosphatase localized in the Golgi. *J Biol Chem 278*, 39866-39873. 10.1074/jbc.M306318200.

Michaelson, L.V., Zäuner, S., Markham, J.E., Haslam, R.P., Desikan, R., Mugford, S., Albrecht, S., Warnecke, D., Sperling, P., Heinz, E., and Napier, J.A. (2009). Functional characterization of a higher plant sphingolipid Delta4-desaturase: defining the role of sphingosine and sphingosine-1-phosphate in *Arabidopsis*. *Plant Physiol 149*, 487-498. 10.1104/pp.108.129411.

Mina, J.G., Okada, Y., Wansadhipathi-Kannangara, N.K., Pratt, S., Shams-Eldin, H., Schwarz, R.T., Steel, P.G., Fawcett, T., and Denny, P.W. (2010). Functional analyses of differentially expressed isoforms of the *Arabidopsis* inositol phosphorylceramide synthase. *Plant Mol Biol 73*, 399-407. 10.1007/s11103-010-9626-3.

Muramoto, T., Iriki, H., Watanabe, J., and Kawata, T. (2019). Recent Advances in CRISPR/Cas9-Mediated Genome Editing in *Dictyostelium*. *Cells 8*. 10.3390/cells8010046.

Nagiec, M.M., Nagiec, E.E., Baltisberger, J.A., Wells, G.B., Lester, R.L., and Dickson, R.C. (1997). Sphingolipid synthesis as a target for antifungal drugs. Complementation of the inositol phosphorylceramide synthase defect in a mutant strain of *Saccharomyces cerevisiae* by the AUR1 gene. *J Biol Chem 272*, 9809-9817.

Nazarova, E.V., Montague, C.R., La, T., Wilburn, K.M., Sukumar, N., Lee, W., Caldwell, S., Russell, D.G., and VanderVen, B.C. (2017). Rv3723/LucA coordinates fatty acid and cholesterol uptake in *Mycobacterium tuberculosis*. *Elife 6*. 10.7554/eLife.26969.

Neuhaus, E.M., Horstmann, H., Almers, W., Maniak, M., and Soldati, T. (1998). Ethane-freezing/methanol-fixation of cell monolayers: a procedure for improved preservation of structure and antigenicity for light and electron microscopies. *J Struct Biol 121*, 326-342. 10.1006/jsbi.1998.3971.

Neuwald, A.F. (1997). An unexpected structural relationship between integral membrane phosphatases and soluble haloperoxidases. *Protein Sci 6*, 1764-1767. 10.1002/pro.5560060817.

Nichols, J.M., Veltman, D., and Kay, R.R. (2015). Chemotaxis of a model organism: progress with *Dictyostelium*. *Curr Opin Cell Biol 36*, 7-12. 10.1016/j.ceb.2015.06.005.

Niekamp, P., Guzman, G., Leier, H.C., Rashidfarrokhi, A., Richina, V., Pott, F., Barisch, C., Holthuis, J.C.M., and Tafesse, F.G. (2021). Sphingomyelin Biosynthesis Is Essential for Phagocytic Signaling during *Mycobacterium tuberculosis* Host Cell Entry. *mBio 12*. 10.1128/mBio.03141-20.

Nolta, K.V., Rodriguez-Paris, J.M., and Steck, T.L. (1994). Analysis of successive endocytic compartments isolated from *Dictyostelium discoideum* by magnetic fractionation. *Biochim Biophys Acta 1224*, 237-246. 10.1016/0167-4889(94)90196-1.

Pandey, A.K., and Sassetti, C.M. (2008). Mycobacterial persistence requires the utilization of host cholesterol. *Proc Natl Acad Sci U S A 105*, 4376-4380. 10.1073/pnas.0711159105.

Paschke, P., Knecht, D.A., Silale, A., Traynor, D., Williams, T.D., Thomason, P.A., Insall, R.H., Chubb, J.R., Kay, R.R., and Veltman, D.M. (2018). Rapid and efficient genetic engineering of both wild type and axenic strains of *Dictyostelium discoideum. PLoS One 13*, e0196809. 10.1371/journal.pone.0196809.

Pathak, D., Mehendale, N., Singh, S., Mallik, R., and Kamat, S.S. (2018). Lipidomics Suggests a New Role for Ceramide Synthase in Phagocytosis. *ACS Chemical Biology 13*, 2280-2287. 10.1021/acschembio.8b00438.

Pattingre, S., Bauvy, C., Levade, T., Levine, B., and Codogno, P. (2009). Ceramide-induced autophagy: to junk or to protect cells? *Autophagy 5*, 558-560. 10.4161/auto.5.4.8390.

Pekkinen, M., Terhal, P.A., Botto, L.D., Henning, P., Mäkitie, R.E., Roschger, P., Jain, A., Kol, M., Kjellberg, M.A., Paschalis, E.P., et al. (2019). Osteoporosis and skeletal dysplasia caused by pathogenic variants in SGMS2. *JCI Insight 4*. 10.1172/jci.insight.126180.

Peng, B., Kopczynski, D., Pratt, B.S., Ejsing, C.S., Burla, B., Hermansson, M., Benke, P.I., Tan, S.H., Chan, M.Y., Torta, F., et al. (2020). LipidCreator workbench to probe the lipidomic landscape. *Nat Commun 11*, 2057. 10.1038/s41467-020-15960-z.

Personnic, N., Striednig, B., Lezan, E., Manske, C., Welin, A., Schmidt, A., and Hilbi, H. (2019). Quorum sensing modulates the formation of virulent *Legionella* persisters within infected cells. *Nat Commun 10*, 5216. 10.1038/s41467-019-13021-8.

Pi, J., Wu, X., and Feng, Y. (2016). Fragmentation patterns of five types of phospholipids by ultra-high-performance liquid chromatography electrospray ionization quadrupole time-of-flight tandem mass spectrometry. *Analytical Methods 8*, 1319-1332. 10.1039/C5AY00776C.

Pukatzki, S., Kessin, R.H., and Mekalanos, J.J. (2002). The human pathogen Pseudomonas aeruginosa utilizes conserved virulence pathways to infect the social amoeba *Dictyostelium discoideum. Proc Natl Acad Sci U S A 99*, 3159-3164. 10.1073/pnas.052704399.

Pukatzki, S., Ma, A.T., Sturtevant, D., Krastins, B., Sarracino, D., Nelson, W.C., Heidelberg, J.F., and Mekalanos, J.J. (2006). Identification of a conserved bacterial protein secretion system in *Vibrio cholerae* using the *Dictyostelium* host model system. *Proc Natl Acad Sci U S A 103*, 1528-1533. 10.1073/pnas.0510322103.

Quiroga, R., Trenchi, A., González Montoro, A., Valdez Taubas, J., and Maccioni, H.J. (2013). Short transmembrane domains with high-volume exoplasmic halves determine retention of Type II membrane proteins in the Golgi complex. *J Cell Sci 126*, 5344-5349. 10.1242/jcs.130658.

Raetz, C.R., and Dowhan, W. (1990). Biosynthesis and function of phospholipids in Escherichia coli. *J Biol Chem 265*, 1235-1238.

Rahmaniyan, M., Curley, R.W., Jr., Obeid, L.M., Hannun, Y.A., and Kraveka, J.M. (2011). Identification of dihydroceramide desaturase as a direct in vitro target for fenretinide. *J Biol Chem 286*, 24754-24764. 10.1074/jbc.M111.250779.

Ravanel, K., de Chassey, B., Cornillon, S., Benghezal, M., Zulianello, L., Gebbie, L., Letourneur, F., and Cosson, P. (2001). Membrane sorting in the endocytic and phagocytic pathway of *Dictyostelium discoideum*. *Eur J Cell Biol 80*, 754-764. 10.1078/0171-9335-00215.

Rennie, E.A., Ebert, B., Miles, G.P., Cahoon, R.E., Christiansen, K.M., Stonebloom, S., Khatab, H., Twell, D., Petzold, C.J., Adams, P.D., et al. (2014). Identification of a sphingolipid α-glucuronosyltransferase that is essential for pollen function in *Arabidopsis*. *Plant Cell 26*, 3314-3325. 10.1105/tpc.114.129171.

Rietveld, A., Neutz, S., Simons, K., and Eaton, S. (1999a). Association of sterol- and glycosylphosphatidylinositol-linked proteins with *Drosophila* raft lipid microdomains. *J Biol Chem 274*, 12049-12054. 10.1074/jbc.274.17.12049.

Rietveld, A., Neutz, S., Simons, K., and Eaton, S. (1999b). Association of Sterol- and Glycosylphosphatidylinositol-linked Proteins with *Drosophila* Raft Lipid Microdomains*. *Journal of Biological Chemistry 274*, 12049-12054. https://doi.org/10.1074/jbc.274.17.12049.

Risselada, H.J., and Marrink, S.J. (2008). The molecular face of lipid rafts in model membranes. *Proc Natl Acad Sci U S A 105*, 17367-17372. 10.1073/pnas.0807527105.

Robson, K.J., Stewart, M.E., Michelsen, S., Lazo, N.D., and Downing, D.T. (1994). 6-Hydroxy-4-sphingenine in human epidermal ceramides. *J Lipid Res 35*, 2060-2068.

Rodriguez-Paris, J.M., Nolta, K.V., and Steck, T.L. (1993). Characterization of lysosomes isolated from *Dictyostelium discoideum* by magnetic fractionation. *J Biol Chem 268*, 9110-9116.

Rouser, G., Kritchevsky, G., Knudson, A.G., Jr., and Simon, G. (1968). Accumulation of a glycerolphospholipid in classical niemann-pick disease. *Lipids 3*, 287-290. 10.1007/bf02531203.

Saito, K., Takakuwa, N., Ohnishi, M., and Oda, Y. (2006). Presence of glucosylceramide in yeast and its relation to alkali tolerance of yeast. *Appl Microbiol Biotechnol 71*, 515-521. 10.1007/s00253-005-0187-3.

Sampaio, J.L., Gerl, M.J., Klose, C., Ejsing, C.S., Beug, H., Simons, K., and Shevchenko, A. (2011a). Membrane lipidome of an epithelial cell line. *Proc Natl Acad Sci U S A 108*, 1903-1907. 10.1073/pnas.1019267108.

Sato, K., Noda, Y., and Yoda, K. (2009). Kei1: a novel subunit of inositolphosphorylceramide synthase, essential for its enzyme activity and Golgi localization. *Mol Biol Cell 20*, 4444-4457. 10.1091/mbc.e09-03-0235.

Schäfer, J.-H., Körner, C., Esch, B.M., Limar, S., Parey, K., Walter, S., Januliene, D., Moeller, A., and Fröhlich, F. (2023). Structure of the ceramide-bound SPOTS complex. *bioRxiv*, 2023.2002.2003.526835. 10.1101/2023.02.03.526835.

Sevova, E.S., Goren, M.A., Schwartz, K.J., Hsu, F.F., Turk, J., Fox, B.G., and Bangs, J.D. (2010). Cell-free synthesis and functional characterization of sphingolipid synthases from parasitic trypanosomatid protozoa. *J Biol Chem 285*, 20580-20587. 10.1074/jbc.M110.127662.

Sharpe, H.J., Stevens, T.J., and Munro, S. (2010). A comprehensive comparison of transmembrane domains reveals organelle-specific properties. *Cell 142*, 158-169. 10.1016/j.cell.2010.05.037.

Snider, J.M., Luberto, C., and Hannun, Y.A. (2019). Approaches for probing and evaluating mammalian sphingolipid metabolism. *Anal Biochem 575*, 70-86. 10.1016/j.ab.2019.03.014.

Snyder, F. (1999). The ether lipid trail: a historical perspective. *Biochim Biophys Acta 1436*, 265-278. 10.1016/s0005-2760(98)00172-6.

Sociale, M., Wulf, A.L., Breiden, B., Klee, K., Thielisch, M., Eckardt, F., Sellin, J., Bülow, M.H., Löbbert, S., Weinstock, N., et al. (2018). Ceramide Synthase Schlank Is a Transcriptional Regulator Adapting Gene Expression to Energy Requirements. *Cell Rep 22*, 967-978. 10.1016/j.celrep.2017.12.090.

Sokoya, T., Parolek, J., Foged, M.M., Danylchuk, D.I., Bozan, M., Sarkar, B., Hilderink, A., Philippi, M., Botto, L.D., Terhal, P.A., et al. (2022). Pathogenic variants of sphingomyelin synthase SMS2 disrupt lipid landscapes in the secretory pathway. *Elife 11*. 10.7554/eLife.79278.

Solomon, J.M., Leung, G.S., and Isberg, R.R. (2003). Intracellular replication of *Mycobacterium marinum* within *Dictyostelium discoideum*: efficient replication in the absence of host coronin. *Infect Immun 71*, 3578-3586. 10.1128/iai.71.6.3578-3586.2003.

Sonnino, S., and Chigorno, V. (2000). Ganglioside molecular species containing C18- and C20-sphingosine in mammalian nervous tissues and neuronal cell cultures. *Biochim Biophys Acta 1469*, 63-77. 10.1016/s0005-2736(00)00210-8.

Speer, A., Sun, J., Danilchanka, O., Meikle, V., Rowland, J.L., Walter, K., Buck, B.R., Pavlenok, M., Hölscher, C., Ehrt, S., and Niederweis, M. (2015). Surface hydrolysis of sphingomyelin by the outer membrane protein Rv0888 supports replication of *Mycobacterium tuberculosis* in macrophages. *Mol Microbiol 97*, 881-897. 10.1111/mmi.13073.

Sullards, M.C., Liu, Y., Chen, Y., and Merrill, A.H., Jr. (2011). Analysis of mammalian sphingolipids by liquid chromatography tandem mass spectrometry (LC-MS/MS) and tissue imaging mass spectrometry (TIMS). *Biochim Biophys Acta 1811*, 838-853. 10.1016/j.bbalip.2011.06.027.

Sutterwala, S.S., Hsu, F.F., Sevova, E.S., Schwartz, K.J., Zhang, K., Key, P., Turk, J., Beverley, S.M., and Bangs, J.D. (2008). Developmentally regulated sphingolipid synthesis in African trypanosomes. *Mol Microbiol 70*, 281-296. 10.1111/j.1365-2958.2008.06393.x.

Symons, J.L., Cho, K.J., Chang, J.T., Du, G., Waxham, M.N., Hancock, J.F., Levental, I., and Levental, K.R. (2021). Lipidomic atlas of mammalian cell membranes reveals hierarchical variation induced by culture conditions, subcellular membranes, and cell lineages. *Soft Matter 17*, 288-297. 10.1039/d0sm00404a.

Tafesse, F.G., Huitema, K., Hermansson, M., van der Poel, S., van den Dikkenberg, J., Uphoff, A., Somerharju, P., and Holthuis, J.C. (2007). Both sphingomyelin synthases SMS1 and SMS2 are required for sphingomyelin homeostasis and growth in human HeLa cells. *J Biol Chem 282*, 17537-17547. 10.1074/jbc.M702423200.

Takesako, K., Kuroda, H., Inoue, T., Haruna, F., Yoshikawa, Y., Kato, I., Uchida, K., Hiratani, T., and Yamaguchi, H. (1993). Biological properties of aureobasidin A, a cyclic depsipeptide antifungal antibiotic. *J Antibiot (Tokyo) 46*, 1414-1420. 10.7164/antibiotics.46.1414.

Ternes, P., Brouwers, J.F., van den Dikkenberg, J., and Holthuis, J.C. (2009). Sphingomyelin synthase SMS2 displays dual activity as ceramide phosphoethanolamine synthase. *J Lipid Res 50*, 2270-2277. 10.1194/jlr.M900230-JLR200.

Ternes, P., Feussner, K., Werner, S., Lerche, J., Iven, T., Heilmann, I., Riezman, H., and Feussner, I. (2011). Disruption of the ceramide synthase LOH1 causes spontaneous cell death in *Arabidopsis thaliana. New Phytol 192*, 841-854. 10.1111/j.1469-8137.2011.03852.x.

Ternes, P., Franke, S., Zähringer, U., Sperling, P., and Heinz, E. (2002). Identification and characterization of a sphingolipid delta 4-desaturase family. *J Biol Chem 277*, 25512-25518. 10.1074/jbc.M202947200.

Ternes, P., Sperling, P., Albrecht, S., Franke, S., Cregg, J.M., Warnecke, D., and Heinz, E. (2006). Identification of fungal sphingolipid C9-methyltransferases by phylogenetic profiling. *J Biol Chem 281*, 5582-5592. 10.1074/jbc.M512864200.

Tønjum, T., Welty, D.B., Jantzen, E., and Small, P.L. (1998). Differentiation of *Mycobacterium ulcerans*, *M. marinum*, and *M. haemophilum*: mapping of their relationships to *M. tuberculosis* by fatty acid profile analysis, DNA-DNA hybridization, and 16S rRNA gene sequence analysis. *J Clin Microbiol 36*, 918-925. 10.1128/jcm.36.4.918-925.1998.

Tosetti, N., Croxatto, A., and Greub, G. (2014). Amoebae as a tool to isolate new bacterial species, to discover new virulence factors and to study the host-pathogen interactions. *Microb Pathog 77*, 125-130. 10.1016/j.micpath.2014.07.009.

Vacaru, A.M., Tafesse, F.G., Ternes, P., Kondylis, V., Hermansson, M., Brouwers, J.F., Somerharju, P., Rabouille, C., and Holthuis, J.C. (2009). Sphingomyelin synthase-related protein SMSr controls ceramide homeostasis in the ER. *J Cell Biol 185*, 1013-1027. 10.1083/jcb.200903152.

Vacaru, A.M., van den Dikkenberg, J., Ternes, P., and Holthuis, J.C. (2013). Ceramide phosphoethanolamine biosynthesis in Drosophila is mediated by a unique ethanolamine phosphotransferase in the Golgi lumen. *J Biol Chem 288*, 11520-11530. 10.1074/jbc.M113.460972.

Veltman, D.M., Akar, G., Bosgraaf, L., and Van Haastert, P.J. (2009). A new set of small, extrachromosomal expression vectors for *Dictyostelium discoideum*. *Plasmid 61*, 110-118. 10.1016/j.plasmid.2008.11.003.

Vines, J.H., and King, J.S. (2019). The endocytic pathways of *Dictyostelium discoideum*. *Int J Dev Biol 63*, 461-471. 10.1387/ijdb.190236jk.

Vines, J.H., Maib, H., Buckley, C.M., Gueho, A., Zhu, Z., Soldati, T., Murray, D.H., and King, J.S. (2023). A PI(3,5)P2 reporter reveals PIKfyve activity and dynamics on macropinosomes and phagosomes. *J Cell Biol 222*. 10.1083/jcb.202209077.

Waggoner, D.W., Xu, J., Singh, I., Jasinska, R., Zhang, Q.X., and Brindley, D.N. (1999). Structural organization of mammalian lipid phosphate phosphatases: implications for signal transduction. *Biochim Biophys Acta 1439*, 299-316. 10.1016/s1388-1981(99)00102-x.

Walkley, S.U., and Vanier, M.T. (2009). Secondary lipid accumulation in lysosomal disease. *Biochim Biophys Acta 1793*, 726-736. 10.1016/j.bbamcr.2008.11.014.

Wang, W., Yang, X., Tangchaiburana, S., Ndeh, R., Markham, J.E., Tsegaye, Y., Dunn, T.M., Wang, G.L., Bellizzi, M., Parsons, J.F., et al. (2008). An inositolphosphorylceramide synthase is involved in regulation of plant programmed cell death associated with defense in *Arabidopsis*. *Plant Cell 20*, 3163-3179. 10.1105/tpc.108.060053.

Waterhouse, A.M., Procter, J.B., Martin, D.M., Clamp, M., and Barton, G.J. (2009). Jalview Version 2--a multiple sequence alignment editor and analysis workbench. *Bioinformatics 25*, 1189-1191. 10.1093/bioinformatics/btp033.

Weeks, G., and Herring, F.G. (1980). The lipid composition and membrane fluidity of *Dictyostelium discoideum* plasma membranes at various stages during differentiation. *J Lipid Res 21*, 681-686.

Yamashita, K., Iriki, H., Kamimura, Y., and Muramoto, T. (2021). CRISPR Toolbox for Genome Editing in *Dictyostelium*. *Front Cell Dev Biol 9*, 721630. 10.3389/fcell.2021.721630.

Zaremberg, V., Gajate, C., Cacharro, L.M., Mollinedo, F., and McMaster, C.R. (2005). Cytotoxicity of an anti-cancer lysophospholipid through selective modification of lipid raft composition. *J Biol Chem 280*, 38047-38058. 10.1074/jbc.M502849200.

Zhang, T., Barclay, L., Walensky, L.D., and Saghatelian, A. (2015). Regulation of mitochondrial ceramide distribution by members of the BCL-2 family. *J Lipid Res 56*, 1501-1510. 10.1194/jlr.M058750.

Supplementary Table 1 (1/4)

H. sapiens enzyme	Annotation	Uniprot acession	Dictybase Protein ID	Dictybase gene ID	Bits score	E-value	sequence identity (percent)
Serine palmitoyltransferase 1	SPTLC1	O15269	DDB_G0268056	sptA	352	2,00E-97	182/442 (41%)
Serine palmitoyltransferase 1	SPTLC1	O15269	DDB_G0291283	sptB	151	4,00E-37	93/308 (30%)
Serine palmitoyltransferase 1	SPTLC1	O15269	DDB_G0280763	hemA	107	1,00E-23	72/242 (29%)
Serine palmitoyltransferase 2	SPTLC2	O15270	DDB_G0268056	sptA	136	2,00E-32	74/246 (30%)
Serine palmitoyltransferase 2	SPTLC2	O15270	DDB_G0291283	sptB	491	1,00E-139	228/483 (47%)
Serine palmitoyltransferase 2	SPTLC2	O15270	DDB_G0280763	hemA	135	3,00E-32	101/348 (29%)
Serine palmitoyltransferase 3	SPTLC3	Q9NUV7	DDB_G0268056	sptA	131	8E-31	74/259 (28%)
Serine palmitoyltransferase 3	SPTLC3	Q9NUV7	DDB_G0291283	sptB	464	1E-131	223/488 (45%)
Serine palmitoyltransferase 3	SPTLC3	Q9NUV7	DDB_G0280763	hemA	131	5E-31	100/359 (27%)
3-ketodihydrosphingosine reductase*	KDSR	Q06136	DDB_G0274015	ksrA-1	171	4,00E-43	102/268 (38%)
3-ketodihydrosphingosine reductase*	KDSR	Q06136	DDB_G0272883	ksrA-2	171	4,00E-43	102/268 (38%)
Dihydroceramide desaturase	DEGS1	O15121	DDB_G0269738	desA	170	7,00E-43	108/320 (33%)
Ceramide synthase	CERS1	P27544	DDB_G0282607	crsA	55,8	2,00E-08	45/187 (24%)
Ceramide synthase	CERS2	Q96G23	DDB_G0282607	crsA	97,4	7,00E-21	65/211 (30%)
Ceramide synthase	CERS3	Q8IU89	DDB_G0282607	crsA	85,9	2,00E-17	61/225 (27%)
Ceramide synthase	CERS4	Q9HA82	DDB_G0282607	crsA	103	1,00E-22	68/218 (31%)
Ceramide synthase	CERS5	Q8N5B7	DDB_G0282607	crsA	109	2,00E-24	64/210 (30%)
Ceramide synthase	CERS6	Q6ZMG9	DDB_G0282607	crsA	120	7,00E-28	71/209 (33%)
Sphingomyelin synthase-related protein 1	SAMD8	Q96LT4	no hit	no hit	no hit	no hit	no hit
Phosphatidylcholine:ceramide cholinephosphotransferase 1	SGMS1	Q86VZ5	no hit	no hit	no hit	no hit	no hit
Ceramide glucosyltransferase	CEGT	Q16739	no hit	no hit	no hit	no hit	no hit
Ceramide transfer protein**	CERT	Q9Y5P4	no hit	no hit	no hit	no hit	no hit
*BLAST search yielded 44 other hits, (with bits score above 50) presented is the one with the highest Bits score and the lowest E-value.							
**BLAST search yielded multiple hits but none of them have bits score above 50.							

Supplementary Table 1 (2/4)

S. cerevisiae enzyme	Annotation	Uniprot acession	Dictybase Protein ID	Dictybase gene ID	Bits score	E-value	sequence identity (percent)
Serine palmitoyltransferase subunit 1	Lcb1	P25045	DDB_G0268056	sptA	285	5,00E-77	170/465 (36%)
Serine palmitoyltransferase subunit 1	Lcb1	P25045	DDB_G0291283	sptB	126	2,00E-29	82/282 (29%)
Serine palmitoyltransferase subunit 1	Lcb1	P25045	DDB_G0280763	hemA	90.9	1,00E-18	76/300 (25%)
Serine palmitoyltransferase subunit 2	Lcb2	P40970	DDB_G0268056	sptA	139	2,00E-33	81/247 (32%)
Serine palmitoyltransferase subunit 2	Lcb2	P40970	DDB_G0291283	sptB	445	1,00E-125	211/447 (47%)
Serine palmitoyltransferase subunit 2	Lcb2	P40970	DDB_G0280763	hemA	140	2,00E-33	111/357 (31%)
3-ketodihydrosphingosine reductase	Tsc10	P38342	DDB_G0274015	ksrA-1	84.3	6,00E-17	73/283 (25%)
3-ketodihydrosphingosine reductase	Tsc10	P38342	DDB_G0272883	ksrA-2	84.3	6,00E-17	73/283 (25%)
Ceramide synthase subunit	Lac1	P28496	DDB_G0282607	crsA	73.6	1,00E-13	60/267 (22%)
Ceramide synthase subunit	Lag1	P38703	DDB_G0282607	crsA	70.5	1,00E-12	44/161 (27%)
Ceramide synthase subunit	Lip1	Q03579	no hit	no hit	no hit	no hit	no hit
Sphinganine hydroxylase	Sur2	P38992	DDB_G0269788	lhsA (proposed)	56.6	1,00E-08	71/267 (26%)
Sphinganine hydroxylase	Sur2	P38992	DDB_G0270946	lhsB (proposed)	53.9	8,00E-08	73/261 (27%)
Sphinganine hydroxylase	Sur2	P38992	DDB_G0279611	lhsC (proposed)	51.2	5,00E-07	63/249 (25%)
Ceramide fatty acid hydroxylase*	Scs7	Q03529	DDB_G0269908	lhsD (proposed)	118	3,00E-27	103/369 (28%)
Inositol phosphorylceramide synthase catalytic subunit	Aur1	P36107	no hit	no hit	no hit	no hit	no hit
Mannosyl phosphorylinositol ceramide synthase	Sur1	P33300	no hit	no hit	no hit	no hit	no hit
Mannosyl phosphorylinositol ceramide synthase regulatory protein	Csg2	P35206	no hit	no hit	no hit	no hit	no hit
Inositolphosphotransferase 1	Ipt1	P38954	no hit	no hit	no hit	no hit	no hit
Mannosyl phosphorylinositol ceramide synthase CSH1	Csh1	P38287	no hit	no hit	no hit	no hit	no hit
Serine palmitoyltransferase-regulating protein	Tsc3	Q3E790	no hit	no hit	no hit	no hit	no hit
Component of the SPOTS complex Orm1	Orm1	P53224	DDB_G0288847	n.a.	73.2	7,00E-14	47/139 (33%)
Component of the SPOTS complex Orm2	Orm2	Q06144	DDB_G0288847	n.a.	51.2	3,00E-07	27/89 (30%)
Phosphatidylinositol-3-phosphatase SAC1	Sac1	P32368	DDB_G0271630	sac1	266	1,00E-71	179/468 (38%)
Phosphatidylinositol-3-phosphatase SAC1	Sac1	P32368	DDB_G0290653	n.a.	265	3,00E-71	168/471 (35%)
Phosphatidylinositol-3-phosphatase SAC1	Sac1	P32368	DDB_G0274537	n.a.	249	2,00E-66	171/497 (34%)
Phosphatidylinositol-3-phosphatase SAC1	Sac1	P32368	DDB_G0292392	Dd5P3	202	4,00E-52	132/433 (30%)
Phosphatidylinositol-3-phosphatase SAC1	Sac1	P32368	DDB_G0281427	fig4	131	7,00E-31	144/543 (26%)
Fatty acid elongase	Elo1	P39540	DDB_G0272012	n.a.	117	5,00E-27	71/195 (36%)
Fatty acid elongase	Elo1	P39540	DDB_G0274669	n.a.	113	7,00E-26	71/194 (36%)
Fatty acid elongase	Elo1	P39540	DDB_G0292896	eloA	108	3,00E-24	71/224 (31%)
Fatty acid elongase	Elo1	P39540	DDB_G0277569	n.a.	102	1,00E-22	82/265 (30%)
Fatty acid elongase	Elo1	P39540	DDB_G0270312	n.a.	97.4	6,00E-21	75/253 (29%)
Fatty acid elongase	Elo1	P39540	DDB_G0271066	n.a.	91.7	3,00E-19	60/196 (30%)
Fatty acid elongase	Elo1	P39540	DDB_G0281821	eloB	80.9	5,00E-16	72/263 (27%)
Fatty acid elongase	Elo2	P25358	DDB_G0292896	eloA	115	2,00E-26	82/225 (36%)
Fatty acid elongase	Elo2	P25358	DDB_G0272012	n.a.	113	1,00E-25	70/194 (36%)
Fatty acid elongase	Elo2	P25358	DDB_G0274669	n.a.	105	2,00E-23	67/193 (34%)
Fatty acid elongase	Elo2	P25358	DDB_G0270312	n.a.	94.4	5,00E-20	70/253 (27%)

Supplementary Table 1 (3/4)

S. cerevisiae enzyme	Annotation	Uniprot acession #	Dictybase Protein ID	Dictybase gene ID	Bits score	E-value	sequence identity (percent)
Fatty acid elongase	Elo2	P25358	DDB_G0271066	n.a.	92.4	2,00E-19	70/243 (28%)
Fatty acid elongase	Elo2	P25358	DDB_G0277569	n.a.	85.1	3,00E-17	74/260 (28%)
Fatty acid elongase	Elo2	P25358	DDB_G0281821	eloB	74.7	5,00E-14	63/268 (23%)
Fatty acid elongase	Elo3	P40319	DDB_G0292896	eloA	89.4	2,00E-18	54/151 (35%)
Fatty acid elongase	Elo3	P40319	DDB_G0274669	n.a.	73.9	9,00E-14	48/155 (31%)
Fatty acid elongase	Elo3	P40319	DDB_G0272012	n.a.	72.4	3,00E-13	46/154 (29%)
Fatty acid elongase	Elo3	P40319	DDB_G0277569	n.a.	71.6	4,00E-13	66/259 (25%)
Fatty acid elongase	Elo3	P40319	DDB_G0281821	eloB	61.6	4,00E-10	47/173 (27%)
Fatty acid elongase	Elo3	P40319	DDB_G0270312	n.a.	61.6	4,00E-10	62/249 (24%)
Fatty acid elongase	Elo3	P40319	DDB_G0271066	n.a.	60.5	1,00E-09	49/178 (27%)
Ceramide binding protein (Svf1)	Svf1	Q05515	n.a.	n.a.	n.a.	n.a.	n.a.
*BLAST search yielded 10 other hits, (with bits score above 50) presented is the one with the highest Bits score and the lowest E-value.							

Supplementary Table 1 (4/4)

A. thaliana enzyme	Annotation	Uniprot acession	Dictybase Protein ID	Dictybase gene ID	Bits score	E-value	sequence identity (percent)
Serine palmitoyltransferase (SPT)	LCB1	Q94IB8	DDB_G0268056	sptA	327	6,00E-90	176/438 (40%)
Serine palmitoyltransferase (SPT)	LCB1	Q94IB8	DDB_G0291283	sptB	127	9,00E-30	95/380 (25%)
Serine palmitoyltransferase (SPT)	LCB1	Q94IB8	DDB_G0280763	hemA	103	1,00E-22	65/242 (26%)
Serine palmitoyltransferase (SPT)	LCB2a	Q9LSZ9	DDB_G0280763	sptA	138	4,00E-33	111/392 (28%)
Serine palmitoyltransferase (SPT)	LCB2a	Q9LSZ9	DDB_G0268056	sptB	498	1,00E-141	233/469 (49%)
Serine palmitoyltransferase (SPT)	LCB2a	Q9LSZ9	DDB_G0291283	hemA	149	2,00E-36	112/376 (29%)
Serine palmitoyltransferase (SPT)	LCB2b	Q9M304	DDB_G0268056	sptA	135	5,00E-32	85/267 (31%)
Serine palmitoyltransferase (SPT)	LCB2b	Q9M304	DDB_G0291283	sptB	498	1,00E-141	232/469 (49%)
Serine palmitoyltransferase (SPT)	LCB2b	Q9M304	DDB_G0280763	hemA	146	1,00E-35	108/359 (30%)
3-dehydrosphinganine reductase	TSC10B	F4JZN6	DDB_G0274015	ksrA-1	119	2,00E-27	87/309 (28%)
3-dehydrosphinganine reductase	TSC10B	F4JZN6	DDB_G0272883	ksrA-2	119	2,00E-27	87/309 (28%)
3-dehydrosphinganine reductase	TSC10A	Q0WRJ2	DDB_G0274015	ksrA-1	120	7,00E-28	83/287 (28%)
3-dehydrosphinganine reductase	TSC10A	Q0WRJ2	DDB_G0272883	ksrA-2	120	7,00E-28	83/287 (28%)
Ceramide synthase	LOH1	Q9LDF2	DDB_G0282607	crsA	102	3,00E-22	84/268 (31%)
Ceramide synthase	LOH2	Q9LJK3	DDB_G0282607	crsA	114	4,00E-26	85/258 (32%)
Ceramide synthase	LOH3	Q6NQI8	DDB_G0282607	crsA	108	3,00E-24	76/246 (30%)
Sphingolipid delta(4)-desaturase	DES1	Q9ZPH4	DDB_G0269738	desA	154	4,00E-38	108/305 (35%)
Sphinganine C4-monooxygenase 1	SBH1	Q8VYI1	DDB_G0269788	lhsA (proposed)	57	6,00E-09	42/142 (29%)
Sphinganine C4-monooxygenase 1	SBH1	Q8VYI1	DDB_G0270946	lhsB (proposed)	53,5	7,00E-08	38/138 (27%)
Sphinganine C4-monooxygenase 1	SBH1	Q8VYI1	DDB_G0279611	lhsC (proposed)	57	6,00E-09	45/147 (30%)
Sphinganine C4-monooxygenase 1	SBH2	Q9AST3	DDB_G0269788	lhsA (proposed)	63.9	5,00E-11	48/142 (33%)
Sphinganine C4-monooxygenase 1	SBH2	Q9AST3	DDB_G0270946	lhsB (proposed)	57.0	7,00E-09	39/134 (29%)
Sphinganine C4-monooxygenase 1	SBH2	Q9AST3	DDB_G0279611	lhsC (proposed)	54.7	3,00E-08	62/235 (26%)
Ceramide fatty acid hydroxylase	FAH1	O48916	DDB_G0269908	lhsD (proposed)	142	1,00E-34	84/230 (36%)
Ceramide fatty acid hydroxylase	FAH2	Q9SUC5	DDB_G0269908	lhsD (proposed)	159	9,00E-40	86/231 (37%)
IPC synthase	IPCS1	Q9M325	no hit	no hit	no hit	no hit	no hit
Inositol phosphorylceramide glucuronosyltransferase 1	IPUT1	Q8GWB7	DDB_G0286945	gtr3	57	2,00E-08	48/184 (26%)
Glycosylinositol phosphorylceramide mannosyl transferase	GMT1	Q9LY62	no hit	no hit	no hit	no hit	no hit
Glucosamine inositolphosphorylceramide transferase	GINT1	Q84WB7	no hit	no hit	no hit	no hit	no hit
Ceramide glucosyltransferase	n.a.	Q944R4	no hit	no hit	no hit	no hit	no hit
Ceramide glucosyltransferase	GCS	O82193	no hit	no hit	no hit	no hit	no hit

*BLAST search of both TSC10A and TSC10B yielded 29 other hits, presented is the one with the highest Bits score and the lowest E-value.

ABBREVIATIONS

3-KDS	3-ketodihydrosphingosine
AbA	AureobasidinA
BCP	Beads Containing Phagosome
Cer	Ceramides
CerS	Ceramide synthase
CSS	Complex Sphingolipid Synthase
CV	Contractile Vacuole
DAG	Diacylglycerol
DHS	Dihydroceramide
EPC	Ethanolamine Phosphoryl Ceramides
ER	Endoplasmic Reticulum
GPI-AP	Glycosylphosphatidylinositol Anchored Proteins
GIPC	Glycosylinositol Phosphorylceramides
GlcCer	glycosylceramide
GPL	Glycerophospholipid
GPI-AP	Glycosylphosphatidylinositol anchored protein
FARAT	Fatty-acyl Reductase Acyl Transferase
Ksr	3-keto-sphinganine reductase
MDG	Monoalkyl-diacyl-glycerols
MCV	Mycobacteria-Containing Vacuole
MIPC	mannosylinositol-phosphorylceramide
$M(IP)_2C$	mannosyldiinositol-phosphorylceramide
PA	Phosphatidic Acid
PC	Phosphatidyl Choline
PDI	Protein Disulfide Isomerase
PE	Phosphatidyl Ethanolamine
PG	Phosphatidyl Glycerol
PI	Phosphatidyl Inositol
PIP	Phosphoinositides
PNS	Post-Nuclear Supernatant
PS	Phosphatidyl Serine
LBPA	Lyso-bis-phosphatidic acid
LC	Liquid Chromatography
LD	Lipid Droplets
LPA	Lyso-phosphatidic Acid
LPC	Lyso-phosphatidyl Choline
LPE	Lyso-phosphatidyl Ethanolamine
LPI	Lyso-phosphatidyl Inositol
LPP	Lipid Phosphate Phosphatase
IPC	Inositol Phosphoryl Ceramides
MS	Mass Spectrometry
MDG	Monoalkyl-diacyl-glycerol
SD	Spinning Disc
SM	Sphingomyelin
SMS	Sphingomyelin Synthase
SPT	Serine Palmitoyl Transferase
TAG	Triacylglycerol
TGN	Trans-golgi Network
TLC	Thin Layer Chromatography
TMD	Transmembrane Domain
VLCFA	Very Long Chain Fatty Acid
WB	Western Blot
WGE	Wheat Germ Extract

STRAINS, PLASMIDS, PRIMERS AND ANTIBODIES

***D. discoideum* strains**	**Relevant characteristics**	**Source/Reference**
AX2	wt, parental strain	
CSS2-mCherry	$G418^r$	This study
mCherry-CSS2	$G418^r$	This study
CSS2-mCherry ZntD-GFP	$G418^r$, Hyg^r	This study
mCherry-CSS2 ZntD-GFP	$G418^r$, Hyg^r	This study
GFP-D4H	Hyg^r	This study
Plasmids		**Source/Reference**
CSS2-mCherry	pDM1210-CSS2	This study
mCherry-CSS2	pDM1208-CSS2	This study
ZntD-GFP	pDM1045-ZntD	This study
GFP-D4H	pDM1043-D4H	This study
pEU-Flexi-CSS1	Amp^r,	This study
pEU-Flexi-CSS2	Amp^r	This study
pEU-Flexi-SMS2	Amp^r	(Kol *et al.*, 2017)
Antibody	**Dilution**	**Source/Reference**
α-p80 (H161, mouse)	1/50	Geneva ab facility, AJ154-M2a
α-p80 (H161, human)	1/50	Geneva ab facility, AJ154-H1
α-VatA (mouse)	1/50	Geneva ab facility, AJ520-M2a
α-VatA (human)	1/50	Geneva ab facility, AJ520-H1
α-VacA (mouse)	1/50	Geneva ab facility, RB256-M2a
α-VacB (mouse)	1/50	Geneva ab facility, RB256-M2a
α-AK426 (mouse)	1/10	Geneva ab facility, AK426-M2a
α-PDI (mouse)	Undiluted	Maniak lab, 221-64-1
CF488A (goat, α-mouse IgG)	1/1000	Biotium/BOT-20018
CF640A (goat, α-mouse IgG)	1/1000	Biotium/BOT-20175
CF640A (goat, α-human IgG)	1/1000	Biotium/BOT-20081-1
AlexaF546 (goat, α-human IgG)	1/1000	Thermo Fischer/A
Primers	**Sequence**	
oMIB99	5'-CCAGATCTGCCAAGGGAAAAATAAACTTAGA-3'	
oMIB100	5'-CCACTAGTGAATTCTTAATTGTAAGTAATACTAG-3'	
oMIB154	5'-AGATCTATGGGAGTACAACAACAATCGG-3'	
oMIB155	5'-ACTAGTCTATTTATTATTAAATTTTGATAAAATATTTTG-3'	
oMIB156	5'-AGATCTAAAATGGGAGTACAACAACAATCGG-3'	
oMIB157	5' ACTAGTTTTATTATTAAATTTTGATAAAATATTTTG-3'	

LIST OF FIGURES

LIST OF TABLES

ACKNOWLEGMENTS

This might be a long one, so please bear with me. First and foremost, I would like to thank my PI and friend, **Caroline Barisch,** for giving me a chance to conduct my studies. The journey has its ups and downs, but I can say it is both intense and fun. Also, I would like to thank **Joost Holthuis** for being the mentor figure, guiding both me and Caro throughout the development of the paper. The help from **Matthijs Kol** is essential for the paper, I won't go far without it. As for mass spectrometry, the expertise of **Florian Fröhlich** and **Stefan Walter** is invaluable. They are both kind and patient in handling my repetitive questions. In my early days of doing lipidomics, **Sebastian Eising** provided excellent instructions.

Throughout my PhD, I received much help and constructive feedback collaborators. Hence, I would like to express my gratitude to **Thierry Soldati** for checking the manuscript, sending me protocol, and making thoughtful suggestions. **Peggy Paschke** provided me with her expertise in genetic engineering of *D. discoideum*, she is generous with her time and help. Also, **Markus Maniak** provides us with *D. discoideum* strains, protocols and helpful insights. **Fikadu Taffesse** and **Jason King**, also provided me with valuable feedback, during their visit to Osnabrück. The review writing experience with **Mélanie Foulon** was fun and pleasant.

The help from **Christine Wolterink** is also instrumental. I am extremely grateful for her steadfast assistance with the authorities. **Sigrid Bröcker-Smidt,** thank you for your kind help with the paperwork. Also for **Sergei Korneev,** for synthetizing click-lipids and for the conversations in the evenings. **Angelika Hilderink** and **Britta Fiedler** provided me with helpful technical support, I would like to thank them as well.

The MIB team is far from boring, here I would like to mention them. **Aby Anand** annoyed me throughout my PhD, I wanted to say nice things to him, but the words just did not come out**. Edwin Ufelmann,** who greatly contributed to my work, has proven to be a reliable student. **Iris Hube**, thank you for being a good friend of mine and helping me and Aby in establish our roots in Germany. **Deise Schäfer**, thank you for the great time we had together with the rest of the MIB team, especially during the BBQ in Ibbenbüren. **Anna Mazur** and **Vana Hüttel**, thank you for being such an amazing friend and colleague, helping each other out as we progress in our research work. **Danica Müller,** thank you for your wonderful presence and also for taking your time to check my German abstract. **Sarah Polkehn** and **Fynn Kamp**, thank you for the great time we had together.

The MCB team is also dear to me. **Tolu Sokoya** (my man), your calmness and your dedication are an inspiration to me. **Michael Timme**, thank you for the friendship and the awesome time we had together. **Tobi Adeosun**, I had a lot of fun moments with you. Also thank you for checking

my manuscript. **Milena Wessing,** you are awesome. **Katharina Kott** and **Elisabeth Südhoff,** thank you for the pleasant conversations, you are also awesome. **Christian Schröer** and **Sebastian Bieker**, you guys are cool.

I met so many beautiful people in the University of Osnabrück. Shoutout to: **Leo Breitsprecher** and **Rico Franzkoch** from the Psathaki group**; Ben Pauli, Shiksha Ajmera, Sharvari Harshe, Swagatika Dash** from the **Kost** group**; Bianca Esch** from **Froehlich** group; **Linnet Bischof** from the Heinisch group; **Kim Chi Vho** and **Izabella Ćwiklińska** from Gupta group; and **Malavika Pramod**; not excluding people I fail to mention.

Special thanks to my former flatmate, **Felix Wille,** for helping me out during the moving in process to my current flat. Also to my confessor, **Fr. Libin Chitteh**, for his patience and listening ear; and to **Ákos T. Kovács** who provided me with generous post-Master career promotion and support. **Philipp Grunner**, I really grateful for your participation in the career seminar. **Robert** and **Sumi Olinski**, thank you for hosting me when I am in Denmark and for the long lasting friendship. My longtime friend, **Moniqe Daba Faye**, is always loyal and listens to my problems. She also proofread my manuscript.

I like biology. My high school teacher, **Mrs. Noviana Ingrid**, inspired me to continue my pursuit in Biology. One time, when me and my classmates went to this out-of-town Biology competition, she went so far as to fund us from her own pocket. My Bachelor thesis supervisor and friend, **Mrs. Tresnawati Purwadaria,** helped a lot throughout my career. Without her mentorship, I am left uninspired. I would also like to thank my **Mom** and **Dad**, for their love and support. My siblings, **Nico Listian** and **Christo Listian,** are my best friends. I have received so much support, and I am humbled to have made it this far.

Most importantly, I would like to thank my **Lord Jesus** and **Mother Mary**.

Erklärung über die Eigenständigkeit der erbrachten wissenschaftlichen Leistung

Ich erkläre hiermit, dass ich diese Arbeit ohne unerlaubte Hilfe Dritter und ohne Verwendung anderer als der angegebenen Hilfsmittel angefertigt habe. Die direkt oder indirekt aus anderen Quellen übernommenen Daten sind mit der Quelle gekennzeichnet. Bei der Auswahl und Auswertung des nachfolgenden Materials haben mich die unten aufgeführten Personen wie jeweils beschrieben entgeltlich / unentgeltlich unterstützt.

1. Die Experimente zur zellfreien Expression (CFE) wurden, soweit angegeben, von Dr. Matthijs Kol (Molekulare Zellbiologie, Universität Osnabrück) durchgeführt.

2. Die Immunfärbung von *D. discoideum* für die CSS2-Lokalisierung und der intrazelluläre Wachstumstest von *M. marinum* wurden, soweit angegeben, von Edwin Ufelmann (Molekulare Infektionsbiologie, Universität Osnabrück) durchgeführt.

An der inhaltlichen Aufbereitung des Materials der vorliegenden Arbeit waren keine weiteren Personen beteiligt. Insbesondere habe ich keine bezahlte Hilfe von Vermittlungs- oder Beratungsdiensten (Doktorväter oder andere Personen) in Anspruch genommen. Niemand hat von mir direkt oder indirekt irgendwelche geldwerten Vorteile für Arbeiten erhalten, die mit dem Inhalt der vorliegenden Arbeit in Zusammenhang stehen. Die Dissertation ist in gleicher oder ähnlicher Form bei keiner anderen Prüfungsbehörde im In- oder Ausland eingereicht worden.

Osnabrück, den

_____

Stevanus Aditya Listian